DOTTORATO DI RICERCA IN SCIENZE CHIMICHE

CICLO XXXIII

COORDINATORE Prof. PIERO BAGLIONI

^{14}C - AMS MEASUREMENTS OF MICROGRAM-SIZED SAMPLES: HARDWARE DEVELOPMENTS AND APPLICATIONS TO CULTURAL HERITAGE

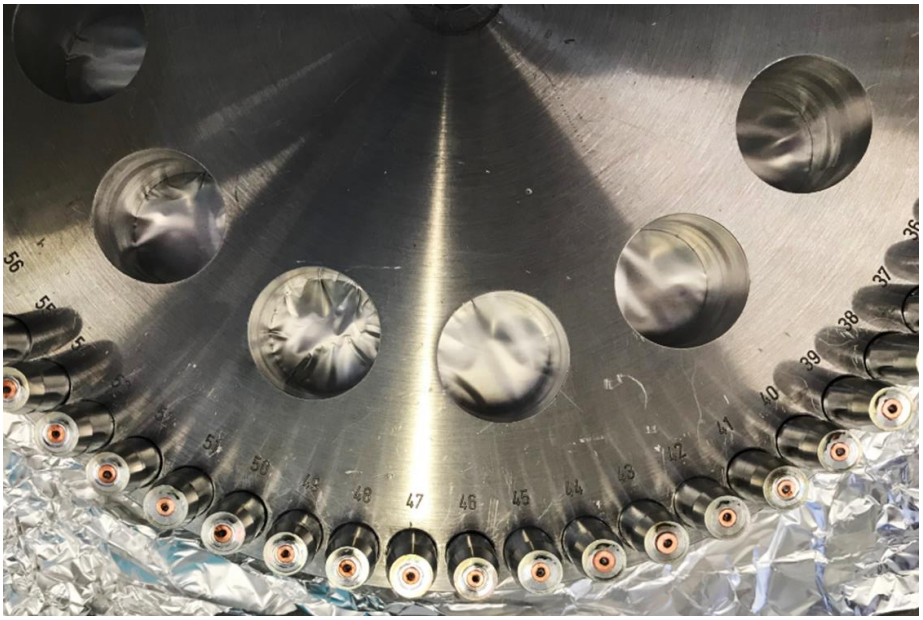

Dottorando
Dott. Serena Barone

Tutore
Dott. Mariaelena Fedi

DOTTORATO DI RICERCA IN SCIENZE CHIMICHE

CICLO XXXIII

COORDINATORE Prof. PIERO BAGLIONI

^{14}C - AMS MEASUREMENTS OF MICROGRAM-SIZED SAMPLES: HARDWARE DEVELOPMENTS AND APPLICATIONS TO CULTURAL HERITAGE

Settore Scientifico Disciplinare FIS/07

Dottorando
Dott. Serena Barone

_____
(firma)

Tutore
Dott. Mariaelena Fedi

_____
(firma)

Coordinatore
Prof. Piero Baglioni

_____
(firma)

Anni 2017/2020

Table of contents

Introduction

In the field of Cultural Heritage and archaeology, knowing the period in which an artefact is produced or being able to date biological remains is of fundamental importance. For these studies, many different techniques cooperate together to reconstruct and understand our history. Among them, radiocarbon dating is surely one of the most widespread dating techniques. It allows us to date all those organic and inorganic materials which have been exchanging carbon with a carbon reservoir until a certain moment (e.g. the death of an organism or the definite isolation of the inorganic system from the reservoir itself).

One of the basics in radiocarbon dating is the need to collect a sample, whose mass typically varies according to the kind of materials. Considering the possibility to measure the residual ^{14}C abundance by Accelerator Mass Spectrometry (AMS), sample masses are usually relatively small, i.e. of the order of magnitude of tens of milligrams. However, in some particular cases, the mass required for the analysis may become problematic: indeed, there can be some applications in which the amount of mass required would alter the integrity and spoil the legibility of the object to be dated (e. g. when a central portion of the object should be collected), or the amount of mass that we can collect is already very small (e.g. in case of highly degraded materials or samples for which a particular selective pre-treatment is mandatory). For this reason, especially in the most recent times, the interest in reducing the mass required for the ^{14}C measurements has increased. As a matter of fact, systems specifically designed for microsamples measurements have been developed: in particular, two different approaches have been used, one based on the use of ion sources optimized for gaseous CO_2 samples [1], the other based on solid graphite samples [2] [3]. The former method surely is less time consuming and with lower probability of contaminations, since the graphitization step is avoided. However, since the whole sample is directly injected into the source, there is no possibility of re-measuring the sample and verify the reproducibility *a posteriori.* Moreover, since in our laboratory the graphitization process

efficiency is not a problem and the actual experimental conditions would need several expansive operations to perform measurements on gas samples, we chose the solid samples method.

My Ph.D. research has been focused on reducing the amount of mass needed to perform radiocarbon measurements down to about 50 µg of graphite. During these three years, I have worked at INFN-LABEC laboratory (Istituto Nazionale di Fisica Nucleare - Laboratorio di tecniche nucleari per i Beni Culturali), in Florence. At LABEC, radiocarbon measurements are typically performed preparing samples of about 700 µg of C (final carbon mass at the end of the sample preparation process). In order to reduce the mass of the treated samples, the first part of the project has been represented by the upgrade of the pre-existing graphitization system and the following optimization of the new installed experimental set-up for microsamples. We installed new graphitization reactors, reducing their volumes in order to improve the collected pressure to favour the graphitization reaction. New reactors were equipped with a small quartz tube used as the "hot" part and a silver cold finger. We also designed and assembled small ovens and small Peltier-based devices, used to reach the temperature needed to trigger the reaction and to trap the unwanted water produced during the graphitization reaction, respectively. We installed new pressure gauges, sensitive to low pressures, and we assembled a home-made data acquisition system based on an Arduino board. In addition to the optimization of the graphitization set-up, the optimization of the AMS measurements in the Tandem accelerator was necessary as well. We performed microsamples beam runs using dedicated operating conditions to test the achievable precision and accuracy.

The second part of this Ph.D. project consisted in studying new possible applications for our new microsamples set-up. Among all the possible applications, we decided to focus on two feasibility studies: dating of mortars and of organic inks on papyrus.

The present thesis discusses all the fundamental steps of the project, concerning both the set-up upgrades and the case studies, and it is so divided:

- The first chapter briefly introduces the principles of radiocarbon dating and

of Accelerator Mass Spectrometry (AMS) technique; it also includes a detailed description of the experimental set-up installed at LABEC laboratory, which is used for the pre-treatment and measurements in case of the typical large mass samples. A discussion on the importance of reducing the mass needed for the measurement and the issues arising from such an action are also present at the end of the chapter.

- The second chapter is focused on the upgrade and optimization of the graphitization set-up for microsamples: the modifications in the experimental set-up needed to deal with different issues are explained in details and the several tests performed to verify the reliability of the graphitization reactions are discussed.
- The third chapter describes the optimization of the AMS measurements for microsamples: the strategy applied to optimize the beam transport along the AMS beam line is present as well as a detailed discussion about the tests performed to verify the reproducibility and reliability of our measurements.
- The fourth chapter is about radiocarbon dating of mortars: being a very heterogeneous material, mortar dating brings along many issues that are still discussed in the radiocarbon international community; the selection of the carbonaceous fraction of interest and the removal of possible contaminations is difficult and a particular aggressive and selective pre-treatment is necessary, resulting in a significant mass loss. For this reason, the newly developed experimental set-up for microsamples is expected to be suitable for this kind of application.
- In the fifth chapter, the feasibility study about radiocarbon dating of organic carbon-based inks is presented: one of the main issues of this kind of applications is that a portion of text has to be collected for the analysis, hence minimising the invasiveness of the analysis is mandatory. For this study, test samples were prepared and an efficient pre-treatment for the removal of possible contaminations and the extraction of carbon particles from ink was

identified.

Chapter 1: Radiocarbon and Accelerator Mass Spectrometry

1.1 Principles of radiocarbon dating

^{14}C dating is a radiometric dating method, based on the measurements of the residual concentration of that carbon isotope inside specific materials. This method was firstly developed in 1940s by Willard Frank Libby, who was awarded the Chemistry Nobel Prize in 1960 for his research [4].

By radiocarbon, we can date those materials which have been exchanging carbon with the atmosphere or any other carbon reservoir until a certain moment, i.e. the death of an organism which the material derives from, or the complete isolation of the system from the environment.

^{14}C is the only natural instable isotope of carbon. Its decay follows equation (1.1):

$$^{14}C \longrightarrow {}^{14}N + \beta^{-} + \bar{\nu} \tag{1.1}$$

Radiocarbon is produced in the atmosphere by the interactions between thermal neutrons, by-product of cosmic rays, and atmospheric nitrogen, following the nuclear reaction:

$$^{14}N(n,p)^{14}C \tag{1.2}$$

Once formed, ^{14}C rapidly oxidizes to $^{14}CO_2$ and scatters throughout the atmosphere. In this chemical form, it enters the different carbon reservoirs (e.g. atmosphere, biosphere, oceans) thanks to chemical and biological processes, such as photosynthesis and CO_2 dissolution [5]. ^{14}C is thus assimilated by all the living beings, in a concentration[1] which is roughly equal to the one of the atmosphere ($\approx 1.2 \cdot 10^{-12}$ [6]). As long as there are exchanges with the external environment, there is an equilibrium between the

[1] By "concentration", here we refer to the isotopic ratio $^{14}C/^{12}C$, considering that the abundance of ^{12}C is about the 99% of the all-natural carbon on earth.

assimilated ^{14}C and the decaying ^{14}C. When the exchanges with the environment have somehow stopped (e.g. the living organism dies), the ^{14}C concentration starts decreasing with a trend given by the exponential decay law. Thus, at a given time t, we will have:

$$\left[{}^{14}C\right]_t = \left[{}^{14}C\right]_0 \cdot e^{-t/\tau} \tag{1.3}$$

where $\left[{}^{14}C\right]_0$ is the radiocarbon concentration at the death of the organism, or at the moment of the system isolation from the carbon reservoir, and τ is the mean-life of ^{14}C. Assuming τ as the so-called Libby's mean-life (8033 years) and $\left[{}^{14}C\right]_0$ as the radiocarbon concentration in 1950, we can obtain the so-called conventional radiocarbon age (t_{RC}) from equation (1.3):

$$t_{RC} = \tau \ln \frac{\left[{}^{14}C\right]_0}{\left[{}^{14}C\right]_t} \tag{1.4}$$

Conventional radiocarbon age is expressed in years Before Present (yrs BP), in which 1950 is conventionally assumed as present.

However, the radiocarbon conventional age does not represent the real age of a sample, because some of the hypotheses that support equation (1.4) are true only at a first approximation. In Appendix A, further details are discussed about the hypotheses supporting the conventional radiocarbon age.

To obtain the best estimate of the real age of a sample, the conventional radiocarbon age must be calibrated, as it is used to say, using appropriate calibration curves. A calibration curve describes the relationship between a conventional radiocarbon age and the corresponding calendar date (see Figure 1.1). Each calibration curve commonly accepted is built by combining ages that have been measured using different dating methods.

For example, a portion of the calibration curve has been built by dating tree rings both by radiocarbon dating and dendrochronology. In a tree, only the outer ring is in equilibrium with the atmosphere; each tree ring thus represents only a single year of growth. Therefore, the radiocarbon concentration of a single tree ring is representative of the concentration in the atmosphere during its formation year. If we date all the tree rings by dendrochronology and, at the same time, we measure their ^{14}C concentrations, we can build a calibration curve of radiocarbon age against the calendar age. Using tree rings, it is possible to build a calibration curve down to about 10000 years ago. Other materials that have been used to build the curve are speleothems and corals, which can be dated through the U-Th method, and varves, which are dated by counting and measuring their growth strata.

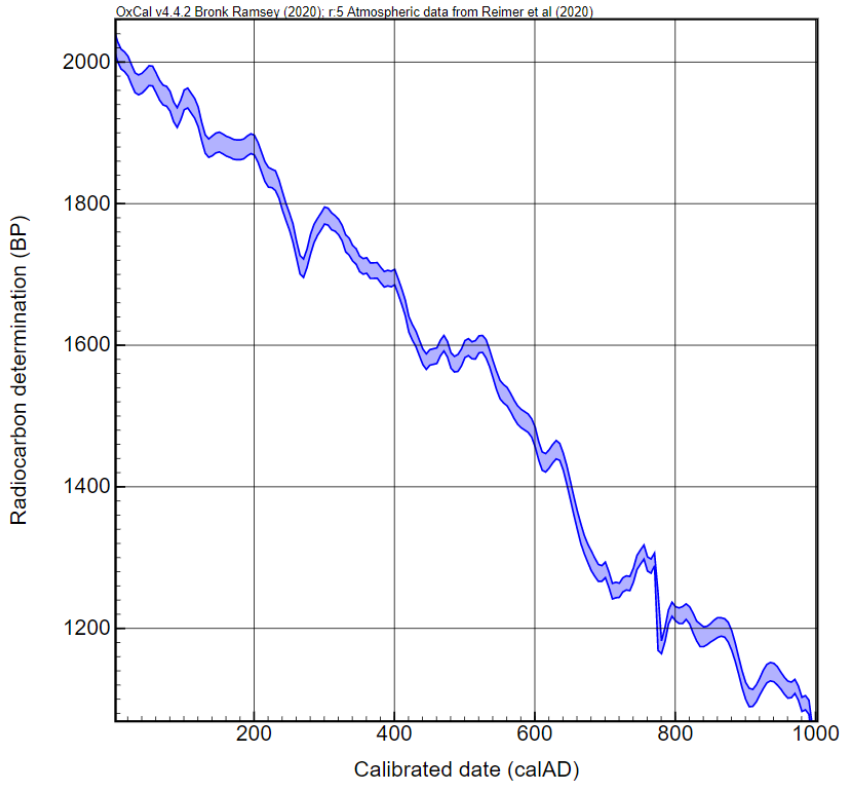

Figure 1. 1 A portion of the calibration curve IntCal20 used to date terrestrial samples.

All the different calibration datasets “assembled” together contribute to the IntCal20 and Marine20 calibration curves, used by the whole radiocarbon community to date terrestrial and marine samples, respectively, down to 55000 years ago [7] [8].

For the calibration, different software can be used, as for example OxCal, developed by the Oxford Radiocarbon Accelerator Unit [16]. An example of calibration obtained using Oxcal version 4.3.2 is visible in Figure 1.2: on the X and the Y axes, the calendar age and the conventional radiocarbon age are reported, respectively; in blue, the calibration curve is represented, together with its experimental error.

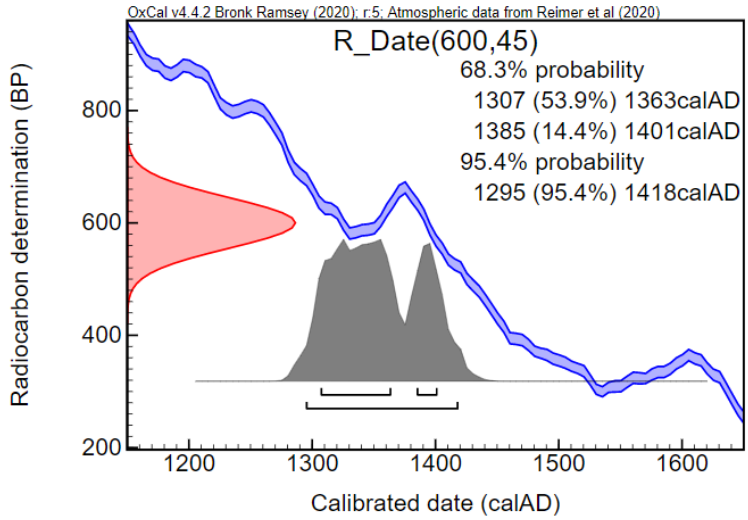

Figure 1. 2 Example of calibration of the radiocarbon conventional age of a sample, using Oxcal.

To obtain the probability distribution which represents the calibrated age, Oxcal uses the Bayes’ theorem [9]:

$$P(t|y) \propto P(y|t)P(t) \propto \frac{\exp\left(-\frac{\left(r-r(t)\right)^2}{2\left(s^2+s^2(t)\right)}\right)}{\sqrt{s^2+s^2(t)}} \qquad (1.5)$$

In equation 1.5, t is the date of the event we would like to determine, y is the measurement result, i.e. $y = r \pm s$ (in red in Figure 1.2), $r(t)$ and $s(t)$ describe the

coefficient of the normal distribution associated to each of the point of the calibration curve (in blue in Figure 1.2). The result of calibration is the conditional probability $P(t|y)$ of obtaining t given the measurement result y and it is represented in grey in the Figure. For a single value of conventional radiocarbon age, it is possible to obtain multiple ranges of real age t.

1.2 Accelerator Mass Spectrometry

Accelerator Mass Spectrometry (AMS) is an experimental technique that allows us to measure the relative abundance of rare isotopes, discriminating them according to their masses, energy and charge state [10]. One of the most widespread application of the AMS technique is the measurement of radiocarbon concentration: instead of measuring the decays, atoms as ions are accelerated to medium-high energies using a particle accelerator [11], thus achieving an extremely low sensitivity (down to about 10^{-15}) and allowing us to reduce the sample masses of about three order of magnitude with respect to the masses required for the measurement of the activity [12].

In AMS, a particle accelerator and its beam transport system are employed as a sort of high sensitivity mass spectrometer: in particular, Tandem accelerators have become the "standard" AMS machines. ^{14}C concentration cannot be measured using a simple mass spectrometer, not only because of the very low concentration of this particular isotope, but also because of the presence of different interferences, that must be removed during the measurements. These interferences are elemental and molecular isobars, such as ^{14}N, ^{13}CH and $^{12}CH_2$, which basically have the same mass as ^{14}C and cannot be distinguished from it.

Using a Tandem accelerator, however, allows us to suppress all these interferences during the measurements:

- the simple fact that a negative ion beam is extracted from the accelerator source allows us to remove the ^{14}N interference: ^{14}N, as a matter of fact, does not form stable negative ions [9].
- The other molecular isobars, such as ^{13}CH and $^{12}CH_2$, are instead suppressed

during the stripping process at the accelerator high voltage terminal: together with the charge state exchange, the loss of electrons causes the so-called Coulomb explosion. The bonds, which hold the molecules together, break apart. The molecules lose their stability and are further accelerated as fragments with mass clearly different from 14.

Referring to the 3MV Tandem accelerator installed at INFN-LABEC laboratory in Florence [13], in the following paragraph the functioning of the accelerator is explained.

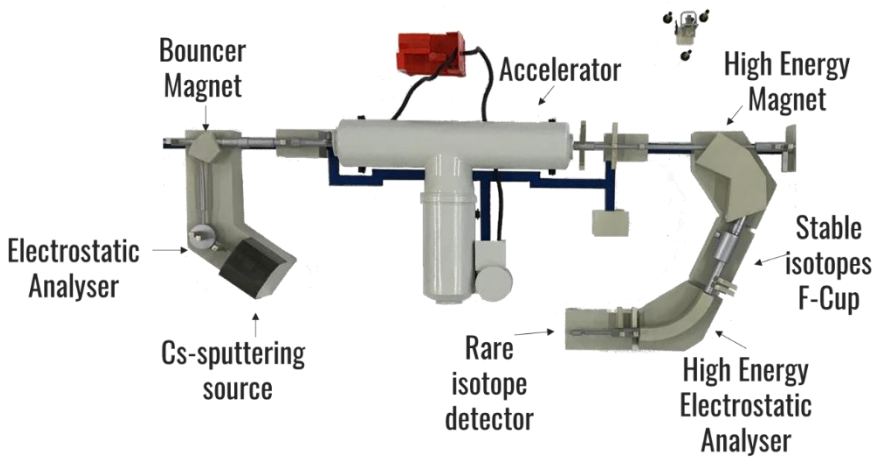

Figure 1.3 Schematic representation of the 3 MV Tandem accelerator installed at INFN-LABEC laboratory; only the components related to the AMS beam line are shown.

1.2.1 The Tandem accelerator for AMS

The Tandem accelerator consists in three main parts: the low-energy side, which goes from the ion source to the accelerator tube; the accelerator itself, with the high voltage terminal; the high-energy part, from the exit of the accelerator to the detector. Along the beam line there are different tools, such as Faraday Cups and Beam Profile Monitors, that help analysing and transport the particle beam from the ion source to the detector.

The ion source used for the AMS analyses is a Caesium-sputtering source, equipped with a carousel with 59 positions, where samples to be measured are allocated as graphite pellets in aluminium supports. In order to extract the ion beam, low energy

heavy ions, in this case Cs^+ ions, are used to bombard the target/sample, thus causing the ejection of the light atoms. These atoms are then negatively ionized thanks to the interaction with Cs itself. In such a source, it is clear that, in order to have a reliable current output, a good alignment between the impinging Cs+ beam and the surface of the target is fundamental. It is possible to choose different sputtering positions: during a typical beam run, each graphite pellet is measured in 9 different positions so as to not form "craters" in the pellet surface (these craters would modify the total geometry of the electric field inside the source). The strength and the tightness of the sample pellet is essential as well.

The extracted negative ions are accelerated out from the source into the beam line by a total voltage of 35 kV.

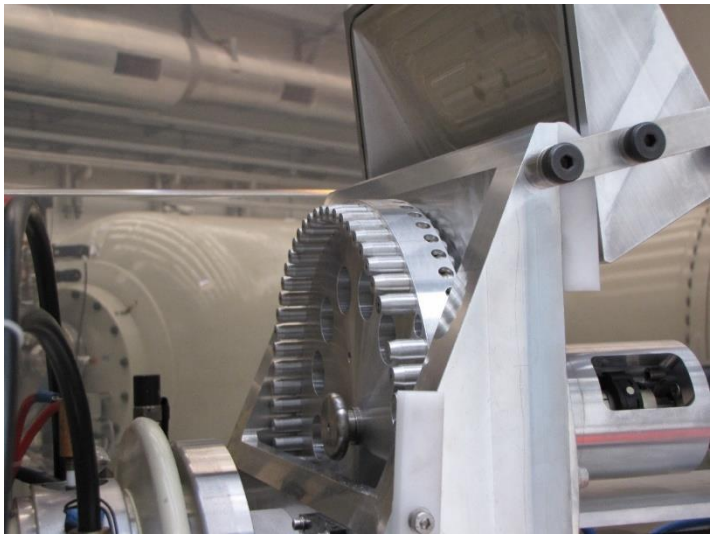

Figure 1. 4 The Cs-sputtering ion source of the AMS beam line installed at LABEC. The carousel with the samples pressed in the aluminium holders can be seen.

On the beam line, electrostatic and magnetic "filters" are used in order to "clean" the ion beam and select the ion of interest.

The first "filter" is an electrostatic analyser (ESA), which selects the ions depending on their energy-to-charge ratio (E/q). Basically, the ESA is a parallel plates capacitor, whose surfaces are designed following specific geometries. Only those ions that fulfil the

following equation are transmitted through the analyser:

$$\mathcal{E}\, r = 2\frac{E}{q} \tag{1.6}$$

where $\mathcal{E}$ represents the applied electric field and r is the ESA bending radius, q and E represent respectively the charge of the ions and their energy.

In our case, ions with a ratio E/q of 35 keV over 1e are selected.

Downstream the ESA, the Bouncer Magnet selects the ions according to their masses, using the Lorentz force:

$$\mathcal{B}\, r = \frac{\sqrt{2mE}}{q} \tag{1.7}$$

From equation (1.7), we can say that ions with different masses will travel the same trajectory by varying the applied magnetic field $\mathcal{B}$ or the ion energy E. During radiocarbon measurements, in addition to ^{14}C, we also need to measure both ^{12}C, necessary to obtain the isotopic ratios (i.e. the "concentrations") of samples, and ^{13}C, necessary to evaluate the corrections for the isotopic fractionation. The different masses are rapidly injected one after the other by varying the energy of the ion beam: the magnetic field is kept constant, so that the magnetic hysteresis can be avoided. In our typical measurement set-up, every cycle of injection has a duration of about 10 ms. During each injection cycle, each mass (12, 13 and 14) is sequentially injected during different time ranges, which depend on the expected abundance of that specific mass: for example, ^{14}C is injected for most of the time (about 8 ms), because its concentration is much smaller than the concentrations of the other two isotopes of interest[2].

Downstream the bouncer magnet, the negative ions are then accelerated to the high

[2] These time ranges refer to the typical measurements set-up. They may be changed depending on the need of the measurements (see Paragraph 3.1)

voltage terminal. Here the ions change their charge state as a consequence of the so-called stripping process. At the high voltage terminal, the accelerator tube is filled with gas, commonly called stripper (Argon, in the case of LABEC). When the accelerated ion collides with the gas particles, it has a certain probability to lose one or more electrons, hence changing its charge state. The likelihood to have a specific charge state depends on the thickness of the stripper and on the speed of the ion at the moment of stripping. Once the equilibrium thickness is reached, the most likely charge state depends on the ion speed only. At the exit of the accelerator, the ions have a distribution of charge states.

At the end of the accelerator tube, on the high energy side, the ions energy thus depends on the charge state; for monoatomic ions, we have:

$$E_f = E_i + (q+1)e\Delta V \tag{1.8}$$

where E_i is the ion energy exiting the ion source, q is the ion charge after the stripping process and ΔV is the terminal voltage. At LABEC, during typical radiocarbon measurement, the terminal voltage is set at 2.5 MV and, among all the possible charge states, the most likely is the +3. Thus, in the end, the ions with a +3 charge have an energy of about 10 MeV, plus the energy acquired in the extraction from the source.

On the high energy side, there is another magnet, which selects the ions accordingly to their masses: for example, during a radiocarbon measurement, we select only those ions with charge state +3 and mass 14 ($^{14}C^{+3}$).

After the magnet, the ion beam is further analysed through another ESA, which transmits only those ions with a E/q ratio of 10 MeV/3e, so that any other possible interferences are removed.

Radiocarbon counts are measured using a solid state silicon detector downstream the final ESA. ^{12}C and ^{13}C abundances are measured as ion currents exploiting two off-line Faraday Cups which are installed after the exit of the high energy magnet along inner trajectories. The use of Faraday cups is possible because the expected ^{12}C and ^{13}C ion

currents are well above the typical sensitivity limits of such devices. It is clear that, if the extracted current from a sample is lower than expected, while keeping the same injection times, the instantaneous ^{12}C and ^{13}C currents will be lower as well and the Faraday cups would not be necessarily suitable for the measurement.

1.3 Sample preparation for the measurement

As can be inferred from paragraph 1.2.1, to measure the radiocarbon content in a material or object by AMS, we need to collect a sample, whose mass is relatively small. How much large is the sample surely depends on which the material we want to date is: the required mass usually is in the order of few tens of milligrams[3].

However, as said in the paragraph above, we cannot use the sample as it is, but the samples must be converted into a chemical form that is suitable for the ion source we are using for the measurements. In particular, the ion source used at LABEC admits exclusively solid samples, i.e. graphite. In addition, due to the possible contaminations that may be present in the sample, we need to extract only the carbon fraction that is of interest for the dating.

Therefore, we treat all the samples we want to date.

Removal of all the possible contaminations and extraction of the carbonaceous fraction of interest is usually performed thanks to a preliminary physical and chemical pre-treatment. As far as this operation is concerned, no standard protocol exists. Instead, each procedure is modulated depending on the material to be analysed and/or on which contaminations we may expect. Indeed, for samples collected from an archaeological site or excavation, we expect natural contaminations such as carbonates and humic acids from the soil, while for those samples within museum contexts, we may expect contaminations from possible restoration work, such as synthetic resins (see [14] as example).

[3] For materials like wood or charcoal, we talk about 10-50 mg, depending on the preservation state and on the possibility of having undergone restoration; if we want to date more complex materials, e.g. bones, we need to take a sample of about 100-500 mg.

Further details about the possible pre-treatments will be discussed when the case studies are presented later in this thesis.

After the pre-treatment needed to remove the contaminants, samples are combusted and graphitized, as explained in the following paragraph.

1.3.1 Sample combustion and graphitization

In Figure 1.5, the diagram of the combustion/graphitization line installed at LABEC [13] is presented.

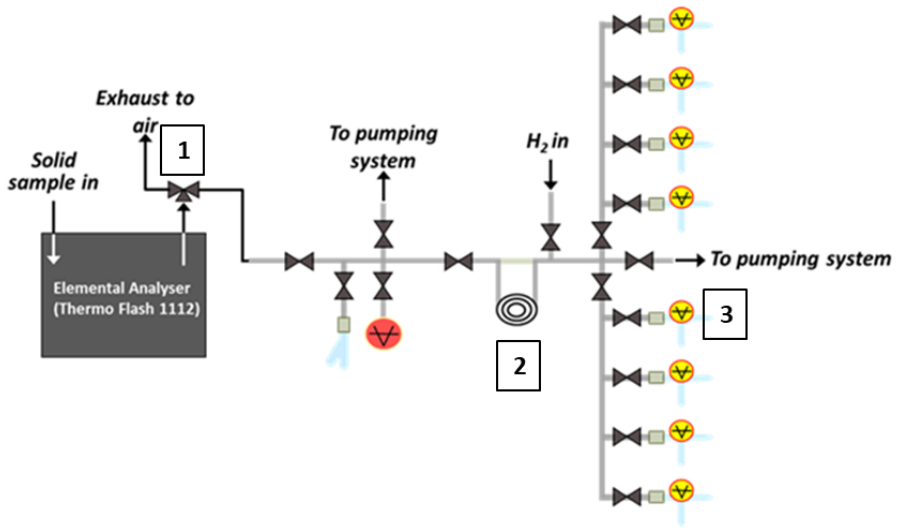

Figure 1. 5 Diagram of the graphitization line installed at LABEC in Florence. With reference to the text, the switching valve, the cryogenic CO_2 coil trap and the graphitization reactor are indicated by numbers 1, 2 and 3, respectively.

Combustion is needed to extract carbon from the samples as CO_2, that will be graphitized afterwards. For the combustion, an elemental analyser CHN (Thermo Flash EA 1112) is installed. The elemental analyser (EA) is composed of a combustion column, filled with different reagents needed to either oxidize or reduce the evolving gases, a gas-chromatographic column and a gas detector.

The sample to be dated is weighed and closed inside a tin capsule. In Table 1.1, typical masses depending on the sample material are reported. The capsule is inserted into the

combustion column, which is heated up to 950°C: here, a flux of oxygen allows the triggering of the flash combustion.

Sample material	Combusted mass (mg)
Oxalic acid	4.45
Cyclohexanone 2,4 DNPH	1.50
Charcoal	1.25
Wood	1.80
Textile (linen, cotton…)	1.80
Collagen	2.00

Table 1. 1 Sample masses for combustion depending on the material. Regarding the Oxalic acid, it is important to keep in mind that this material is highly hygroscopic, hence the combustion CO_2 yield is lower than expected.

The gases are transported by a "carrier" (He) through the analyser. After the combustion column, they pass through the gas-chromatographic column: this column is filled with an adsorbent polymer, which holds and releases the gases depending on their affinity for it. The different gases retention times inside the column allow us to distinguish and separate them. The output of the analyser is shown as a chromatogram, where the signals due to the different gases are represented as a function of time (see Figure 1.6).

While the other gases N_2 and H_2O are released into the atmosphere, only CO_2 is collected. Actually, the analyser outlet is connected to the graphitization line via a three-way switching valve: as CO_2 passes, the valve is commuted to allow for the gas and the carrier flowing into the line.

Usually, between two samples, a blank combustion – without any sample inserted into the EA – is performed, in order to check whether the combustion have been complete and thus the possible presence of contaminations. Moreover, to further minimized the cross-contamination risk, after the blank combustion, when the total mass is sufficient, a very small fraction of the cleaned sample that has to be then

processed is burnt: in this way, should the EA introduce a contamination due to the previous combustion, the effect would be of the same radiocarbon concentration of the sample itself [15].

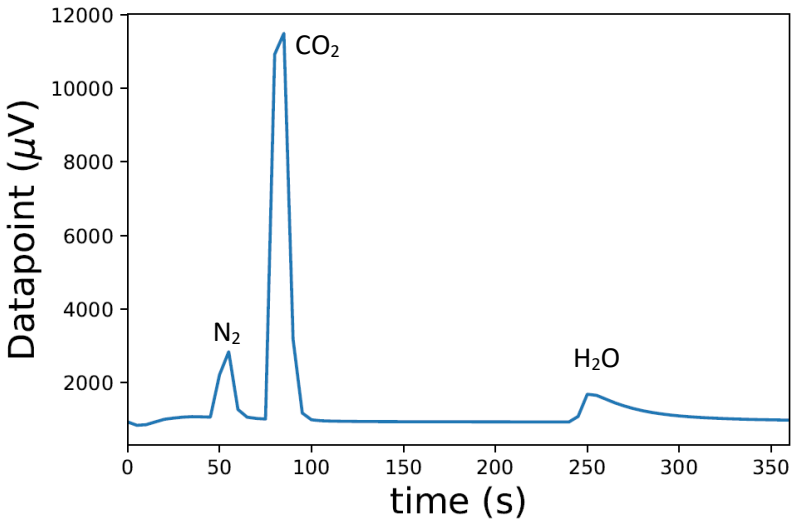

Figure 1. 6 Example of a chromatogram of cyclohexanone 2,4 DNPH.

While not in operation, the graphitization line is usually kept in vacuum (~ 10^{-4} mbar). As already mentioned above, when the chromatogram shows the passage of CO_2, the gas is transferred into the graphitization line through the switching valve (1 in Figure 1.5). The cryogenic trap indicated with 2 in Figure 1.5 is immersed into liquid nitrogen, which brings the system close to -196°C, allowing the condensation of only CO_2, while the carrier He remains as a gas. Helium can be then removed via the pumping system, while the CO_2 remains trapped in the graphitization line.

Each graphitization reactor (see 3 in Figure 1.5) is made up by two quartz tubes: one is used as a cold finger, while the other one is the actual reactor. The total internal volume is about 6 cm^3. After pumping of helium, CO_2 is recollected into one of the graphitization reactors by immersing the cold finger into liquid nitrogen. Thus, the CO_2 pressure is measured: usually, to have as uniform graphite pellets as possible, we collect an amount of CO_2 of (270±20) mbar, which corresponds to about 700 µg of graphite at

the end of the reaction.

The graphitization reaction is [16]:

$$CO_2 + 2H_2 \xrightarrow{Fe,600°C} C + 2H_2O \quad (1.9)$$

The reaction triggers at 600°C in presence of Fe as catalyst. Usually, we work with a H_2 excess, in order to increase the chances of a complete reduction of CO_2 to C. Moreover, to have a correct trend of the reaction, the cold finger is kept at about -30°C by a Peltier cooling system, which traps the unwanted water, which is produced according to (1.9).

The reaction is monitored by acquiring the gas pressure inside the reactor in real time.

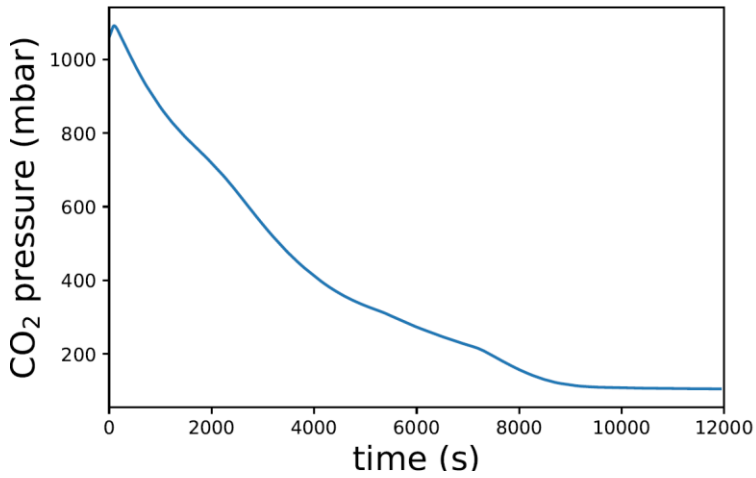

Figure 1. 7 Graphic of a graphitization reaction for our typical samples, obtained collected about 270 mbar CO_2.

In Figure 1.7 the trend of a typical graphitization is represented. The CO_2 pressure is reported versus time: when the pressure reaches a plateau (after about 2.5 hours), we can consider the reaction finished. In the Figure, the presence of a residue at the end of the reaction is visible: this residue is due to the excess of H_2 added to start the graphitization.

At the end of the reaction, the obtained graphite plus the iron powder is pressed as a pellet into an aluminium support, which is specifically designed to fit in the ion source of the accelerator (see Figure 1.8).

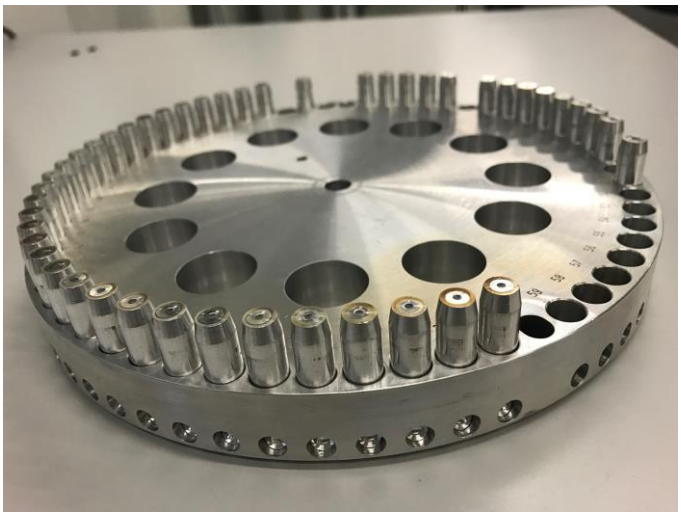

Figure 1. 8 Samples pressed into their aluminium holders and mounted in the carousel, ready to be put into the accelerator ion source.

1.4 The importance of measuring microsamples

As already explained in paragraph 1.3.1, in our laboratory, the graphitized mass is typically about 700 µg. If we consider e.g. the case of a charcoal, this mass derives from the combustion of about 1.2 mg. Considering that, when a charcoal is very badly preserved, we can even have a pre-treatment yield as low as 30%, we should collect 5÷10 mg of raw material at least for the radiocarbon measurement. This mass is usually relatively small for the majority of applications of this technique.

However, there can be some possible applications in which the invasiveness of the analysis becomes problematic, because the required mass could spoil the legibility of the object or the available mass itself could not be sufficient. For instance, this may be the case if we want to date a particular material, such as the pigment of a painting [17] or the organic ink of a written document (see chapter 5), when collecting a sample to

be dated means removing a visible part of the object. In addition, this may be the case of all those applications when a strong and highly selective pre-treatment procedure leads to small residual masses (see e.g. chapter 4).

Reducing the sample masses is also useful when we deal with highly degraded materials. This kind of samples can be unfortunately very difficult to be dated due to the residual very small amount of material combined with a high probability of presence of contamination. An example is well represented by archaeological bones: after the death of an organism, its bones undergo a series of chemical and physical transformations, called diagenesis, which lead to the depolymerisation and to the deterioration of collagen (the material of interest for the dating). Moreover, the action of humic acids or bacteria in the soil increase the possibility of introduction of contaminants inside the sample. For these reasons, a particular "aggressive" and highly selective pre-treatment is needed for these materials, thus reducing the already small masses.

Measuring microsamples is useful not only for Cultural Heritage applications, but also for environmental studies. In order to estimate the source apportionment of particulate matter, two different carbon sub-fractions are analysed: elemental carbon and organic carbon [18]. However, to collect enough material for the analysis, in case of measurements using a combustion-graphitization set-up similar to that described in paragraph 1.3.1, samplers optimized for "big" volumes are needed, thus making difficult the application of this technique on large-scale in typical sampling campaigns. Moreover, if the particulate matter is collected from very remote sites, the situation can even worse, considering the fact that the particulate matter presence in the air is already very low.

In the most recent times, reducing the mass of the sample to be dated to study these kinds of applications has thus become an important key issue to be solved. For this reason, we decided to focus our attention in modifying our dating process so as to reduce the mass of the samples to be dated down to 50 µg. Doing this, we would gain about an order of magnitude in mass, which would allow us studying new possible application for radiocarbon dating.

1.4.1 Problems of microsamples

The possibility to reduce the sample mass to perform radiocarbon dating is a big advantage for many applications, but there are many issues we need to take care of. Indeed, measuring samples with masses of about few tens of micrograms does not only involve lowering the masses of the samples we want to date. First of all, the same experimental set-up used for the "typical" large samples is not suitable for these very small samples and changes of hardware must be taken into account. Below, the most important issues are explained in details.

- Using reactor volumes that are the same of the reactors for the big samples is expected to cause a significant decrease of the graphitization rate. Indeed, when lowering the masses of samples, the CO_2 collected after the combustion is obviously much lower than the one collected for the typical samples. This implies that inside the "big" reactors, the chance that CO_2 and H_2 "collide" is very low, making the graphitization lasts for longer or not triggering at all. Moreover, working with too low pressures makes difficult, if not impossible, to monitor the graphitization reaction in real time. As explained in paragraph 1.3.1, the graphitization reaction is monitored by measuring the pressure inside the reactor and analysing its trend. However, if the pressure is too low, the pressure gauge may not be sensitive to that pressure range[4].
- Since we are dealing with very small samples, we have to minimize the mass loss possibility between one preparation step and the other. Therefore, we need to modify some stages in the process. For example, at the end of the graphitization reaction, in our typical large samples procedure, we need to transfer the graphite + iron powder into the aluminium sample holder: in this passage, some powder may be dispersed or may remain inside the quartz tube

[4] We use capacitive pressure gauges, whose response is independent with respect to the gas which fills our reactors. They are optimized for a particular pressure range (usually 3 orders of magnitude). Hence, if we use a pressure gauge sensitive to atmospheric pressure, we will have a reliable pressure reading down to about 1 mbar.

of the reactor. Such an effect should be of course avoided.

- When reducing the size of the samples, we expect an increase in the percentage of external contaminants; this is a consequence of the fact that the external contaminants in the environment interact with a smaller mass, thus leading to a more severe contaminant/sample ratio.
- As already explained in paragraph 1.2, measuring the ^{14}C concentration is a destructive analysis. Due to sputtering, the graphite pellet inside the ion source is consumed while the measurement is going on. For this reason, when measuring small samples, we need to pay attention not to consume the whole sample without obtaining a relevant statistic. Moreover, we expect that, during the measurement, the currents extracted from the small samples would be very low, maybe lower than the sensitivity of the Faraday cups used to measure the ^{12}C and ^{13}C abundances.

In this work, we dealt with all the problematics explained above. During the three years of Ph.D., I have worked on the upgrade of the pre-existing experimental set-up and its optimization for the measurement of microsamples, as will be explained in the following chapters.

Chapter 2: Graphitization set-up upgrades

2.1 Preliminary tests at VERA (Vienna)

Before starting the experimental set-up upgrades, we performed preliminary tests working on lower graphite samples in order to estimate the possible limits of the existing system, especially concerning the AMS beam line.

A set of small samples with different graphite masses were prepared at VERA laboratory (Vienna Environmental Research Accelerator) in Vienna. In Table 2.1, the prepared samples are reported.

Lab.code	Material	CO_2 pressure (mbar)	Mass of graphite (µg)
V3	NIST OxAcII	237	130
V5	Blank	405	215
V6	Blank	405	215
V7	NIST OxAcII	431	230
V10	NIST OxAcII	128	70
V11	Blank	275	150
V13	Blank	138	70
V14	NIST OxAcII	142	75

Table 2. 1 Samples prepared at VERA laboratory with their related graphite masses (the reported masses are estimated on the basis of the collected CO2 pressures and the known volume of the reactors).

The set included standard (NIST Oxalic acid II) and blank (Cyclohexanone 2,4 DNPH), samples[5], with graphite masses ranging between 70 and 230 µg, well below our typical

[5] In each AMS measurement, samples from standard reference materials, with a certified ^{14}C concentration, and blank materials, with nominally no radiocarbon, are typically prepared and measured (see Appendix B for details). Here, NIST OxAcII is the primary standard, SRM 4990C, provided by US National Institute of Standard and Technology (NIST); blank is Cyclohexanone 2,4 DNPH, provided by Santis Analytical Italia (as spare for Thermo Flash EA 1112).

mass samples measured at LABEC (about 700 µg). All the samples were prepared according to [2]. The graphite pellets with their original support were then "adapted" in order to fit our aluminium sample holders and then allocated into the ion source of LABEC accelerator for the AMS measurement. All the details about the beam transport, which has to be adapted to these small samples, will be given in chapter 3.

In Figure 2.1, the ^{12}C currents measured for the NIST Oxalic acid II samples are reported as normalized to the extracted currents of the larger samples measured in the same AMS run.

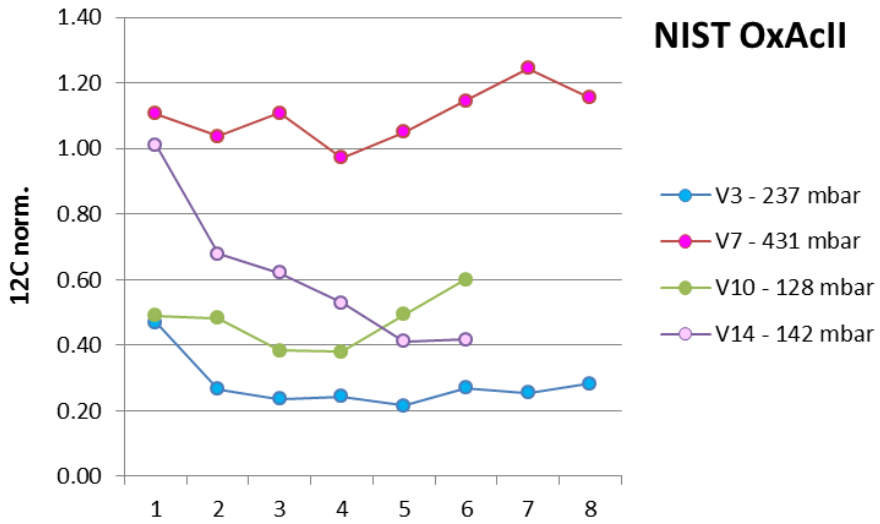

Figure 2. 1 Measured ^{12}C currents for NIST Oxalic acid II samples prepared at VERA. On the x axis, the number of repetitions are reported. The measured currents of sample V3 is lower than the others, even though its mass is estimated to be larger. This may be explained by assuming that its graphitization reaction was not complete and hence the C mass at the end was lower than expected.

The measured currents were generally satisfying, being – at least – about half of the typical currents obtained measuring larger samples. Moreover, we were able to measure the pellets for a sufficient time period, allowing us to collect a pretty good statistics, considering the small masses: at the end of the measurements, we obtained an experimental uncertainty on the measured radiocarbon concentration of 2 – 4%. As

for the background, ^{14}C concentrations measured in blanks were slightly higher than those measured for traditional large samples. This result was also expected (as discussed in the previous chapter).

Considering the measurements results, we observed that, provided some required adjustments of the beam transport conditions, that will be explained into details in chapter 3, we could focus on samples as small as about 50 µg of graphite. Thus the upgrades of the graphitization hardware and procedure were designed to match that mass goal.

2.2 The new graphitization set-up and procedure

2.2.1 The hardware upgrade

As explained in paragraph 1.4.1, lowering the mass of the samples to be dated requires experimental set-up upgrades both of the preparation line and of the AMS measurement procedures or set-up.

In particular, for the graphitization set-up, one of the key points to be addressed is represented by the too big volumes of the "traditional" reactors (about 6 cm^3), which may cause issues in the triggering of the reaction and make the reaction impossible to be monitored due to a low sensitivity of the used pressure gauges.

With the aim at reducing the internal volume of the graphitization reactors, during the first part of the Ph.D. project, we focused on designing new reaction chambers (Figure 2.2 A) to be integrated into the pre-existing graphitization line (described in paragraph 1.3.1, see Figure 2.2 B and C). We aimed at installing two new reactors, replacing two of the large ones.

The core of the new reactors is a Swagelok® Ultra-torr stainless steel vacuum fitting, chosen for its high vacuum seal performances and for the possibility to be coupled to different materials, such as quartz[6].

[6] In a Swagelok® Ultra-torr fitting, vacuum sealing is possible thanks to Viton® o-rings that provide tightness on the external surface of the inserted tube, without deforming or flatten the tube itself.

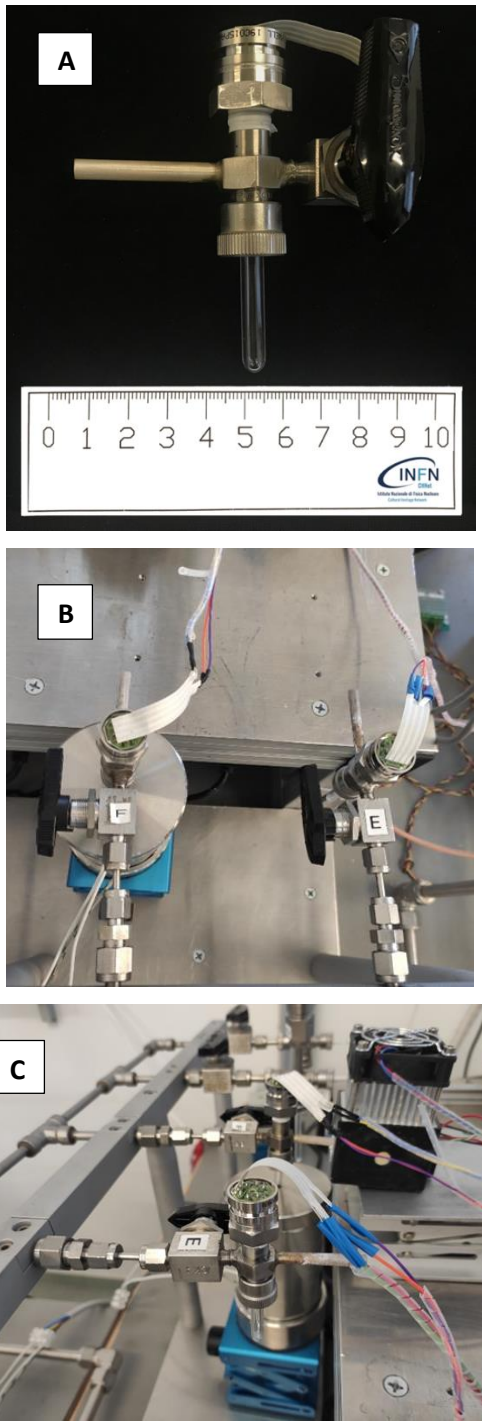

Figure 2. 2 The new small reactor in details (A) and how it is integrated into the pre-existing graphitization line (B) (C).

The different elements of the reactor were directly mounted on the body of the Ultra-torr fitting (see Figure 2.2 A). When possible according to the geometry and the type of components, the parts were directly soldered onto the fitting to minimize both the volume and the use of o-rings. To isolate each small reactor from the rest of the graphitization line, we chose a valve with an inner diameter that was smaller than the rest of the line (1/8" instead of 1/4") and a reducing fitting was used to adapt the new reactors to the original line. To further reduce the internal volume, the quartz tube, in which the reaction actually takes place and which can be also used as a trap for CO_2 when immersed in liquid nitrogen, was chosen as shorter than the one of the big reactors. Instead of using another "empty" tube as cold finger for the trapping of H_2O during the reaction, we chose a small silver bar with a very thin and short canal inside. The silver bar was also drilled from the external part to lighten the overall structure, thus reducing the heat load to be refrigerated. Silver was used due to its high thermal conductivity, which allows us to maintain the same cooling capacity as the big reactors while keeping the internal volume as low as possible.

To measure the gases pressure inside the reactor and thus also monitor how the reaction is going on, a small capacitive and temperature compensated sensor was used (Honeywell 19 mm series). In the perspective of reducing the internal volume of the reactors, we chose this particular sensor thanks to its sensitivity range combined with a very small dead volume. Since the sensor output signal is in the mV range, the voltage output was firstly amplified: the system I projected is based on a 17 MHz rail-to-rail input-output operational amplifier, mounted on a printed circuit board specifically designed (see Figure 2.3 A). The amplified signal is then acquired via a home-developed system based on an Arduino board (Figure 2.3 B). A script was specifically written for the purpose to acquire the pressure and to show in real time the trend of the reaction.

All the components selected for the new graphitization reactors allowed us to considerably reduce their internal volume, which is now about 1/4 than the internal volume of the large reactors.

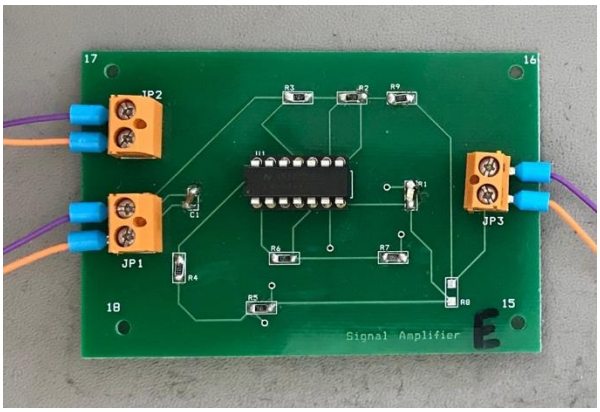

(a)

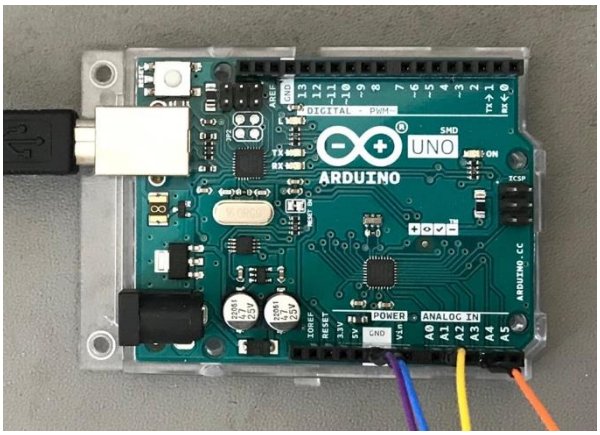

(b)

Figure 2. 3 The printed circuit board specifically designed for the signal amplifier (A) and the Arduino board used to acquire the pressure gauge signal (B).

As explained in paragraph 1.3.1, an oven and a cooling system are necessary for the graphitization reaction: the former is used to reach the temperature needed to trigger the reaction, while the latter is used to trap the forming unwanted water. The different size of the new reactors with respect to the big ones made necessary to design new oven and new Peltier system. In Figure 2.4, both the new home-design oven (A) and Peltier cooling system (B) are shown.

The small oven (Figure 2.4 A) is based on a single cartridge heating element (240 V, 100 W), housed in a copper core. The oven is designed to heat the reactor up to 600°C, without warming up the other elements. For this reason, thermal insulation is

guaranteed by protecting the copper core with Superwool® blanket. This ceramic fibre was chosen as insulating material because it shows very good thermal performances and, contrary to other coating materials, is not classified as carcinogenic or dangerous (e.g. no special requirement for dust control is needed and it is also considered a non-hazardous waste in case of disposal).

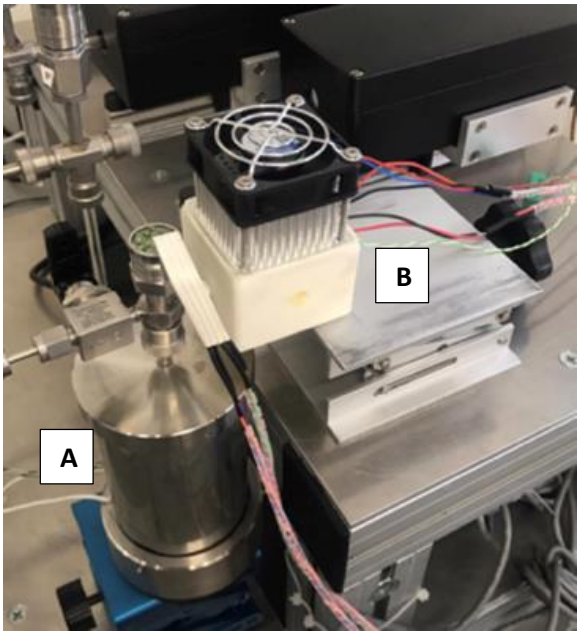

Figure 2. 4 The new small home-designed oven (A) and Peltier cooling system (B).

The home-designed cooling device (Figure 2.4 B) is based on two small Peltier modules thermally coupled in series. Heat dissipation from the hot side of the most external Peltier cell is obtained through air cooling, using a high thermal conductivity heatsink and a fan. The system is optimized to reach -25°C, sufficient to trap H_2O.

2.2.2 The new copper inserts

As explained in paragraph 1.4.1, when dealing with small masses we need to modify some of the steps of the pre-treatment procedure in order to avoid mass losses where possible.

In our large sample procedure, the iron powder is directly inserted into the reaction tube; while forming, the graphite adheres just on the iron particles, so that, at the end of the graphitization process, the mixture of carbon and iron is transferred from the tube to the aluminum holder and there pressed. It is clear that in the last operation, we may lose some material. Hence, we designed new copper inserts (see Figure 2.5), following [2].

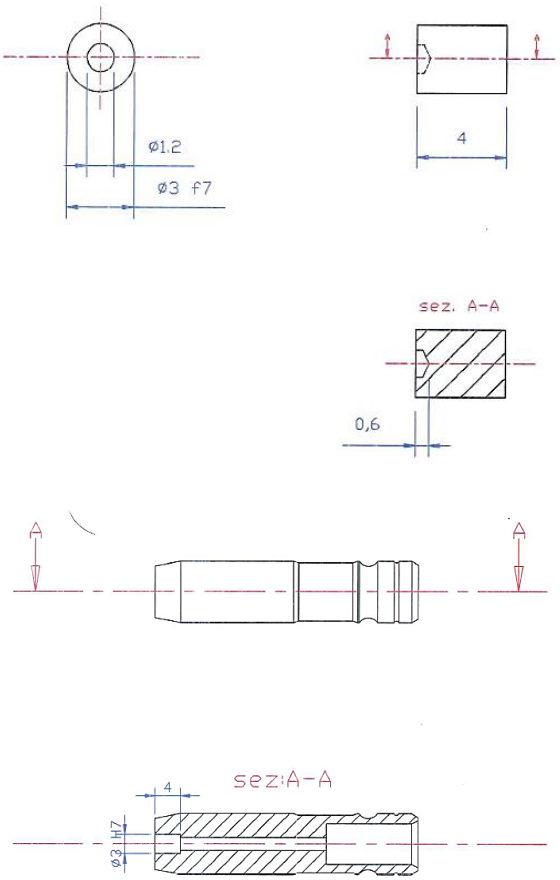

Figure 2. 5 Technical drawing of the Cu inserts and the modified aluminium holder.

Iron is directly pressed into these inserts and then they are introduced into the quartz tube of the reactor. During the graphitization reaction, the graphite deposits directly on the iron pressed onto the Cu inserts. After the reaction has finished, the Cu inserts are

mounted into the aluminium holders, which are properly modified to fit them (see Figure 2.6). In this way, the possible mass loss, that may occur when transferring the powder from the reactor to the aluminium holder, is minimized.

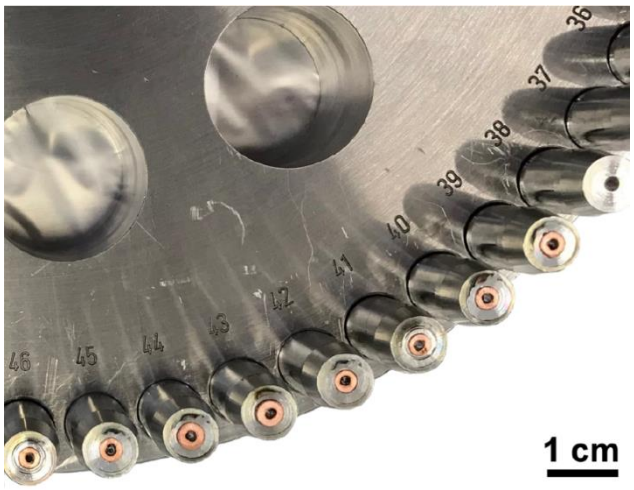

Figure 2. 6 The aluminium holders allocated into the carrousel of the ion source of the accelerator: Cu inserts used for small samples graphitization are mounted into the "traditional" holders, which have been modified on purpose (as comparison, on the right, position 38, a traditional graphite pellet can be seen).

2.3 Working with the new graphitization reactors

Before the application of the new experimental set-up, we decided to test the reactors, preparing standards, blank samples and internal standards with certified radiocarbon concentrations. These tests were necessary to understand if the configuration of reactor-oven-cooling device worked, which its limits might be and how much sample mass we needed to obtain our goal, i.e. about 50 µg of graphite at the end of the reaction.

In the typical set-up used for the "big" samples, we observed that in order to obtain 600-700 µg of graphite at the end of the reaction, we needed to collect about 270 mbar of CO_2, as described in paragraph 1.3.1. Considering the yield of the graphitization reaction non-dependant from the amount of initial CO_2, a simple calculation can be used to estimate the CO_2 suitable for our goal: we decided to collect 100 mbar (which would

correspond to 25 mbar in the big reactors).

In Table 2.2, the comparison between typical sample masses that are burnt in the big reactors and those burnt in the new small ones are shown.

Material	Sample mass for the big reactors (mg)	Sample mass for the new small reactors (mg)
Oxalic acid	4.5	0.6
Cyclohexanone 2,4 DNPH	1.5	0.2
Charcoal	1.3	0.2
Collagen	2.0	0.4

Table 2. 2 For some of the materials usually treated in our laboratory, comparison between the typical sample masses that are burnt for graphitization in the big reactors and those burnt to be graphitised in the new small reactors. Regarding the Oxalic acid, this material is highly hygroscopic: the reported mass should be intended as the sum of oxalic acid itself and the absorbed water from the environment.

The reported masses for the small reactors correspond to the above-mentioned 100 mbar of CO_2 measured in the reactor, or, in other words, to about 50 µg of C at the end of the reaction. If we compare this mass to the typical graphite masses obtained in the big reactors, actually we can notice a loss in efficiency of the overall combustion-graphitization process. In fact, while for the big reactors we can estimate an efficiency of about 85%, for the small reactors, this efficiency is lower, about 50%. This discrepancy is likely to be connected to the sample combustion in the elemental analyser. As described in paragraph 1.3.1, the produced CO_2 is transferred into the graphitization line by manually switching a connection valve when the carbon dioxide is starting to flow out of the EA. This is done by an operator when the gas signal starts being distinguishable from the background. When a small sample is combusted, the peak-to-background ratio is clearly lower than when burning a large mass; thus, we can hypothesize that, in this case, even a tiny variation of the switching moment can produce a relevant variation of the selected amount of gas.

Another aspect we observed is about the non-reproducible behaviour of the

graphitization reactions (see Figure 2.7): most of them had very different durations, even though they started from the same amount of collected CO_2 and added H_2.

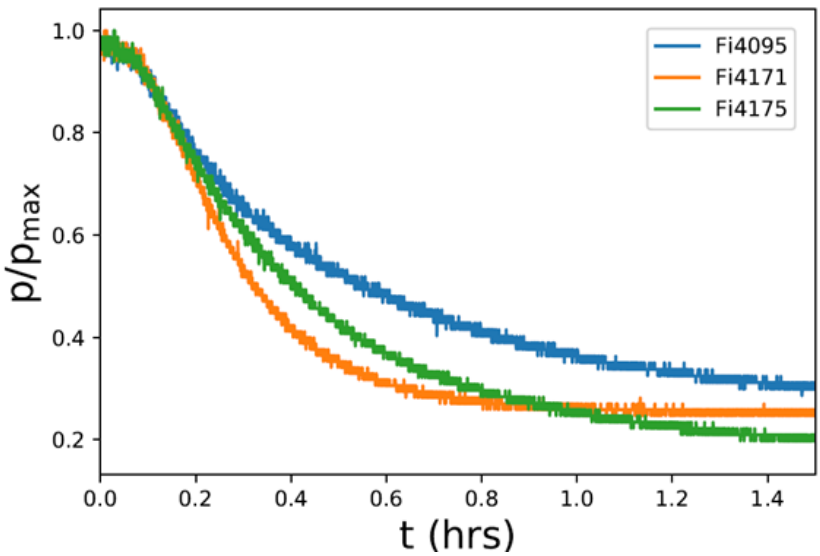

Figure 2. 7 Comparison of the different graphitization behaviours in samples Fi4095, Fi4151 and Fi4171 (NIST Oxalic acid II). It is clear how the trend of the reactions is very different one from the other.

We identified the cause of this behaviour in the different compactness of the iron catalyst pressed in the Cu supports: the stronger the iron was pressed, the smaller was the overall surface of the catalyst which is exposed to the external environment, thus the longer takes the reaction. The non-uniformity in the compactness of the iron obviously derived from the method used to press the iron: pressing was performed "by hand" using a hammer and home-designed pressing tools. However, it is clear that using the hammer didn't allow us to control the strength used in the operation.

With the purpose to make the pressing process as reproducible as possible, we re-design the pressing tools and replaced the hammer with a mini pellet press, usually used for pressing KBr pellets in FTIR analysis (Figure 2.8).

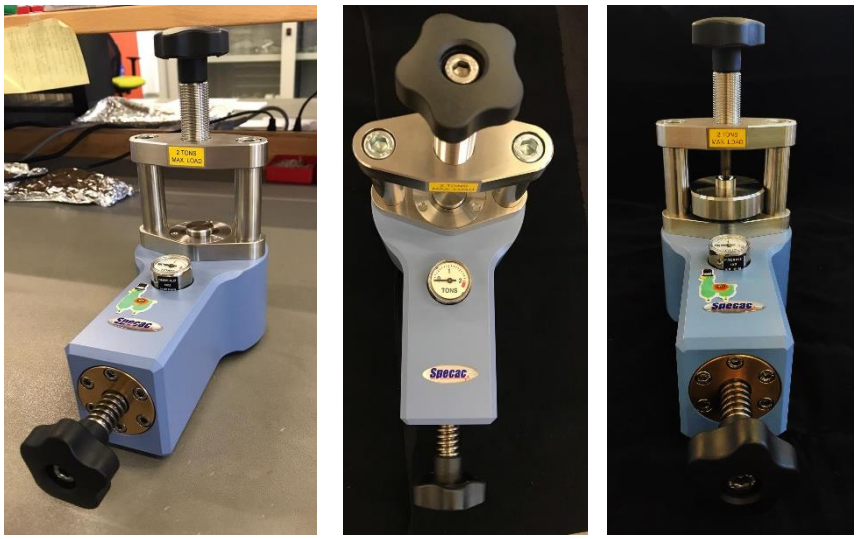

Figure 2. 8 The mini pellets press used to press the iron catalyst into the Cu inserts of the small samples.

Using the pellet press allowed us to better control the pressing strength, therefore having more uniform behaviours and durations of the graphitization process, as shown in Figure 2.9.

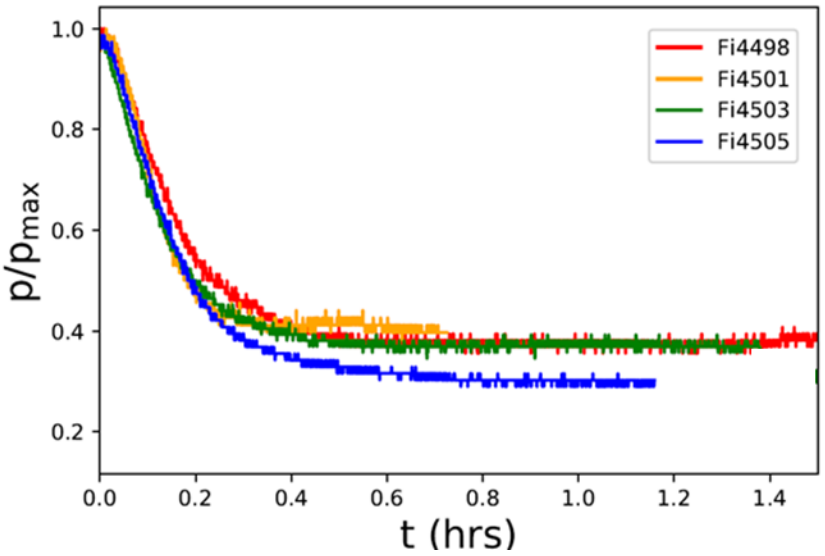

Figure 2. 9 Comparison of graphitization behaviours of samples Fi4498, Fi4501, Fi4503 and Fi4505 (NIST Oxalic acid II). A more uniform trend can be seen.

Moreover, we observed that reactions were faster (Figure 2.10). When using the hammer, reactions were pretty slow and didn't finish until one or two hours passed (some of them took even longer), while, when using the pellet press, all the reactions were basically completed after 20-30 minutes.

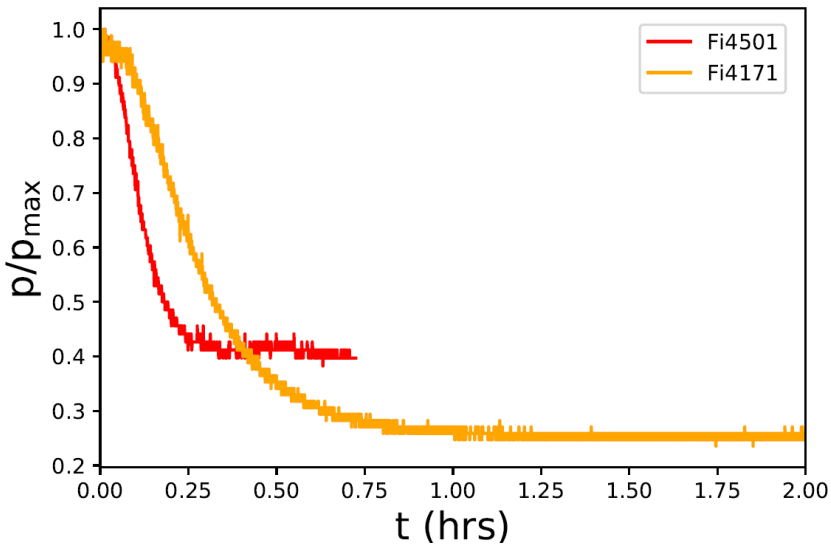

Figure 2. 10 Comparison between graphitization behaviours of samples Fi4501 (mini pellet press) and Fi4171 (hammer. We can observe how much the first reaction is faster.

However, we noticed that the faster reactions had higher gas residues, losing a bit of efficiency with respect to the slow reactions. We hypothesize that even this effect is correlated to the way the iron is pressed into the Cu inserts: pressing the iron by the hammer, we may expect that its distribution is not uniform or flat, but instead more "globular"; in this way, more iron surface may be available during the graphitization reaction, hence the efficiency of the reaction may be higher. Instead, if we press the iron using the mini pellet press, we expect a uniform, flat distribution of the iron into the Cu inserts: in this way, less iron surface would be available, but the graphite would deposit more uniformly onto the catalyst.

Having more uniform reactions, hence more uniform graphite pellets, is important for the following AMS measurement: in this way, we will have more uniform ion currents

extracted from the samples, thus having more precise measurements, as explained in further details in Chapter 3.

Chapter 3: AMS upgrades

3.1 Optimization of the beam measurements conditions

As far as the AMS measurements are concerned, when dealing with smaller size graphite samples, one of the key issues is to “preserve” the sample during the measurement so as to collect the needed statistics at the end. As explained in paragraph 1.4.1, the sputtering process to extract the ion beam implies the progressive consumption of the graphite pellet, so, if our sample is already small, we risk to consume it all without being able to consider our measurement as reliable. Thus, probably even more than in routine measurements of typical large samples, we have to pay attention to the efficiency of beam extraction from the sputtering source and of course to the beam transport as well as to the stability of the beam itself during the whole run period. With reference to the experimental set-up described in paragraph 1.2, the optimization of the measurements and the necessary upgrades are discussed in the following.

A satisfying beam extraction can be achieved exploiting the possibility to adjust the sputtering positions with respect to the centre of the source optical axis, in order to minimize the possibility to sputter on copper inserts. To check the relative position of the graphite pellet with respect to the system centre, we measured the extracted currents while scanning the sputtering positions on the horizontal (X) and vertical (Y) directions. For these measurements, for convenience, we used a large sample graphite pellet. In Figure 3.1 and 3.2, the measured extracted currents are reported versus the scanned positions on the X and Y directions, respectively. In both the directions, we can observe a sort of flat-top distribution of current, corresponding the diameter of the large graphite pellet (2 mm). With respect to the centre of pellet, the diameter of the graphite microsamples, about 1.2 mm, is indicated with the red lines in the Figures: we chose the new sputtering positions inside those ranges. Since the good intervals are very limited, we selected 5 sputtering positions for the analysis instead of the typical 9 positions used for larger samples.

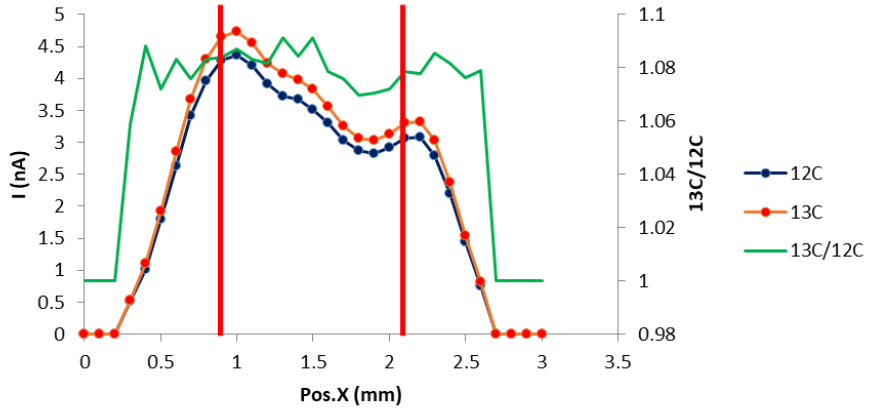

Figure 3. 1 Measured extracted currents while scanning on the X directions. The X position range selected to choose the sputtering positions is highlighted in red.

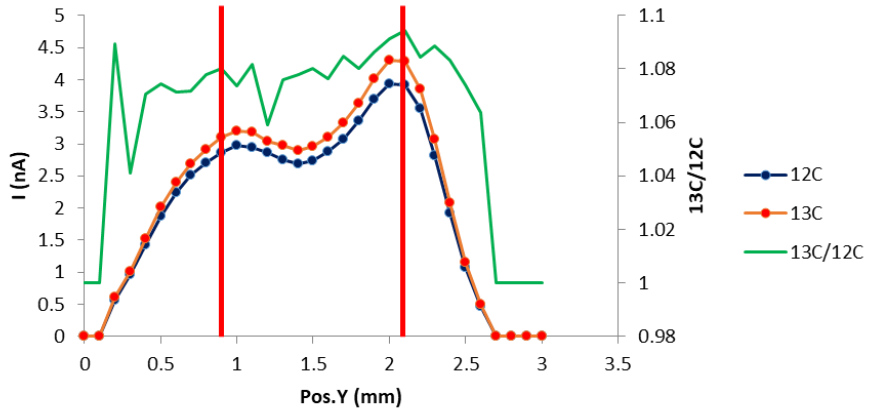

Figure 3. 2 Measured extracted currents while scanning on the Y directions. The Y position range selected to choose the sputtering positions is highlighted in red.

Considering the overall beam currents measured just after the first electrostatic analyser (see Figure 1.3), typical values extracted from 50 µg graphite pellets are of the order of 10 µA.

As mentioned in paragraph 1.4.1, another crucial point is represented by the stability of the best beam transport condition over time. In our set-up, this is achieved by an active feedback on the accelerator terminal voltage. This feedback is driven by the ^{13}C current measurement on the high energy side, after the exit of the analysing magnet.

The dedicated Faraday cup consists of two adjacent slits: the sum of the currents read on each of the slits gives us the total ^{13}C current, i.e. the amount of ^{13}C ions. Otherwise, the difference between the two currents gives us the information about the centring of the particles with respect to the beam axis. When this signal moves from zero, i.e. when the beam moves from the centred trajectory, it triggers the feedback system that slightly modifies the accelerator terminal voltage to account for this change, modifying the final energy of the analysed particles and thus correcting back the direction of the beam inside the magnet chamber. It is thus evident that a precise and accurate measurement of stable isotopes currents is fundamental not only for the isotopic ratios themselves (which are necessary for data analysis, as explained in Appendix B), but also to guarantee the stability of the beam trajectory during the whole duration of the beam run.

The measurement range of Faraday cups depends on the characteristics of the current-to-voltage converter used to collect the signal. Thus, in case we measure a current much lower than the typical currents for which the system is optimized, we may expect to reach the detection limit of the instrumentation, losing the reliability of the of the currents measurement.

In order to avoid any possible and more expensive upgrade of electronics, we chose to optimize bouncer injection times of the three different carbon masses into the accelerator. New injection times were chosen with the aim at balancing the clear necessity to acquire as much as ^{14}C counts as possible in each injection cycle with the requirement to increase the “instantaneous” stable isotopes currents acquired by the high energy Faraday cups (keeping them in the order of few nA, as when we measure larger mass samples). In particular, the selected injection times are:

- Mass 14: 8.5 ms.
- Mass 13: 1.8 ms.
- Mass 12: 0.018 ms.

As already explained in paragraph 1.2.1, in the final part of the beam line, the beam current is too low to monitor its transport using Faraday cups. The optimization of beam

transport is yet even more important when measuring microsamples and dealing with lower currents. A further control on the ion beam position would be needed. For this reason, we installed a new silicon photodiode detector (5 × 5 cm^2, 300 µm thickness) on the high energy side, at the end of the beam line after our final selection element, the electrostatic analyser [19] (Figure 3.3).

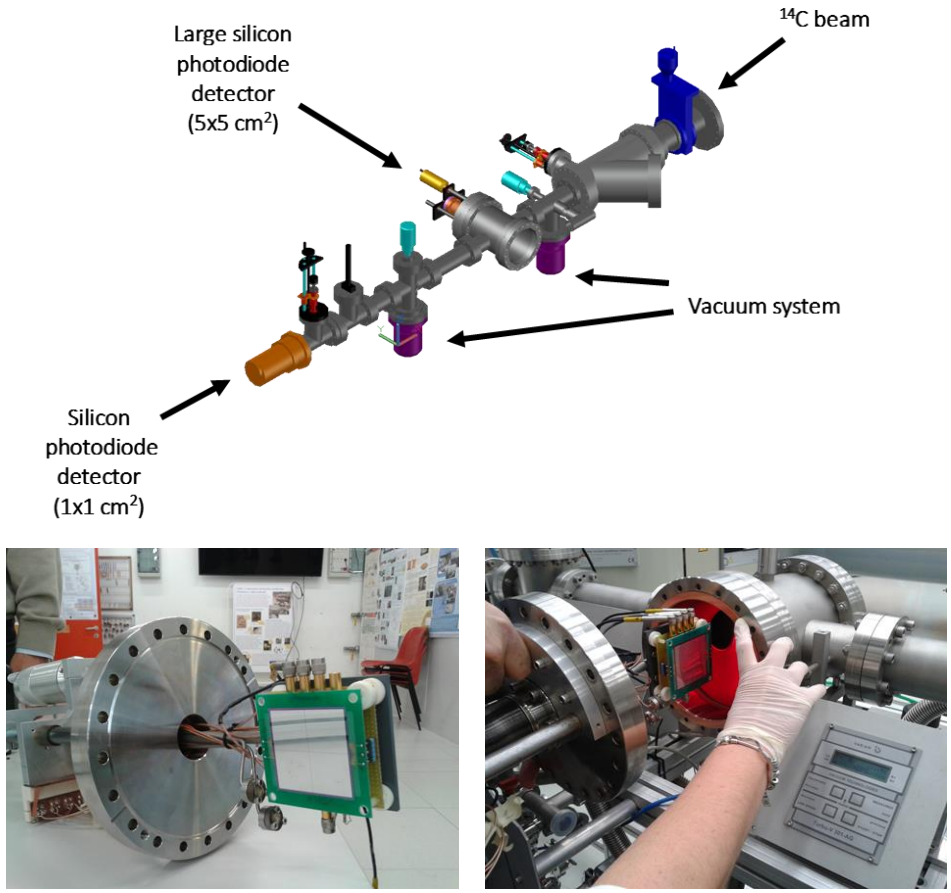

Figure 3. 3 Schematic representation of the final part of the AMS beam line and photos of the detector during the installation.

The detector is mounted on an extractable arm, which allows us to only insert it when needed during the beam transport optimization.

This silicon photodiode detector is divided into four sectors: each of the four

independently acquires the signals (i.e. the ^{14}C counts) and returns a spectrum; the sum of the counts in the four spectra gives us the total amount of the acquired ^{14}C ions, while their subtraction or comparison allows us to check the beam transversal position with respect to the optical axis of the accelerator beam line.

As an example, Figure 3.4 shows a schematic representation of the new silicon detector and its functioning. In the case shown in the upper part of the figure, it is possible to notice that particle beam has drifted too much on the left, since only sector A and C registered counts due to 14C in the spectra; in the lower part, after the re-tuning, the beam looks much more centred and it is possible to detect ^{14}C counts on all the four spectra.

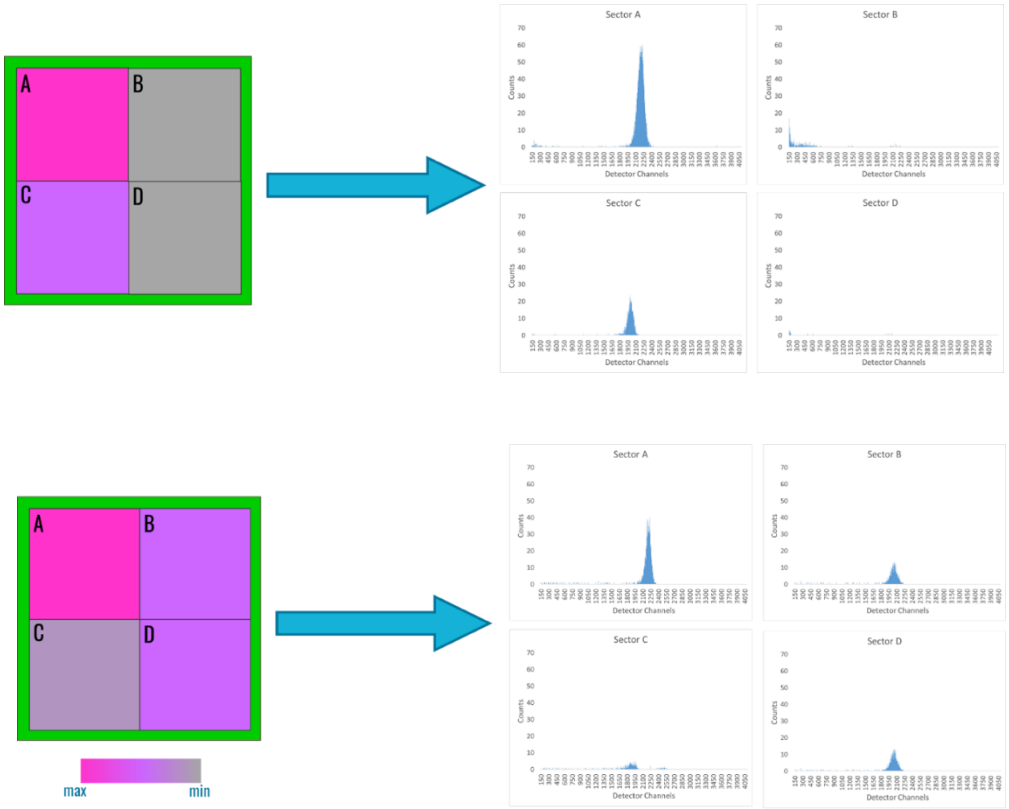

Figure 3. 4 Schematic representation of the four sectors silicon photodiode detector and how it works.

Therefore, the use of this new detector provides us an additional feedback for the

position of the beam, allowing for a better beam transport and thus a better control on the possible counts loss during the beam run.

3.2 Testing the new set-up

In order to check the reliability of the new experimental set-up and the new measurements conditions, described in the paragraphs above, we performed AMS test beam runs: during these tests, we measured standard samples and blank samples. In particular:

- NIST Oxalic acid II, called "primary standard", with a certified radiocarbon concentration, to verify the reproducibility of the measurement during the beam run;
- Cyclohexanone 2,4 DNPH, called "blank", with a nominal null ^{14}C concentration, to evaluate the background;
- IAEA C7 (oxalic acid) and C2 (travertine), called "internal secondary standards", with a certified radiocarbon concentration, used to verify the accuracy of the measurements.

3.2.1 Verifying extracted currents, precision and background

In Figure 3.5, the ^{12}C currents[7] extracted from NIST Oxalic acid II samples and measured on the high energy side of the Tandem accelerator are shown. Figure 3.5 (A) shows the currents of pellets pressed using the hammer (see paragraph 2.3), while Figure 3.5 (B) shows the ^{12}C currents of those pellets prepared using the mini pellet press. Currents are shown versus what we call number of repetitions. In fact, each sample into the source is sputtered for a short period of the order of few minutes, after which the following sample is in turn inserted into the sputtering position and measured. Once the last pellet mounted into the carrousel has been measured, the measurement starts again with the first sample in the queue. Several repetitions are

[7] The extracted currents are normalized to the whole duration of an injection cycle.

performed until the needed statistics is achieved for each of the samples. In Figure 3.5, each point represents the average ^{12}C current for each repetition.

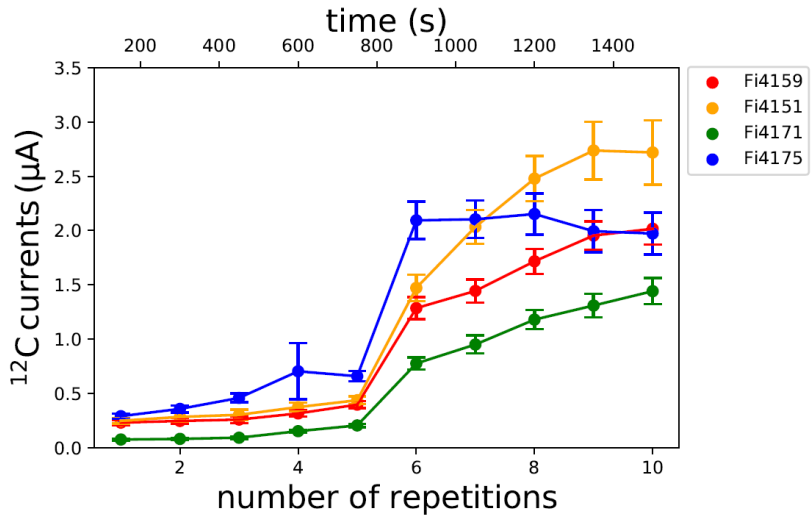

(a)

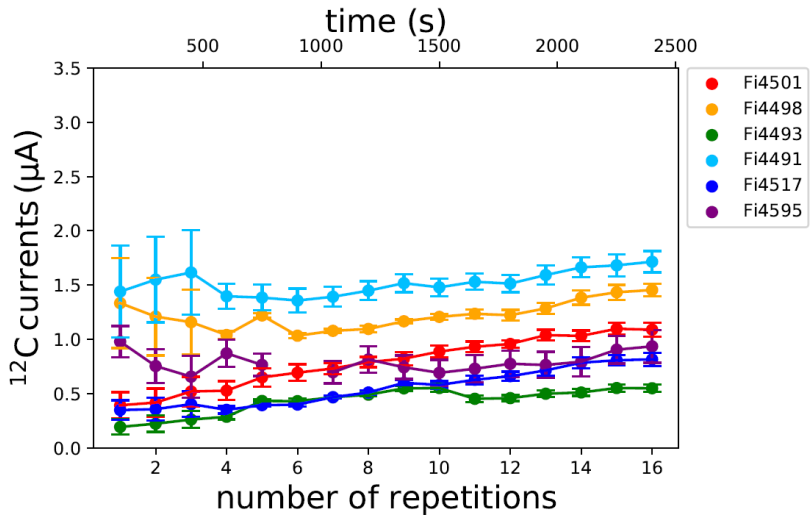

(b)

Figure 3. 5 ^{12}C currents measured on the high energy side of the Tandem accelerator for NIST Oxalic Acid II samples pressed using the hammer (a) and the mini pellet press (b). Currents are reported as normalised to the overall duration of each injection cycle.

^{12}C currents for the hammer-pressed samples show a peculiar behaviour: they start

increasing as the number of repetitions increased, reaching pretty stable values, as average, basically around the tenth turn.

The press-pressed samples, instead, show a much uniform trend: even though these currents never reach the maximum values of the previous samples, they are very stable, with a slightly increasing trend as the repetitions continue.

However, for both these sets of samples (hammer-pressed and press-pressed), the acquired currents after all the repetitions (each lasting for 150 s) suggest that such samples can be measured for more than this number of turns, with the obvious consequence of possibly improving the ^{14}C statistics and thus the AMS measurement precision.

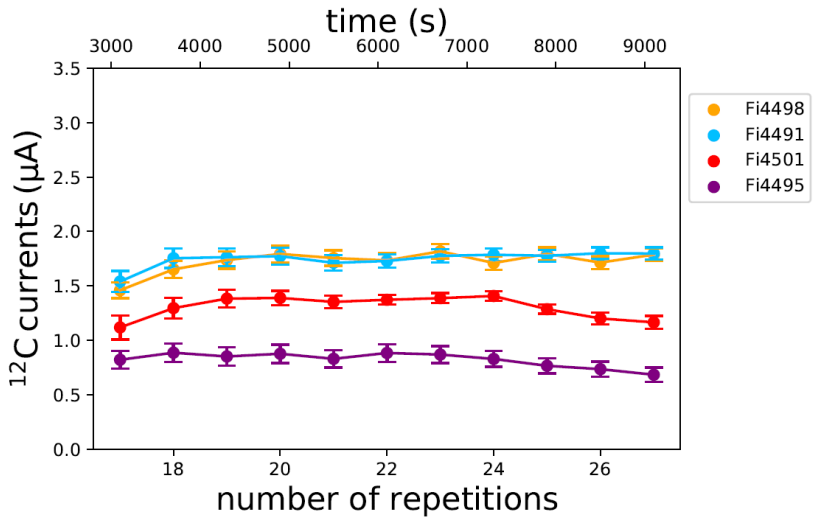

Figure 3. 6 ^{12}C currents measured on the high energy side of the Tandem accelerator for NIST Oxalic Acid II samples pressed using the mini pellet press; the repetitions acquired after those shown in Figure 3.5 B are shown.

Since the measured ^{12}C currents were promising, we decided to test the sample endurance to sputtering. In Figure 3.6, the ^{12}C currents measured after the 16th repetition (with reference to Figure 3.5 B) are shown. As we can see, the measured

currents continued to be stable even if stressed until the 27th repetition[8]. Hence, our samples may last even over 2 hours and half, which is a very satisfying result, considering that the average measuring time of a sample is usually around 1 hour – 1 hour and a half.

In Figure 3.7, the $^{14}C/^{12}C$ raw ratios measured in three different sets of standard samples are shown. Each graph refers to a separate beam run and shows the average ratios as measured after the several repetitions performed, as for example shown above in Figure 3.5. Inside each beam run, the concentrations measured are in satisfying agreement one with another, suggesting a good reproducibility of the measurements.

Interesting indications also came from blank samples. As expected (see paragraph 1.4.1), we obtained $^{14}C/^{12}C$ values larger than in our routine AMS measurements, meaning a background that is slightly worse than usual. In fact, in these conditions, possible modern contaminations become more critical and particular care has to be taken when handling samples. These effects can be minimized and the background can be improved by using a laminar flow box during the process of preparing the samples. In particular, we chose to work under a laminar flow box to press the iron powder into the Cu inserts and, after graphitization, to mount them into the aluminium supports before setting them into the source. In Figure 3.8, we can notice to which extent working in these conditions has indeed contributed to improve our process background. $^{14}C/^{12}C$ isotopic ratios were corrected for isotopic fractionation, exploiting $^{13}C/^{12}C$ ratios measured along the AMS beam line and normalized to a set of standard samples prepared and measured within the same beam run.

[8] It has to be noticed that after the 16th repetition, each repetition was 600 seconds long, not 150.

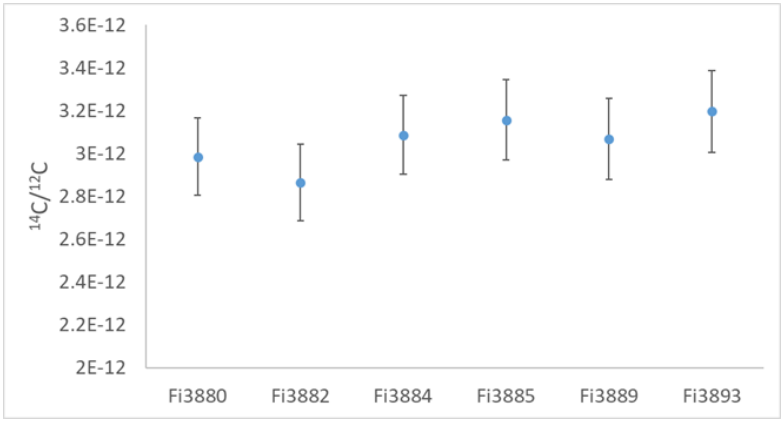

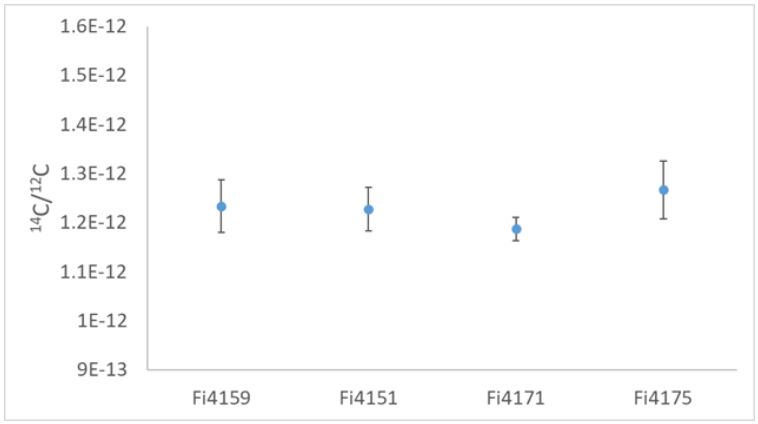

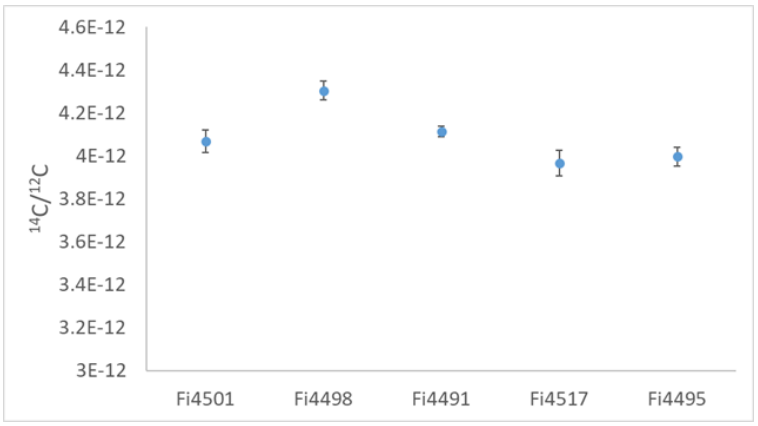

Figure 3. 7 $^{14}C/^{12}C$ isotopic ratios as averaged over the whole acquired repetitions, samples prepared from NIST Oxalic Acid II standard reference material. Each graphic represents the ^{14}C concentrations measured in a beam run.

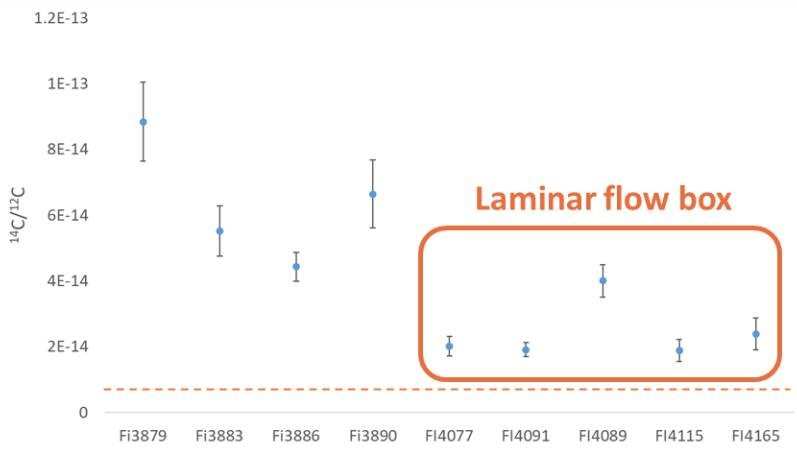

Figure 3. 8 ^{14}C concentrations measured for some blank samples.

3.2.2 Verifying the achievable accuracy

To verify the accuracy of the overall process, the measured radiocarbon concentrations of IAEA C7 and IAEA C2 samples are reported in Table 3.1, together with the certified radiocarbon concentrations. Concentrations are reported as percent of Modern Carbon (pMC, see Appendix B for further details). The shown data were obtained by correcting the measured $^{14}C/^{12}C$ isotopic ratios according to background counts and isotopic fractionation, considering $^{13}C/^{12}C$ also measured using the accelerator, and by normalizing them to the ratio measured for standards.

The measured concentrations are in good agreement with the certified ones, proving our measurements to be accurate.

In addition to the aforementioned internal secondary standards, that helped us to verify the reliability of our measurements, further tests were performed analysing unknown samples which were already measured with the typical experimental set-up for large samples.

Material	Lab Code	^{14}C conc. (pMC)	Certified conc. (pMC)
IAEA C7 (Oxalic Acid)	Fi3881	49.40 ± 0.96	49.53 ± 0.12
	Fi3887	48.39 ± 0.92	
	Fi4083	49.37 ± 0.49	
	Fi4092	48.43 ± 0.38	
	Fi4494	49.50 ± 0.71	
	Fi4502	50.18 ± 0.87	
IAEA C2 (Travertine)	Fi4152	40.7 ± 1.1	41.14 ± 0.03
	Fi4507	41.50 ± 0.78	
	Fi4513	41.69 ± 0.99	

Table 3. 1 Radiocarbon concentrations measured for some samples prepared from IAEA standard reference materials: IAEA C7 is oxalic acid, IAEA C2 is travertine.

In the context of a restoration campaign conducted by the "Museo Egizio" of Turin, we had the possibility to date a wide set of samples, consisting in more than fifty animal mummies. From this set, using the small samples set-up, we prepared and dated two samples:

- C.2353/11: we had already dated it with the typical experimental set-up, thus it represents a sort of "control" sample for our new experimental set-up;
- C.2350/6: its mass after the pre-treatment was insufficient for the typical samples analysis.

Table 3.2 shows the measured radiocarbon concentrations. The two fractions of C.2353/11, the "typical" sample (lab code Fi3607) and the "micro" sample (lab code Fi4503), are consistent one with another, suggesting that our set-up is reliable. This result supports the accuracy of the measurement of C.2550/6. It is worth noticing that, considering its bad preservation state and the small amount of the recovered material at the end of the pre-treatment, without the set-up optimized for small masses, the

dating of this sample would have not been possible otherwise.

Samples	Lab code	^{14}C conc. (pMC)
C.2353/11	Fi3607	75.71 ± 0.43
	Fi4503	75.3 ± 1.0
C.2350/6	Fi4506	75.84 ± 0.70

Table 3. 2 Measured radiocarbon concentrations of the samples from the mummies set of the "Museo Egizio" of Turin. Sample Fi3607 was prepared using the typical samples set-up, while Fi4503 and Fi4506 were prepared.

Sample	Lab code	14C conc (pMC)
Burial_6	Fi3107	80.1 ± 1.8
	Fi4502	80.6 ± 1.4

Table 3. 3 Measured radiocarbon concentrations of the samples from the Uffizi museum archaeological excavation. Sample Fi3107 was prepared using the typical set-up while sample Fi4502 was prepared using the microsample set-up.

Another case in which the comparison between the typical set-up and the microsample set-up has been possible was the study of an archaeological excavation in the area of the Uffizi museum, in Florence. In this context, different burial grounds were analysed and a set of bone samples was measured, using the typical set-up. Samples were all dated around the second half of the IV century CE. The collagen extracted from the sample labelled as Burial_6 was dated using both our typical set-up for big samples (lab code Fi3107) and the new one (lab code Fi4502). A precision is worth to be done about Fi3107. Actually, this sample gave a very low yield of datable material (bone collagen), so that we were able to collect a CO_2 pressure that was lower than the typical amount of CO_2. Dating this sample with the typical set-up implied a low precision of the measurement (see Table 3.3). When the new set-up for microgram samples was ready, we prepared another fraction of Burial_6: Fi4502 was consistent with Fi3107, and the precision was even slightly better. This is a very satisfying result, considering that we

can expect that microsample measurements have a slightly worse precision (with respect to typical masses samples) due to lower statistics. In this case, then, we can say that, when the amount of mass is too low for the typical set-up, using the microsample set-up is preferable, since, as shown in this case, it can provide a more precise result.

3.3 Summary of the experimental set-up upgrades

To conclude this part of the thesis about the experimental set-up and move on to the different applications we studied during this project, I wanted to briefly summarise what discussed until now.

The purpose of this project is to reduce the required mass for radiocarbon measurements down to about 50 µg of graphite. This can be particularly useful especially when dealing with Cultural Heritage application, where minimising the invasiveness of the analysis is of fundamental importance.

The already existing sample preparation experimental set-up has been upgraded and optimized. In particular, new small graphitization reactor, together with smaller ovens and Peltier cooling systems, have been designed to solve those problems related to the too big volumes of the reactors and the possible trigger of the reactions. Moreover, in order to limit the mass losses during the pre-treatment, new Cu inserts have been designed: the iron catalyst for the reaction is pressed into these inserts and the graphite deposits directly on them.

As for the AMS measurements, the beam transport has been optimized for the small samples and their low currents and a new silicon photodiode detector has been installed to have a better control on the position of the beam, thus avoiding the loss of ^{14}C counts during the measurements. In this way, the samples are preserved as much as possible, until we gain enough statistics for reliable results. The test performed on different standards have given encouraging results: reproducibility, background, attainable precision and accuracy have been measured to be satisfying.

In the next chapters, two new possible applications of the new experimental set-up will be described in details.

Chapter 4: Radiocarbon dating of mortars

4.1 Mortars: definitions and components

Mortars are among the oldest man-made products, used since ancient times as a binding media to construct buildings or walls: these materials have the characteristic of hardening, becoming a strong, resistant and cohesive material, which keeps together bricks and/or stones, improving the duration of the wall structure over time [20] [21]. Their earliest use is attested in archaeological sites in Palestine and Turkey dated back to 12000 BCE [22]; other evidences can be found in the Kuni island (French Polynesia 11000 BCE), Syria (4250 BCE) [23], China (2000 BCE) [24], Ancient Egypt (1400 – 1200 BCE) [25]. With the Greeks and later the Romans (since 1st millennium BCE), the use of mortars was improved and effectively implemented in wall structures and buildings [26]. Moreover, the first attested documents with recipes and instructions about the composition and the use of mortars date back to this period: the most famous and important one is "*De Architectura*" by the Roman author Vitruvius (25 BCE) [27].

Generally, mortars are made up by a binder, which can harden in specific conditions, some aggregates, as e.g. sand or other minerals that are mixed with the material later evolving into the binder and that are added to avoid the excessive shrinking of the binder itself, water and possible additives, which are added to improve the characteristics of the mortar. Especially in ancient times, the materials used to produce a mortar varied depending on the availability of the raw materials in the surroundings; as a result, we now deal with a vast variability of materials, made up by different constituents and characterized by different properties, so that generally speaking about "mortars" is often not enough to understand the particular situation we are analysing.

For this reason, a specific legislature exists, given by the Italian National Unification (UNI, Ente Nazionale Italiano di Unificazione[9]), to better define the materials and the

[9] The Italian National Unification is a private non-profit association that performs regulatory activities in Italy, especially for industrial, commercial and service sectors. Speaking about mortars, the legislature is written in the document UNI 10924 (2001), which regards the specific

characteristics of mortars. Considering the different type of mortars that can be produced, different classifications exist, depending on the composition, on the function or on the collocation inside the wall structure. In particular, the classification according to the composition of the mortar is in turn divided on the basis of the type of binder, the type of aggregates or the type of additives used.

For the application I'm going to present in this chapter, the most useful classification is the one based on the nature of the binder. We can distinguish:

- Non-hydraulic mortars: produced by mixing together an aerial binder, such as lime ($Ca(OH)_2$), aggregates (usually in a 1:2 or 1:3 ratio with respect to the binder) and water, in such a proportion to make the mixture plastic and malleable. These mortars harden reacting with the CO_2 present in the air giving a matrix of $CaCO_3$, as a result. These mortars are the most used mortars in ancient times;
- Naturally hydraulic mortars: made of a hydraulic binder, which is lime that naturally contains clay or other impurities. These impurities give the mortar the property of hardening in humid environment, even underwater;
- Gypsum mortars: obtained mixing gypsum powder with water. Their hardening process is really fast and it is due to the water evaporation and the consequent formation of gypsum crystals;
- Bastard mortars: produced when different binders are mixed together in different proportion, depending on the use. Usually they are used to improve the hardening process or the properties of the mortar itself, or to lower the price of the material;
- Concrete: produced since ancient times by mixing lime, stones and Pozzolana, which is a fine, sandy volcanic ash. The use of this particular ash gives the binder hydraulic properties.

Considering the different types of mortars and the principles radiocarbon dating

classifications and terminology to use when referring to mortars.

method is based on (see Chapter 1), it is clear that the type of mortar that is more suitable for the dating is, in fact, the non-hydraulic mortar, since it is the only one that involves the atmospheric CO_2 in its hardening process, as shown in the following paragraph.

4.1.1 Non-hydraulic mortars

Non-hydraulic mortars are produced mixing an aerial binder, aggregates and water, in proportion suitable for the type of use: in particular, the volumetric proportion 1:3 (binder: aggregates) has been pointed out as reference, because it was indicated by Vitruvius in his work [28]

Among the aerial binders, air lime was the most widespread and used in the Mediterranean basin, mostly by the Greeks and the Romans.

Air lime is produced starting from limestone. Limestone is a sedimentary rock composed mainly of calcium carbonate ($CaCO_3$) with possible magnesium carbonate impurities. It is formed by the deposition either of the skeletons of small creatures and/or plants (organic limestone), by chemical precipitation, or by deposition of fragments of limestone rock on the beds of seas and lakes [29]. Usually, the most "pure" carbonates, with a calcium carbonate content of almost 95%, are chosen to produce the mortar.

In Figure 4.1, the process to produce an air lime mortar is shown. Limestone is crushed and heated at a temperature above 900°C: this first step is called calcination and involves the dissociation of $CaCO_3$ in CaO and gaseous CO_2 (see reaction 4.1).

$$CaCO_3 \xrightarrow{850-900°C} CaO + CO_2 \uparrow \tag{4.1}$$

The product of reaction 4.1 is a fine grained porous calcium oxide, with enough exposed surface to correctly perform the successive steps of hydration and setting of the mortar [30].

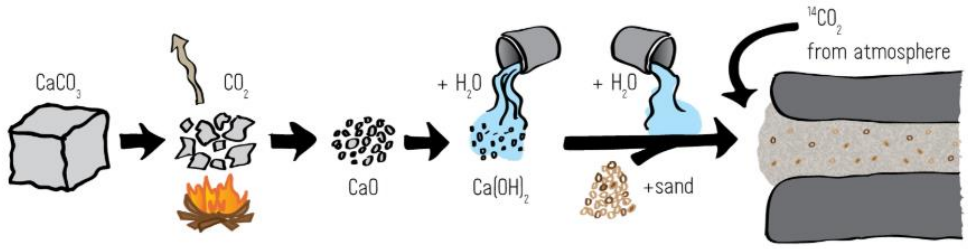

Figure 4. 1 Schematic representation of the production process of an aerial lime mortar [31].

Calcination proceeds from the outer surface of the limestone fragments inwards and gets as slow as the more compact the material is. In case of more porous stones, the CO_2 dissociates more rapidly, producing a very porous CaO. Instead, if the CO_2 stays in contact with the CaO crystals, it favours their growth, giving a product which will be more compact hence less reactive. Obviously, the size of the stones put into the oven for the calcination is also important: if the fragments are too big, the dissociation of the carbon dioxide will be difficult, causing a very slow calcination reaction with a less reactive CaO.

The degree of calcination is affected by the temperature at which the process is performed. Calcite ($CaCO_3$) typically dissociates into CO_2 at 898°C at the pressure of 1 atmosphere [32]. To ensure a complete calcination, even for bigger fragments, the temperature can be increased above 1100°C; however, exposing the material at too high temperatures for too long favours the growth of the CaO crystals (see above), and therefore it should be avoided.

Another important factor that must be taken into account is the possible non-dispersion of the CO_2 produced during the reaction: this may react again with the newly formed CaO crystals, producing $CaCO_3$ lumps. These $CaCO_3$ lumps, as well as possible "uncooked" limestone fragments, may represent a critical issue for the radiocarbon dating, as explained in the following paragraphs.

The CaO produced by calcination is called "quicklime" and it cannot be used as it is as a binder. Quicklime must be hydrated, so as to form a plastic material, easy to work with and with the property of harden in air. The hydration process is called "slaking" and

follows reaction 4.2:

$$CaO + H_2O \rightarrow Ca(OH)_2 \quad (4.2)$$

The slaking reaction is highly exothermic and water is generally added in excess, since most of it will evaporate during the reaction due to the reached high temperature. Nevertheless, at the end of the reaction, a part of water remains as a thin film around the $Ca(OH)_2$ particles, now called "slaked lime" or lime putty[10] [33].

The lime putty looks like a white, plastic paste. From the chemical-physical point of view, it is a calcium hydroxide suspension in water, with a peculiar thixotropic behaviour [34]. Traditionally, the lime putty was let aging under water for a period of 6 to even more than 24 months: the aging changes the crystal habit of the $Ca(OH)_2$ crystals, thus improving the mechanical properties of the future mortar.

Once they are used in the structure, air lime mortars set through the so-called carbonation process (see equation 4.3):

$$Ca(OH)_2 + CO_2 + H_2O \rightarrow CaCO_3 + 2H_2O \quad (4.3)$$

Actually, the entire hardening process occurs in different steps [35]:

- initial hardening due the evaporation of water inside the lime putty;
- diffusion of gaseous CO_2 through the pores of the mortar;
- dissolution of the CO_2 in the pore water;
- dissolution of the $Ca(OH)_2$ in the pore water;
- solution reaction between $Ca(OH)_2$ and CO_2;
- precipitation of solid $CaCO_3$.

The hardening through drying can be relatively fast, from few hours to few days,

[10] Actually, different forms of slaked lime can be produced, depending on the amount of water added for the hydration. Lime putty was used as binder for ancient historical mortars. Nowadays, slaked lime is industrially produced and sold as a dry powder.

depending on the environmental conditions. During this phase, loss of plasticity and workability of the material can be observed. The full carbonation, instead, can be a really slow process and it can take even years to complete. The calcium carbonate that forms during this process is called “anthropogenic” carbonate, in contrast to the “geogenic” carbonate that refers to the limestone. Since during carbonation, the atmospheric CO_2 is involved in the reaction, we can hypothesize that a mortar that hardens following this process contains a radiocarbon concentration which is equal to the one in atmosphere at the moment of the hardening (of course isotopic fractionation must be taken into account). After hardening, in principle, no more exchanges between the mortar and the atmosphere occur, hence we can identify the anthropogenic carbonate as a good candidate for radiocarbon dating [36].

4.2 ^{14}C and mortars

As explained in the paragraph above, the aerial lime binder in a non-hydraulic mortar hypothetically meets all the requirements for radiocarbon dating. Besides, the date that would be obtained when dating the binder would be the exact moment of the hardening of the mortar, a moment really close to the setting of the mortar, that is the building of the masonry. In this way, we would be able to date for example a building in an archaeological site, even if no organic samples such as wooden structures (or wooden beam), textile decorations or charcoal residues closely related to the building are found in the site.

What said until now works really well in theory, but many issues arise when it comes to the practice. A brief analysis is discussed in the following.

The application of radiocarbon dating to mortars has been studied since the second half of 1960 [37]. However, since the early days of mortar dating, it has been noticed that different interferences did not allow a reliable measurement of this material [38]. As a matter of fact, if we want to perform the radiocarbon dating of mortars, we must take into account some important factors, which may alter the results of the measurements. In particular:

- We can expect our measurements to be accurate only if the time period between the setting of the mortar and its complete hardening is smaller than the typical experimental error of the radiocarbon measurements (few decades): as explained before, carbonation generally needs from few months to few years to complete. This time range depends on how much difficult "reaching" a part of the masonry is for the CO_2. If, for example, we consider the inner part of a very thick wall, it may take even a hundred of years for the carbonation to be complete [39].
- One of the fundamental principles of radiocarbon dating is that the sample to be dated should be considered as a closed system. For the mortar, this happens right after the complete hardening of the binder, because it is the moment in which the absorption of the atmospheric CO_2 stops. However, this condition is not always respected, since dissolution and consequent recrystallization phenomena may happen due to e.g. water percolation. The recrystallization causes an apparent rejuvenation of the mortar sample.
- When we want to date a sample by radiocarbon, we have to isolate the carbon fraction of interest, avoiding all the possible contaminations. In particular, for the mortars, one of the possible contaminations is the residual uncooked $CaCO_3$ from the calcination process: these residues represent a fossil carbon contamination and will contribute to the apparent aging of the sample. Other possible contaminations are those aggregates which have a carbonate composition: also in this case, we would have a fossil carbonate contamination, with an apparent aging of the mortar sample.

Considering what discussed above, the radiocarbon dating of mortars presents many technical issues and particular care must be taken for both the sampling of the mortar and the pre-treatment.

For instance, a critical aspect is the choice of the area of the masonry in which the sample is collected: we should avoid those parts of the wall that are too exposed to rain water (usually the outer walls of a building) or to capillarity rise water (ground floors).

Moreover, we should avoid those samples which are collected in the deepest part of the wall, since, as said before, we would risk to have a partially carbonated sample, not suitable for the dating.

In order to find the best candidates for the analysis, a mineralogical-petrographical characterization is mandatory: contaminants can be present inside the mortar itself, due to possible carbonate aggregates, that must be removed; moreover, the complete carbonation of the mortar has to be checked, since otherwise the results of the dating would be altered. Even though we followed all the right procedures as for the sampling, there can still be samples which are not suitable for dating due to many factor, such as the "wrong" nature of the binder or too fine-grained aggregates, which are difficult to be removed. All these factors cannot be *a priori* defined and we need to "look inside" our samples thoroughly to find the best candidates and to choose an efficient pre-treatment.

The mineralogical and petrographical knowledge of the sample components is important not only in the choice of the pre-treatment, but also in the interpretation of the results.

For the characterization, different techniques can be used depending on which aspect of the mortar we want to define. In general, these mortars characteristics can be observed:

- the nature of the binder (aerial or hydraulic) and the grain size of the binder matrix;
- the degree of carbonation of the binder;
- the mineral composition of the aggregates, the possible presence of carbonates and their grain size;
- the presence of lumps and their nature (binder lumps or uncooked limestone).

Each characterization technique does not give us full view on the nature of the mortars and usually different techniques, that give complementary information, are used together to obtain the details useful for the dating.

In addition to the preliminary mineralogical-petrographical characterization,

considering the heterogeneity of the material itself and the many different technologies according to which historical mortars were produced in the past, no "standard" procedure to then isolate the binder exists. In fact, the pre-treatment to extract the carbon fraction of interest for the dating is modified and adapted depending on the nature of the binder, the possible presence of carbonate aggregates and their size. Among the possible pre-treatments, two procedures (or combinations of the two [40]) have taken hold in the radiocarbon dating community. In the following paragraphs, they are briefly explained. Both the two procedures have given controversial results and the experiments are still going on.

4.2.1 Sequential dissolution

The so-called sequential dissolution procedure was developed in 1997 [36] and it is based on the observation that the anthropogenic carbonate of the mortar is typically very fine-grained, porous and powdered and that can react very quickly in acid. The geogenic carbonates, instead, are harder and the rate of their reaction with acid is expected to be much slower [41].

For the extraction of the datable fraction, ortophosphoric acid (85% solution in water) is poured over the mortar under vacuum. CO_2 is produced during the reaction between acid and calcium carbonate of the binder:

$$CaCO_3 + H_3PO_4 \rightarrow CaHPO_4 + CO_2 + H_2O \quad (4.4)$$

In theory, the anthropogenic carbonate dissolves much easier and a quicker rate than the geogenic one. Thus, if we collect different fractions of CO_2 at different times of the reaction and we measure the radiocarbon content of each fraction, we can obtain a sort of "age profile" of the sample (Figure 4.2), which should suggest us the nature of the binder and its aggregates and the presence of possible contaminants.

Before the chemical reaction, a first mechanical selection is made: the mortar sample is gently crushed and the powder is sieved through a fine mesh (generally < 75 μm); this

process should break the soft, porous anthropogenic carbonate of the binder, while leaving the harder limestone intact. The fine powder that passes through the mesh is collected and used for the chemical separation.

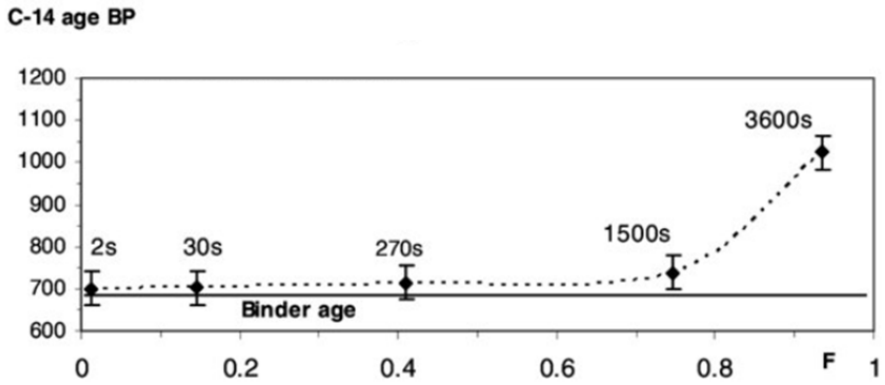

Figure 4. 2 Example of age profile obtained by measuring the ^{14}C concentrations of different CO_2 fractions [42].

These age profiles have been modelled, depending on different criteria, in order to provide guidelines for the interpretation of the results [43]. Following the theory behind this method, the radiocarbon ages of first CO_2 fractions can be associated to the ^{14}C content of the binder, while the ages obtained for the successive fractions are to be linked to the contribution of the aggregates in the dissolution reaction. Generally, when a plateau of ages can be observed in the first fractions, as in Figure 4.2, the ages obtained are more reliable. However, Figure 4.2 represents one of the most ideal cases: very often these age profiles are actually very complicated because many factors can influence the trend of the ages for the sequential CO_2 fractions, such as the presence of very fine-grained carbonate aggregates that would react even faster than the binder. For this reason, in the most recent times, the importance of the characterization of the mortar before the dating has been noticed [40] [44].

4.2.2 The Cryo2Sonic method

As an alternative to the sequential dissolution method, a mechanical separation

method has been proposed [45]. This procedure, called Cryo2Sonic, is based on the mechanical fragmentation of the mortar components and the separation of the binder thanks to the use of an ultrasonic bath: in as mentioned above, the anthropogenic carbonate of the mortar has a fragile structure, much more breakable with respect to the more compact geogenic carbonate. The ultrasonication breaks the crystals of the binder, generating a carbonate suspension with a low sedimentation speed due the very small size of the carbonate particles. The procedure consists in four steps [46] [47]:

- The mortar sample undergoes several thermal shocks, being first immersed in liquid nitrogen and then heated in the oven at 80°C. This cycle is repeated multiple times and finally the sample is gently crushed with a hammer.
- The mortar powder is sieved through a fine mesh (< 100 µm). The smaller the mesh, the more selective this step is. The selected fine powder is then put in a beaker with deionized water and let setting down.
- The beaker is put in an ultrasonic bath for 10 minutes. The generated suspension is collected with a pipette and removed. This suspension is called “sand” and is expected to contain all the fine-grained contaminations, such as the second crystallization carbonates.
- The residue in the beaker is put into the ultrasonic bath again for 30 minutes. During this step, the crystals of the binder will break and will go into suspension. At the end of the sonication, the suspended part is collected, centrifuged and dried at 80°C. This fraction is called “susp” and represents the fraction of interest for the dating measurement.

Compared to the sequential dissolution procedure, the main advantages of this methodology are 1) avoiding the difficulties in handling time-evolved fractions of CO_2 and 2) the limited number of analysis to perform for each mortar sample.

Even for this procedure, however, it has recently been noticed that performing Cryo2Sonic blindly without any previous characterization of the mortar leads to results that are very difficult to interpret, thus the method has been implemented by modifying some steps of the purification protocol and adding a more extensive characterization of

the mortars before and after the purification treatment [48].

4.2.3 Lime lumps: a particular case

The procedures described above are meant to be applied on the mortar samples in bulk, when the material of interest to be collected is just the binder. However, in some particular cases, we can collect a particular component for the mortar: the lime lumps, small binder fragments that can be found in the sample with a whitish colour and a not-defined outline [49]. From a micromorphological point of view, these lumps are composed of very small, well-packed crystals in a compact structure and differ completely from that of the surrounding matrix [50]. Obviously, it is mandatory to distinguish the "real" lime lumps from those fragments of uncooked limestone or overcooked limestone[11], which, in case of dating, would apparently age the mortar. For this reason, even in this case, the characterization is highly suggested so as to avoid possible contaminations.

As far as the radiocarbon context is concerned, lime lumps have been analysed using both the sequential dissolution and the Cryo2Sonic methods [51] [46]. In general, the ^{14}C measurements of lime lumps give more homogeneous results, close to the expected age and easy to interpret. As long as lime lumps deriving from the carbonation of the lime putty are considered, these represent good mortar fractions to date, because they can be considered as lacking of contaminations. However, they should not substitute the analysis of the bulk mortar, instead the two components, lumps and binder, should be coupled together to have a better control on the results.

4.3 Mortar dating at LABEC: experimental set-up and feasibility study

In the context of Cultural Heritage applications, which this thesis is framed with, we expect to have the possibility to analyse mortars from historical buildings. However,

[11] Overcooked limestone fragments are pieces of the original stone used to produce quick lime, that have been left too much at high temperature. These fragments are characterized by a very slow hydration and carbonation and have a dusty aspect with big pores on the inside.

collecting a mortar sample can be very invasive. In fact, dating is just a limited part of all the studies, including mineralogical, petrographical and structural analyses, that can be performed on mortars. Mortar cores of 2-4 cm diameter, 20 cm long are usually collected, but only a small fraction is available for dating. In addition, considering everything that has been discussed above, we have to keep in mind that the pre-treatment to isolate the binder is mandatory: the more selective this pre-treatment is, the higher the chances of having an accurate measurement are. In this case, a selective pre-treatment means using a sieve with a very fine mesh or repeating the ultrasonication multiple times or even select only a very small fraction of CO_2 from the dissolution: in each of the options, the expected mass loss at the end of the process is very high.

In this framework, the new experimental set-up optimized for microsamples appears to be a perfect tool to be used in case of mortar dating. In this way, we would minimise the mass required for the measurements, allowing the use of a more “aggressive” pre-treatment and also the possibility to date lime lumps (usually characterized by very small masses, in the order of few milligrams).

Since in general the sequential dissolution method has proven to be more reliable than the Cryo2Sonic (see the works cited in this chapter), we decided to follow the former approach for the dating of mortars, even though we modified it, selecting only the first fraction of CO_2. In order to do this, an improvement of our experimental set-up has been needed. As a matter of fact, we used to extract the CO_2 from the carbonates using the elemental analyser: the temperature of the column combustion allowed for the dissociation of $CaCO_3$ into CO_2, even though this worked only for “fragile” carbonates, such as travertine or foraminifera, but not for stronger carbonates like marble. However, with the combustion in elemental analyser there is no possibility to select a single fraction of CO_2, instead all the gas produced during the dissociation is transferred into the graphitization reactors.

Hence, we considered the possibility to design a new “piece” of the graphitization line which allowed us to carry out the acid digestion of the carbonates and to select a precise

fraction of CO_2. Coupling the acidification line with the new experimental set-up for microsamples allowed us to reduce the size of the carbonate samples to be analysed, thus keeping highly selective the pre-treatment and allowing us even to analyse the small lime lumps.

The characteristics of this new experimental set-up are described in the following paragraph.

4.3.1 The new acidification line

Figure 4.3 shows a schematic representation of the new acidification line integrated into the graphitization line described in paragraph 1.3.1.

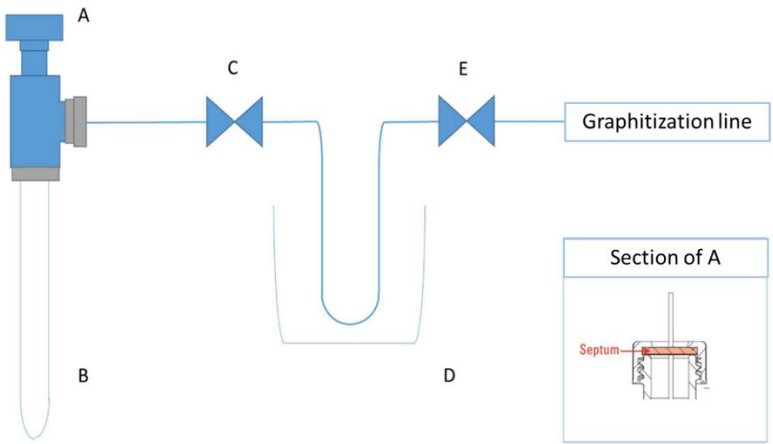

Figure 4. 3 Schematic representation of the acidification line.

The carbonate sample is put into a quartz tube (B in figure). Here is where the reaction with the acid takes place. Once the quartz tube is evacuated (residual pressure ≈ 10^{-4} mbar), the H_3PO_4 acid is inserted into the quartz tube using a syringe through a PTFE/silicone membrane (A in figure). This material is used because it meets all the requirements for this application:

- resistance to acid;
- resistance to temperatures between -40°C and 200°C;

- resistance to multiple perforations;
- capability to guarantee vacuum-tightness.

The dissolution reaction of the carbonates (Reaction 4.4 in paragraph 4.3.1) produces water vapours, which are trapped in a coil immersed in liquid nitrogen vapours (D in figure): in fact, the relative position of the liquid nitrogen vessel D and the trap itself is adjusted in such a way to reach an intermediate temperature, which is low enough to trap H_2O without freezing CO_2. Trapping the water is mandatory: considering the graphitization reaction (see paragraph 1.3.1), the presence of water inside the reactor would shift the equilibrium and not all the CO_2 would be reduced to graphite. Moreover, if the content of water is too high, the reaction does not even take place.

The acidification line is separated from the rest of the graphitization line by a valve (E in figure): this allows us to potentially select only one or multiple fractions of CO_2 produced during the digestion, as the reaction is going on. The CO_2 fractions are then cryogenically transferred to one of the graphitization reactors, following the procedure already described in paragraph 1.3.1.

4.3.2 Optimization of the new experimental set-up

Once the new acidification line was integrated into the graphitization line, different tests were carried out using mortars with known provenance and composition in order to verify the reproducibility of the acidification procedure and to understand the dependence of the CO_2 yield with respect to the mass and composition of the sample. For the tests, two binders associated to two different mortars were used:

- one was selected from an aerial mortar with silicate aggregates, whose carbonation was verified to be complete. Indicated in the following as M1, this mortar was used to verify the procedure since its composition is very simple.
- the other binder was selected from a mortar produced using “Pietra Alberese”, a limestone typically found in the areas surrounding Florence and largely used during Reinassance, with a percentage of clay mineral that was estimated to be of about 12% in this case. Indicated in the following as A12, the mass of this

binder is attributed to both calcite and to amorphous silicate. These silicates derive from the original clay minerals impurities of the limestone and can be observed through FTIR spectroscopy (see Figure 4.4). Obviously, their presence has to be taken into account, since more mass is needed to produce the same amount of CO_2 that can be obtained with pure calcite.

To better understand the trend of the dissolution reaction and the rate at which CO_2 is produced, we first performed a very rough test, using a 30 mg M1 sample. The material was inserted into the reaction tube B and the ortophosphoric acid was poured on it via the syringe through the membrane, as described in the previous paragraph. In Figure 4.5, the CO_2 pressure collected in one of larger graphitization reactors as a function of time is represented. Time 0 is identified as the beginning of the effervescence. We can observe that more than half of the CO_2 produced is collected in the first 4 minutes of the reaction, when the effervescence is stronger. Afterwards, the production rate of CO_2 is slower and slower as the reaction goes on.

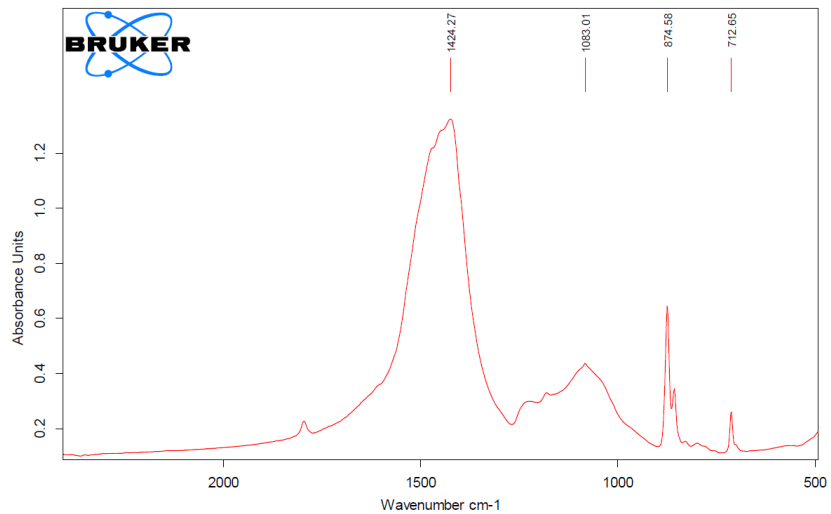

Figure 4. 4 FTIR spectrum of the sample A12. The peaks at 1424 cm-1, 875 cm-1 and 713 cm-1 refer to the carbonate phase of the mortar. In the region around 1083 cm-1 the overlapping signals of silicate phases can be observed.

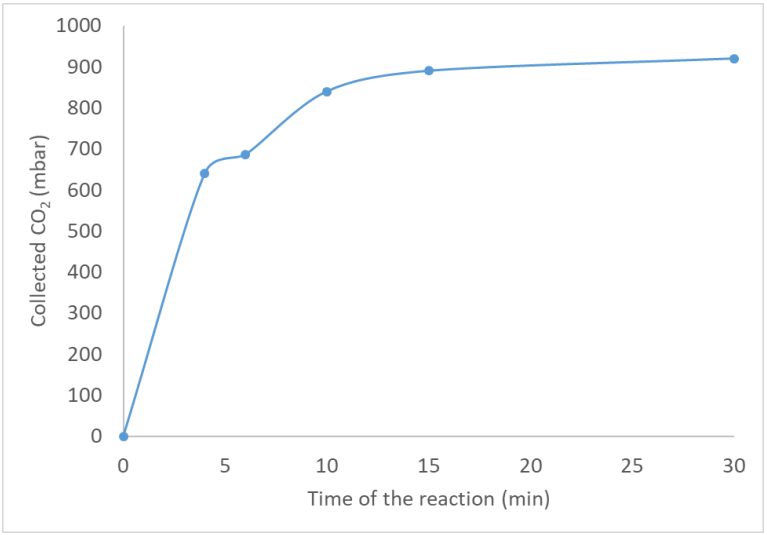

Figure 4. 5 Evolution of the CO_2 during the acidification process.

Considering that our typical large samples are graphitised starting from about 250 mbar CO2, it is clear that just after 1-2 minutes, we could collect the needed gas amount. In such a situation, we would indeed collect the first evolving fractions, thus matching the idea to collect what is highly probable to be the needed anthropogenic component. However, it is also clear that working with such massive sample is not really feasible, as for all the reasons discussed in the first part of paragraph 4.3. We thus decided to optimize the procedure in the case of microsamples. From both the binder M1 and A12, different fractions of 1.5 mg (mass comparable to the one of lime lumps) were selected, 3 from M1 and 2 from A12, and the same procedure was used for each fraction so as to verify the reproducibility of the method. This time, the CO_2 produced during the reaction was collected in the graphitization reactors optimized for the small samples. In Figure 4.6 and 4.7 the CO_2 pressures collected are reported versus the time from the beginning of the reactions. Considering that we were using the microsamples set-up and so our aim was to collect at least 100 mbar of CO_2, we can draw some interesting information from the results we obtained.

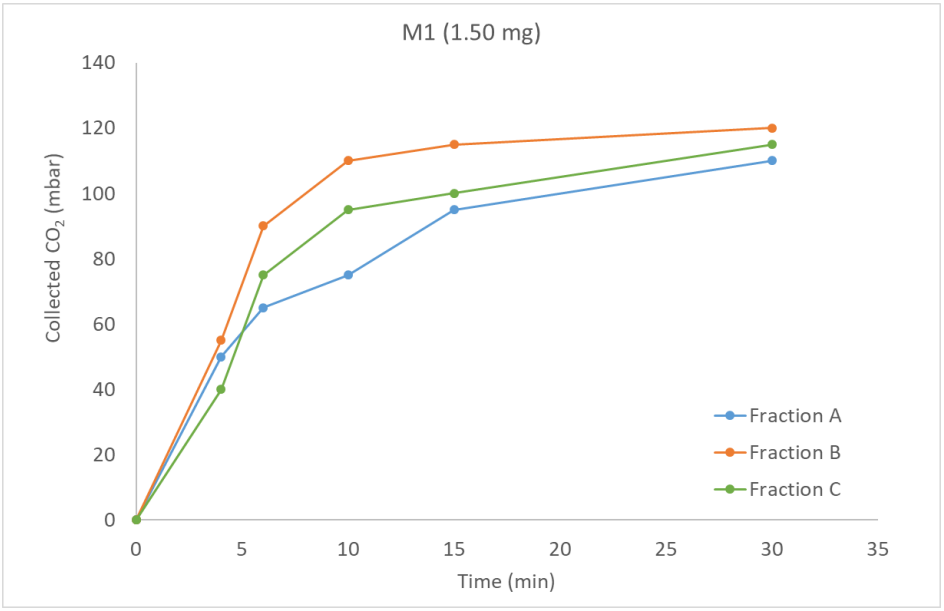

Figure 4. 6 Trend of the evolved CO_2 during the acidification process obtained from 1.50 mg of the binder M1.

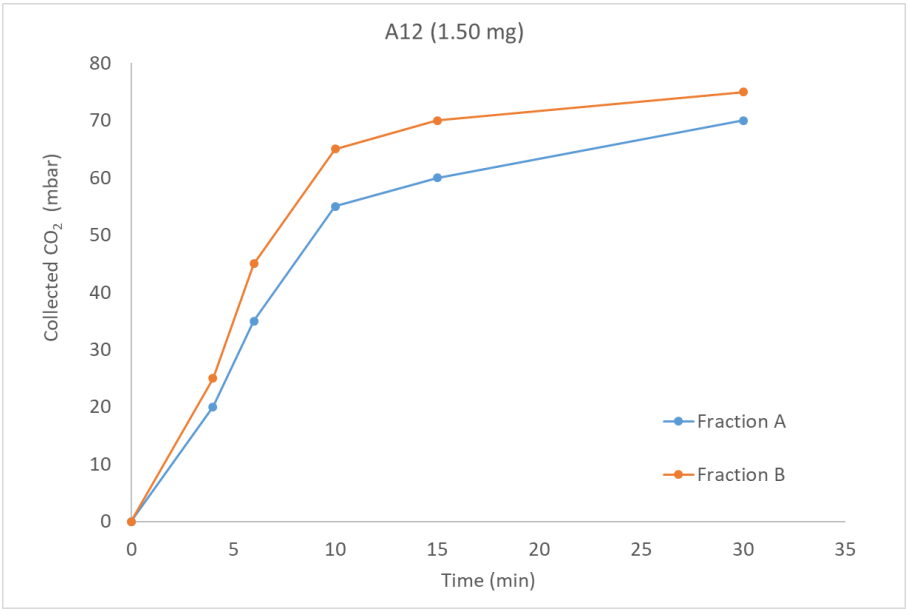

Figure 4. 7 Trend of the evolved CO_2 during the acidification process obtained from 1.50 mg of the binder A12.

For the sample M1, a pure aerial lime binder, we can observe that, in each test, we

collected enough CO_2 for a hypothetical graphitization after 15 minutes. Considering the very small mass used for these tests, comparable with the mass of a lime lump, the result was enough satisfying. However, if we suspect contaminants present inside the mortar sample, such as carbonate aggregates, 15 minutes are not sufficiently selective to be sure that we collected only the CO_2 from the binder, since in this time range these contaminants may start reacting. To shorten the time ranges we need to use bigger masses.

Regarding sample A12, instead, 30 minutes were not enough to collect 100 mbar CO_2. This result was expected, as said before. The partially hydraulic behaviour of the mortar and the consequent presence of amorphous silicates lower the CO_2 yield of the reaction; hence more mass is needed if we want to keep the time ranges shorter (hence more selective).

Once we verified the functioning and the reproducibility of the new set-up for the acid dissolution combined with the microsample experimental set-up, we decided to apply the procedure to a "real" case. We had the chance to take part to an extensive diagnostic campaign about Giotto's bell tower, in the centre of Florence. This campaign was conducted by "Opera di Santa Maria del Fiore Firenze", the no-profit organization that rules the Florence Cathedral and its joined monuments, with the aim at examining in depth the historical and structural aspects of the building. In this context, we were able to analyse the mortars of the bell tower, collecting mortar cores from different levels of the structure. In the following paragraphs the case study is explained in details.

4.4 The case study: Giotto's bell tower

The free standing bell tower by Giotto in Florence is part of the complex buildings of the Santa Maria del Fiore Cathedral in Piazza Duomo, Florence, and one of the masterpieces of the Florentine gothic architecture. Its design was intended to harmonise with the one of the Baptistery and the Cathedral, whose construction was interrupted for almost thirty years [52]: in fact the decorative scheme of the bell tower evokes the one of the cathedral, with the presence of the same polychromy and

geometric patterns given by the use of the three “marbles”, the worldwide well known white marble from Carrara, in the north-western Tuscany, Serpentinite or “green marble” from the hills around Prato, at about 20 km from Florence, and the marlstone or “red marble” from the Maremma region, in the south of Tuscany.

Figure 4. 8 The Giotto's bell tower. In A, the colours represent the different construction phases: the 1st phase in pink, the 2nd in green and the 3rd in white; in B, the original project by Giotto is represented.

The bell tower was designed and built in three different phases, each of them ruled by a different architect (see figure 4.8 A):

- Giotto di Bondone was entrusted with the direction of the construction. He designed the whole building (see Figure 4.8 B), but was able to see only the first part of the project completed, up to the hexagonal stone relief panels;
- After Giotto’s death in 1337, the direction of the work was handed to Andrea

Pisano, who continued following Giotto's direction, repeating his structures and decorations in the first "floor", but modifying the project as the constructions went on. Moreover, Pisano came upon structural issues in Giotto's original project, to which he remedied by reducing the thickness of the walls and adding the half pilasters to reinforce the masonry;

- In 1343 Francesco Talenti continued the construction, being able to complete the bell tower in 1359. He added the mullioned windows with the aim at lightening the whole structure, and ended the tower with a horizontal cornice, modifying the original Giotto's project.

All the phases of the construction are well documented in the literature and the study campaign allowed a more in depth overview of the bell tower history. This is very important for our application because the presence of landmarks for the dating is mandatory to check the reliability of the procedure used.

4.4.1 The mortars of the bell tower

In the context of the study campaign of the bell tower, different mortar cores were collected from two different levels of the building and from its foundations, in such a way that all the different construction phase were represented. Samples were collected using a hand-fed core drill with a 68 mm internal diameter. The cores dimensions were chosen trying to keep the invasiveness as low as possible while having the possibility to gain as much representativeness as possible. In Figure 4.9 the core samples are shown.

Figure 4. 9 The core samples of the bell tower's mortars.

During the study campaign, numerous analyses were performed in order to characterize the mortar cores from both the structural and the mineralogical-petrographical points of view. However, their description lies outside the topic of this thesis, thus we will not discuss them into details here (we suggest consulting [53] for further details).

Instead, here, I'm going to focus on those analyses whose results gave useful information for radiocarbon dating (type of the binder, grain size and nature of the aggregates, presence of lime lumps and their characterization). In particular, the techniques we used to have such information were:

- X-ray diffraction (XRD): this analysis gives qualitative and semi-quantitative information about the mineralogical phases of the sample. It allows for the characterization of the bulk material, the evaluation of the carbonation process and the crystalline components of the bulk mortar or lumps. Even though the analysis is invasive, it is not destructive, so we can re-use the powdered sample for other analyses. In the radiocarbon dating perspective, this is ideal, since we can be sure to date a sample with certain observed characteristics.
- Transmitted light microscopy: this analysis allows us to observe the petrographical features of our sample. The sample reduced in thin sections with a thickness of about 30 μm, embedded into epoxy resin, and it is observed using an optical microscope. Thanks to this analysis we can define the microscopic characteristics of the samples, such as the binder microcrystalline texture, the nature of the aggregates, their grain size and distribution, the presence of lime lumps and the aggregates/binder ratio. The information given by this technique are numerous, however the thin section cannot be used for other analysis. Given the vast heterogeneity of the mortars, we cannot be sure that the sample we are going to date has the very same characteristics of the one we observed (e. g. we can observe the presence of lime lumps and their nature, but we cannot be sure of the nature of the lime lump we want to date if we do not use another non-destructive analysis).

- Scanning electron microscopy (SEM): thanks to this analysis we can obtain information on the morphology as well as elemental maps, useful to evaluate the mineralogical composition of the samples. To perform this analysis, the samples has to be conductive, so as to avoid the accumulation of electric charges, which would interfere with the measurements, and are thus typically covered using graphite. As said above about transmitted light microscopy, even in this case, the sample cannot be re-used for radiocarbon dating.
- Phenolphthalein carbonation test: it is a colorimetric test, which uses the characteristic of phenolphthalein to change colour depending on the pH value. This pH indicator is transparent at neutral values of pH, while its colour turn ns colour into purple with pH values over 8.5, typical of calcium hydroxide. This test should be performed on freshly cut mortar cores and gives us information about the carbonation level of the sample.

All the results of the analysis were useful to identify those mortar samples that were more suitable for radiocarbon dating.

Generally speaking, the mortars of Giotto's bell tower are partially hydraulic mortars, with the typical composition of ancient Florentine mortars: the binder derives from the cooking of "Pietra Alberese" limestone, that, as explained before in paragraph 4.3.2, contains a small percentage of clay minerals which give a slightly hydraulic behaviour to the mortar; as for the aggregates, their composition is mainly siliceous, typical of the material collected from the Arno river. These characteristics were observed thanks to transmitted light microscopy, an example can be seen in Figure 4.10

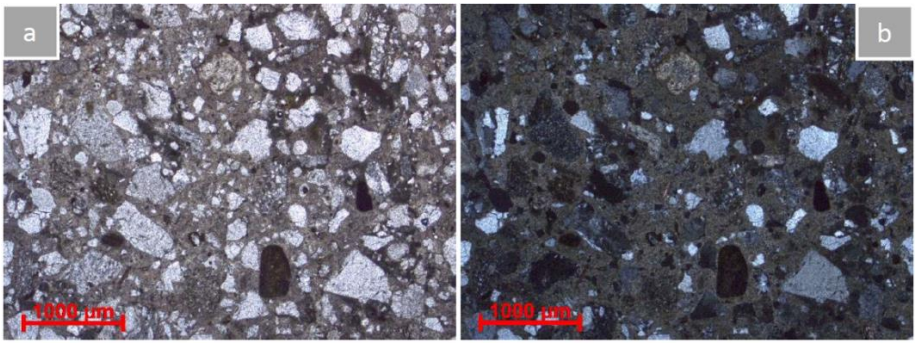

Figure 4. 10 Microphotography of the core sample C60.70m obtained by transmitted light microscopy, at parallel nicols (a) and crossed nicols (b).

Thanks to the characterization analysis, we were able to select two different samples:

- The lime lump G_4 from the mortar core $C_5$0.50m, indicated with G_4_$C_5$0.50m;
- The mortar in bulk from the mortar core C6, indicated with $C_6$0.70m.

The lime lump G_4_$C_5$0.50m was selected due to its whitish colour, its globular form and its powdered consistence, typical physical aspects of a pure binder lumps (see Figure 4.11).

Figure 4. 11 Lump G_4 still inside the mortar core $C_5$0.50m.

Among the different mortar cores, C60.70m was the most suitable for the analysis. All the cores collected from the foundations were discarded because potentially exposed

to capillarity rise of water; other core samples from different levels of the building showed not suitable characteristics for the dating, such as very fine grained carbonated aggregates or not completed carbonation.

Before the dating, the samples underwent a pre-treatment, explained in details in the next paragraph.

4.4.2 Sample pre-treatment and acid dissolution

Before the acid dissolution, sample G_4_$C_5$0.50m was simply crushed into fine powder. Sample $C_6$0.70m, instead, was crushed by gentle hammering and sieved through a mesh of about 63 µm (Figure 4.12).

In Table 4.1 the masses used for the acid dissolution are reported.

Sample name	Type of sample	Mass (mg)
G_4_$C_5$0.50m	Lime lump from the 2nd level of the bell tower	2.00
$C_6$0.70m	Mortar in bulk from the 2nd level of the bell tower	9.11

Table 4. 1 Mass and typology of the samples chosen for the dating.

Figure 4. 12 Sieved mortar sample.

Each sample was inserted inside the quartz tube of the acidification line. Once the line reaches a vacuum of 10^{-4} mbar, H_3PO_4 was syringed into the quartz tube. The CO_2 produced during the reaction was collected until 100 mbar of pressure were reached inside the microsamples reactor. In Figure 4.13 and 4.14 the time ranges and collected pressure for the samples G_4_$C_5$0.50m and $C_6$0.70m respectively are reported.

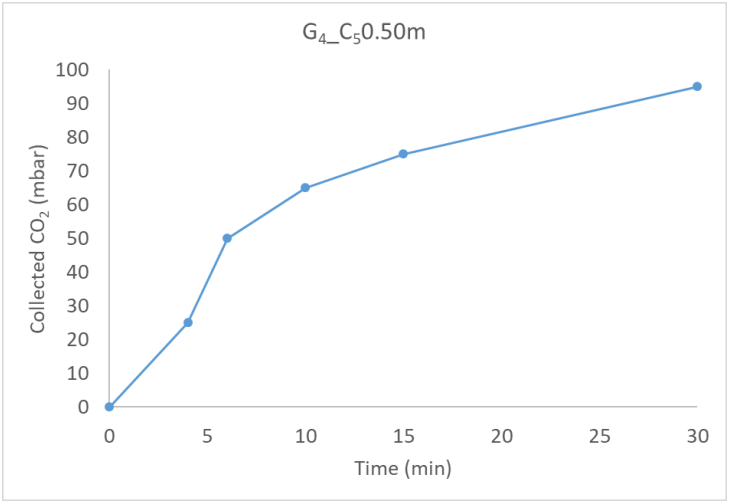

Figure 4. 13 Trend of the evolved CO_2 during the acidification process obtained from 1.50 mg of the lime lump G_4_$C_5$0.50m.

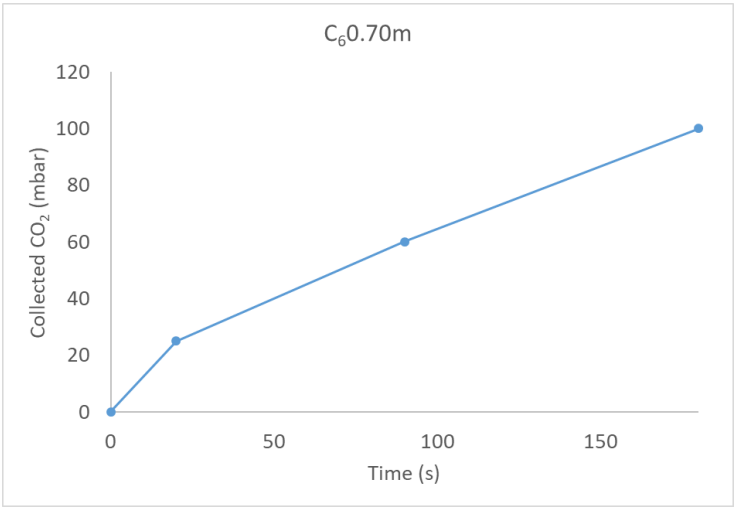

Figure 4. 14 Trend of the evolved CO_2 during the acidification process obtained from about 9 mg of the mortar core $C_6$0.70m.

For the lime lump G_4_$C_5$0.50m the characterization did not highlight any contamination, thus it was possible to extend the time range of the reaction to about 30 minutes, without taking the risk of having contaminants reacting with the acid. Moreover, using longer time rages was useful to collect enough CO_2, since the mass used for the graphitization was very small.

As for $C_6$0.70m, instead, being a mortar in bulk, we collected the CO_2 produced during the reaction for a total of 180 seconds. This time range was much shorter than the one used for the lime lump, but it was still enough to collect 100 mbar of CO_2. While for the lime lumps there were no risks of contaminants, for the mortar in bulk contaminants can still be present in spite of the sieving. Thus, we need to minimize the period of CO_2 collection, reaching at the same time an amount of gas which is enough for the graphitization.

4.4.3 AMS measurements

In Table 4.2 the measured radiocarbon concentrations and conventional radiocarbon ages of the samples are reported.

Samples	Lab code	^{14}C conc. (pMC)	t_{RC} (yrs BP)
G_4_$C_5$0.50m	Fi4164	85.7 ± 2.6	1200 ± 200
$C_6$0.70m	Fi4176	90.1 ± 1.7	830 ± 150

Table 4. 2 Measured radiocarbon concentrations and conventional radiocarbon ages for the samples G_4_$C_5$0.50m and $C_6$0.70m.

It has to be noted that the experimental errors associated to the radiocarbon concentrations are higher than the typical error obtained with the big samples. As already commented, the very small sample masses inserted in the ion source and the low currents extracted during the measurements surely contributed to increasing the experimental error.

In Table 4.3 (and Figure 4.15 and 4.16) the calibrated age of the samples are reported.

The calibrated age of the bulk sample $C_6$0.70m (890 – 1415 CE) resulted compatible

with the expected age of the construction phases of the bell tower. This is a satisfying result, given the fact that the sample was not totally ideal since the binder was not totally aerial. It suggests that the procedure we used (crushing and sieving + collecting the CO_2 from the first seconds of the reaction) can be considered a good strategy to isolate the binder and remove the contaminations.

Regarding the lime lump, though it is consistent with the mortar bulk according to the statistics, its calibrated age (425 – 1220 CE) appears to be slightly older than expected. This may be explained considering a residual very tiny contamination due to the natural hydraulic type of the binder and should be further investigated in the next.

Sample	**t_{RC} (yrs BP)**	**Calibrated age (95% probability)**
G_4_$C_5$0.50m	1200 ± 200	425 – 1220 CE
$C_6$0.70m	830 ± 150	890 – 1415 CE

Table 4. 3 Calibrated ages obtained using Oxcal 4.3 for the samples G_4_$C_5$0.50m and $C_6$0.70m.

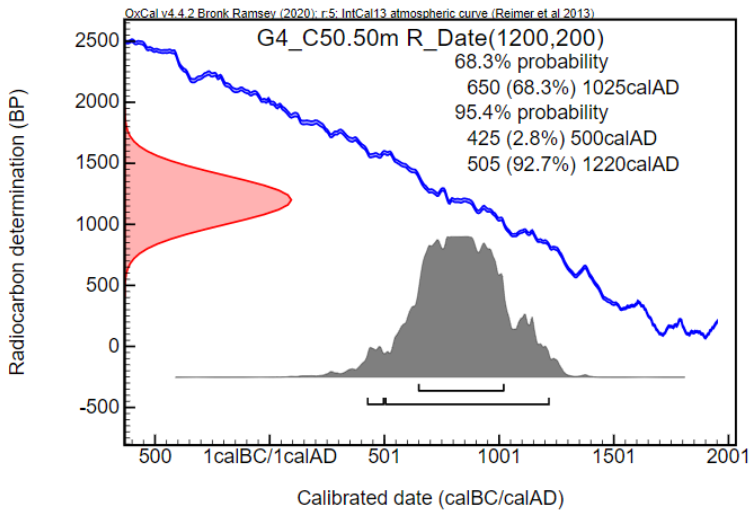

Figure 4. 15 Calibrated age for the sample G4_C50.50m.

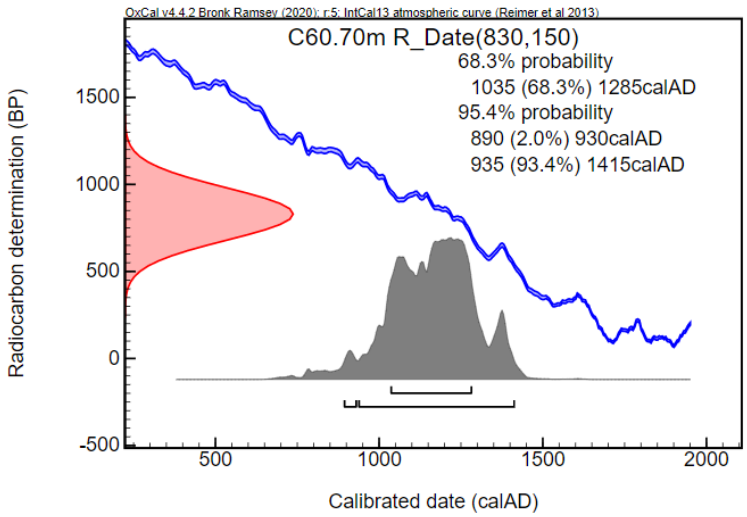

Figure 4. 16 Calibrated age for the sample C60.70m.

4.5 Summary of the case study

This chapter is dedicated to the feasibility study of mortar radiocarbon dating.

Since 1960s, many have investigated the issue of dating mortars by radiocarbon: indeed, this application would be very useful for the dating of building, because when we date the binder of the mortar we identify the “exact” moment when the mortar hardened, hence when the construction was built.

Even though the dating idea is basically simple, its application is not straightforward and mortar dating can be very complicated, due to the numerous contaminants that a mortar may contain: the fraction of interest is indeed the binder, but many other materials, called aggregates, may be added to the mortar to increase its mechanical properties and avoid the excessive shrinking during the hardening; these materials may have a carbonate nature, thus representing a source of contamination for the dating.

However, due to the above mentioned variability of the composition of mortars, it is very difficult to find a standard procedure for mortar dating and studies are still going on. What surely emerged from the numerous studies in the radiocarbon community and from our studies here presented is that characterization procedures of the mortars are

mandatory before the actual dating, in order to identify those samples that are suitable for the analysis.

Moreover, a selective procedure to separate the binder fraction from the aggregates, trying to remove the possible contaminations as much as possible. This procedure consists in crushing the mortar and sieving it with a very fine mesh (< 100 μm); afterwards, the fine sieved powder is reacted to orthophosphoric acid to produce CO_2, which is collected in a graphitization reaction. In order to keep this procedure the more selective possible, we need to use very fine meshes, which leads to a lower yield of material after the sieving, or reduce the time range in which the CO_2 is collected.

The experimental set-up used for our study includes a new acidification line coupled with the microsamples set-up. The acidification line allowed us to choose which time range to use to collect the CO_2, while the microsamples set-up gave us the possibility to reduce the required mass for the dating, preserving the selectiveness of the procedure. We made several tests to better understand how much mass was required for the dating and which time ranges were better, and to find a good balance between the selectiveness of the procedure and the time ranges-mass correlation.

Our feasibility study fits into the context of a study campaign conducted by the "Opera del Duomo" with the aim to examine in depth historical and structural aspects of the Giotto's bell tower. Numerous documentation is available and can be used as a reference for the expected ages of our samples.

Among all the mortar core samples collected for the study campaign, we chose the ones which were more suitable for radiocarbon dating thanks to an in-depth characterization of the mortars.

Samples underwent the procedure mentioned above and the calibrated ages obtained were compatible with the expected ages of the bell tower.

A crucial point in this chapter is that we were able to analyse our samples thanks to our microsample set-up, that allowed us to reduce the mass required for the measurements, thus keeping the pre-treatment of mortar the more selective possible.

Chapter 5: Radiocarbon dating of ancient written documents: a feasibility study

5.1 Radiocarbon dating of written documents

One of the most important key issues in radiocarbon dating is the relationship between the material we are dating and the "event" we actually want to date. In fact, when performing radiocarbon dating, we are always measuring when ^{14}C was fixed in the material from the atmosphere, or from another carbon reservoir in turn in equilibrium with the atmosphere itself, i.e. the death of the organism: this moment can be more or less distant in time with respect to the event we want to date (e.g. the manufacturing of an artefact). This offset depends on the material itself and on the production process of the artefact we are analysing. Hence, in such a case, we are not dating when the artefact was made, but our result should always be interpreted as a *terminus post quem.*

If we are dealing with artefacts that are made of a single homogenous material, e.g. a linen tunic, we simply date a sample collected from it and eventually we can infer which is the correlation between the moment we have determined, when, in this case, the plant was cut to make the material for the artefact, and the event we want to date.

If, instead, we deal with artefacts, like paintings, drawings or written documents, which are made of a support (e.g. canvas, parchment, papyrus or paper) with a layer of binder plus pigment/ink, we can choose which part of the artefact we want to date, in principle at least. In this example, a common, and also "easier", choice is dating the organic material of the support: dating such a component, we can often collect a small portion of the artefact from its edges, minimizing the invasiveness of the measurement, without interfering with the legibility of the artwork and without any particular restriction on the sampled mass. In this way, however, we may expect a possible temporal discrepancy between the age of the support and the manufacture of the document/artwork.

In some cases, this issue is not critical. An example is represented by the famous case

of “Contraste de forms” by the French painter Fernand Léger (1881-1955) of the Peggy Guggenheim Collection [54]. In this work, in order to prove whether the painting was a forgery or not, the support of the artwork was dated by radiocarbon; since the canvas used by the painter was manufactured with plants cut after the death of the artist himself, the painting was definitely identified as a forgery of the late 1950s.

Although the dating of the support may sometimes help with the authentication of the artworks, as in the example above, we cannot always rely on this tool. As a matter of fact, when the obtained result is compatible with the expected period of the document/artwork, this does not unequivocally prove it to be true. Numerous example can be presented on this issues and numerous debates have been and are still discussed (see [55], [56], [57]). One of the criticism the scholars put forward in these debates is that the “authenticity” of the support does not directly prove the authenticity of the document itself: in fact, expert forgers could have used an antique support, contemporary with the artwork they want to reproduce.

To overcome this important issue, the best solution would be directly dating the organic pigment or the organic ink of the artwork/manuscript. As a matter of fact, we can reasonably hypothesise that, in ancient times, inks and colours were produced in small numbers by hand using common and natural materials, so that we can generally expect a short period between their manufacture and their usage. Thus, dating the organic components of inks or colours can give us an age which is likely to be closer to the age of the event we want to date (i.e. the manufacture of the document/artwork) [58].

This particular application brings with itself important issues about the invasiveness of the analysis. If we want to date, for example, the ink of an ancient manuscript, we would have to collect a portion of the text, thus altering the integrity of the document itself. For this reason, we have to keep the collected mass as small as possible for the analysis.

In fact, using the experimental set-up for the “typical” large samples, the analysis would result too invasive for this application. Instead, the only possibility would be using

the new experimental set-up for microsamples, already discussed in Chapter 2, which would allow us to collect much smaller samples.

Among all the possible writing supports in the antiquity, we decided to focus our attention on papyrus, since this material represents one of the most used supports in many civilizations and through many different periods, as for instance in ancient Egypt. Ancient Egyptian papyrus documents have often been found in very bad preservation conditions, often disrupted in many several fragments or re-used as mummy cartonnages, or anyway mixed and glued in rolls. Reconstructing the chronology of such documents is clearly of interest for the archaeological community. Palaeography is typically a powerful tool to date documents. Absolute dating methods such as radiocarbon can be very useful to support palaeographic studies, especially in those case when a counterfeit is suspected [59].

Given the practical interest of this study and the capabilities of the new experimental set-up for microsamples, we decided to study the feasibility to directly date organic ink on papyrus. We started by preparing test samples, following the old manufacturing processes, even though using modern materials. Afterwards, we studied a new procedure to extract the carbon particles of the ink from the test samples, characterizing the collected materials by FTIR (Fourier-Transform Infrared Spectroscopy) and ATR (Attenuated Reflectance Spectroscopy). Finally, we measured the radiocarbon concentration of the ink, to understand if the procedure was effective in removing the possible contaminants and the material of interest for the dating.

5.2 Ancient Egyptian papyri documents

5.2.1 The papyrus: from plant to paper

The *Cyperus papyrus* plant (in Figure 5.1) is a species of aquatic flowering plant belonging to the sedge family Cyperaceae. It has been used by humans, since very long time ago, as it is the source of papyrus paper, one of the first types of paper ever made, used by the Ancient Egyptians since the 3rd millennium BCE.

The papyrus is a tall, robust plant, consisting of leafless trunk with triangular section, that can grow up to 3 to 5 m high, and ending with bright-green umbrelliform inflorescences. In nature, it grows in full sun, in flooded swamps, and on lake margins throughout Africa, Madagascar, and the Mediterranean countries even though it is nearly extinct in its native habitat in the Nile Delta, where in ancient times was widely cultivated.

Figure 5. 1 The Cyperus papyrus plant.

The trunk consists of an outer strong cortex and an inner marrow, made up by 97% of carbohydrates (cellulose, hemicellulose and lignin) and 2-3% of protein-based materials [60]. The presence of cellulose chains, organized in micro then macro-fibrils, makes the material rigid and resistant. These characteristics are intensified by the presence of lignin, with its high molecular weight and amorphous structure.

The most ancient note describing the manufacturing of papyrus paper dates back to Pliny the Elder in his “Naturalis Historia”. In later times, many researchers have studied and discussed his writings about papyri [61] [62] [63] to confirm their accuracy.

The method described by Pliny consists in cutting the papyrus trunk in segments of equal length, removing the cortex, obtaining thin strips taken from near the marrow.

The strips are placed one next to the other, forming a first layer. The second layer consists of other strips, placed again one next to the other and all perpendicular to the first layer. The two overlapping layers are pressed together and then left to dry.

The cohesion among the strips is due to physical bonds: when the layers are pressed together, the air among the strips is removed and the space is occupied by the lymph of the plant, making the whole structure more compact. When the papyrus is completely dried, these bonds are permanently fixed and the cellulose fibres are stuck together into a solid lattice. Moreover, the gum-like substances from the cell sap of the pith of papyrus tend to form hydrogen bonds one with another and, in addition, a layer of starch was added, increasing the adhesion and cohesion even more [64] [65].

5.2.2 The charcoal-based ink

In Ancient Egypt, the most employed inks to write on papyrus paper were red and black inks: the former ones were used to write headers and titles and were produced starting from red pigments like hematite, iron oxide or realgar (arsenic sulphide); the black inks, instead, were usually lampblack or charcoal-based inks [66] and were mostly employed until the 4th century BCE. These inks were stored in the form of small solid pats, inside a palette together with colours (like our modern watercolours).

The ancient recipes of the inks can be found in the writings of Vitruvius (*De Architectura*), Pliny the Elder (*Naturalis Historia*) and Dioscorides (*De Materia Medica*). In particular, regarding the black inks, they were made using a black pigment and an organic binder. The black pigment was obtained by crushing burnt wood (charcoal indeed) or by collecting the soot produced by the combustion of natural resins and oils. Generally, the black pigment consisted in amorphous carbon, powdered by mortar and pestle.

Regarding the binder, depending on the geographical area and the age, different products were used, like Arabic gum, isinglass, egg white, honey and natural oils. In particular, the Ancient Egyptian used to employ the Arabic gum [67] [68]. This gum was obtained from the exudations of two species of *Acacia* tree*, Acacia Senegal and Acacia*

Seyal, which are very common in the eastern Africa. Usually, to stimulate the exudation, incisions were made on the cortex of these plants. The product obtained from the exudation was powdered.

Arabic gum is a complex mixture of glycoproteins (3%) and polysaccharides (97%) predominantly consisting of arabinose, galactose, rhamnose and glucuronic acids, even though its composition may vary depending on the plant species [69] [70]. It is soluble in water, resulting in a viscous solution, easy to apply on a surface, possibly mixed with the pigment powder. After the application on the support, the water in the solution evaporates and the Arabic gum forms a thin transparent film, elastic and strong. Being transparent, this film does not modify the optical properties of the pigments.

5.3 The dating feasibility study: materials and test samples

For the feasibility study on the dating of collected organic components extracted from written papyri, test samples were prepared, following the old recipe as accurately as possible.

We prepared our own organic ink (Figure 5.2) according to the following steps:

- charcoal fragments were obtained from wood combustion of small branches from different origins and plant species (olive, apricot and peach trees) and thus likely to be different in age; fragments were finely crushed them into a mortar before using them;
- Arabic gum was purchased from a fine art shop; it was dissolved in warm water (about 40°C) in the ratio 5g:20 mL;
- the mixture of charcoal powder and Arabic gum solution was filtered (mesh size of about 0.5 mm) to remove the larger fragments.

As for the support, we purchased a modern papyrus foil in a fine art shop: the supplier ensured us that the material had been manufactured according to the traditional procedures, without adding any glues or resins, being the stickiness of the fibres naturally due to the papyrus extractives, as explained in paragraph 5.2.1, on the basis of the old Pliny recipe.

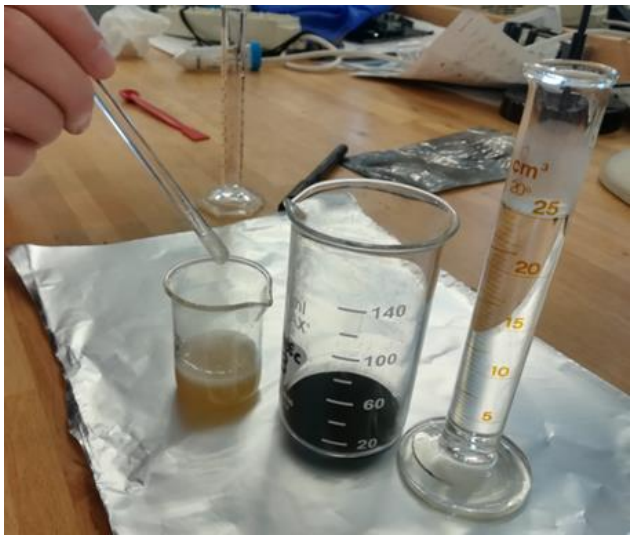

Figure 5. 2 The preparation of the organic ink.

From the same papyrus sheet, two different kind of test samples were prepared:

- the so-called "large tile" samples, obtained covering papyrus about 4x4 cm^2 fragments with a thick layer of home-made ink (about 100 mg before drying), indicated as Ink_ATR1 and Ink_ATR2 in the following (see Figure 5.3 (a)). These samples were used to define the best procedure for the extraction charcoal-like particles from the ink and to verify its effectiveness;
- more realistic samples, obtained writing on smaller papyrus fragments (about 3x3 cm^2), using about 6 mg of inks, as measured before complete drying, indicated as 6mg_0, 6mg_1 and 6mg_2 in the following (see Figure 5.3 (b)).

All the test samples were left in the laboratory for about five months, thus being exposed to natural light, so as to resemble a natural ageing, even though clearly mild.

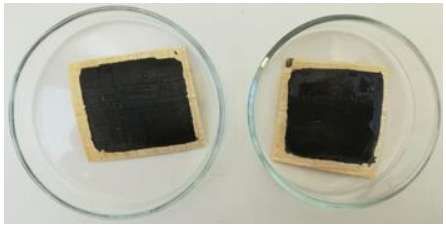

(a)

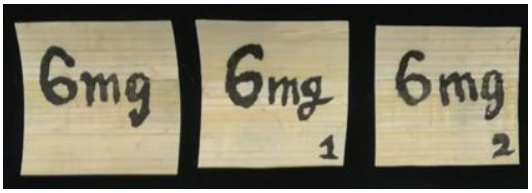

(b)

Figure 5. 3 The different test samples prepared from the same papyrus sheet: the "large tiles" (a) and the more realistic samples (b).

These test samples were characterised for their composition (via FTIR and ATR spectroscopy), as explained in the following paragraph, before and after the sample pre-treatment, in order to check the efficiency of it.

5.4 Characterization of the raw materials

5.4.1 FTIR spectroscopy measurements

The raw materials used to prepare the test samples were characterized both for their composition via FTIR spectroscopy and for their radiocarbon concentrations.

Concerning the FTIR analysis, all the spectra were acquired using a Shimadzu FT-IR 8400S spectrometer (45 scans, 4 cm^{-1} resolution) and elaborated used the software Lab Resolution IR v. 2.16. The samples were analysed in trasmittance on KBr pellets.

As far as the Arabic Gum is concerned (see Figure 5.4), its polysaccharide nature can be observed in the IR spectra by the presence of the 3429 and 1610 cm^{-1} peaks, respectively related to the stretching and bending of the O-H group (blue arrows in figure), and the 2931 and 1417 cm^{-1} peaks, related to the C-H stretching and C-H bending (in green in figure). In the so called fingerprint region of the spectrum, the peaks attributable to the presence of polysaccharides are those at 1074, 1031 and 975 cm^{-1}, related to the stretching of the C-O-H and C-O-C groups (in orange in figure).

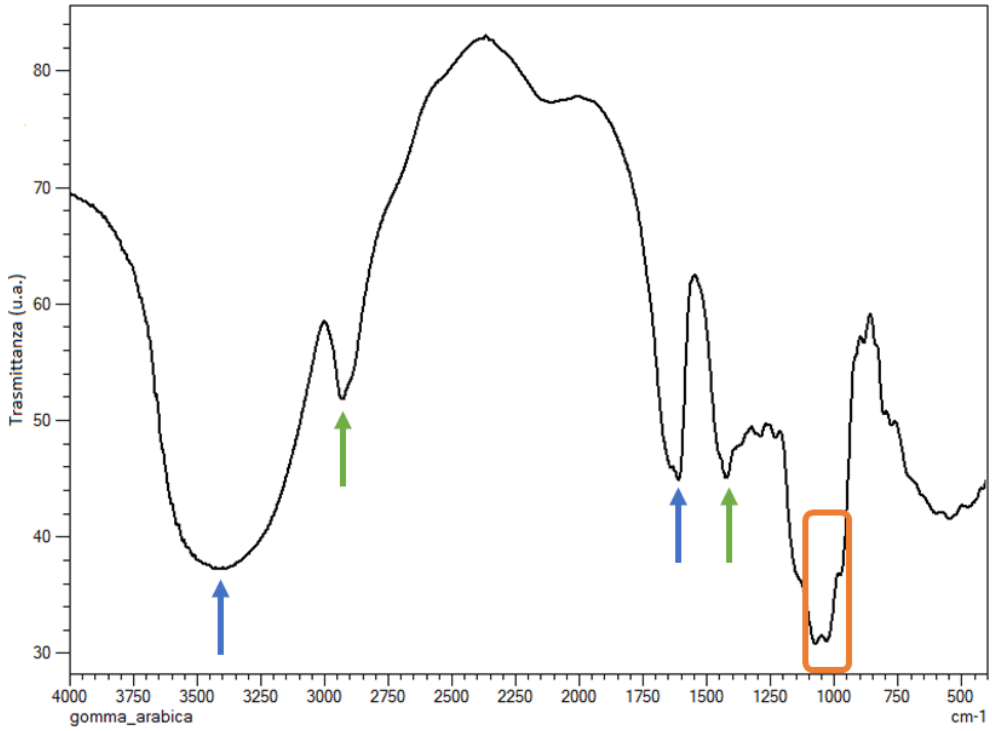

Figure 5. 4 FTIR spectrum of the Arabic gum used to prepare the home-made ink.

The papyrus sheet is clearly expected to be mostly composed of cellulose, as in fact is well visible in the IR spectrum (Figure 5.5). Indeed, the cellulose, like the Arabic gum, is a polysaccharide, thus peaks related to the O-H stretching (3385 cm^{-1}) and bending (1627 cm^{-1}) (in blue in figure) and the C-H stretching (2920 cm^{-1}) (in green) are visible. In the fingerprint region, the presence of 1161, 1107 and 1037 cm^{-1} peaks are ascribable to the cellulose as principal component and to the lignin and hemicellulose, even though the cellulose signals could overlap the ones of lignin and hemicellulose (in orange in figure).

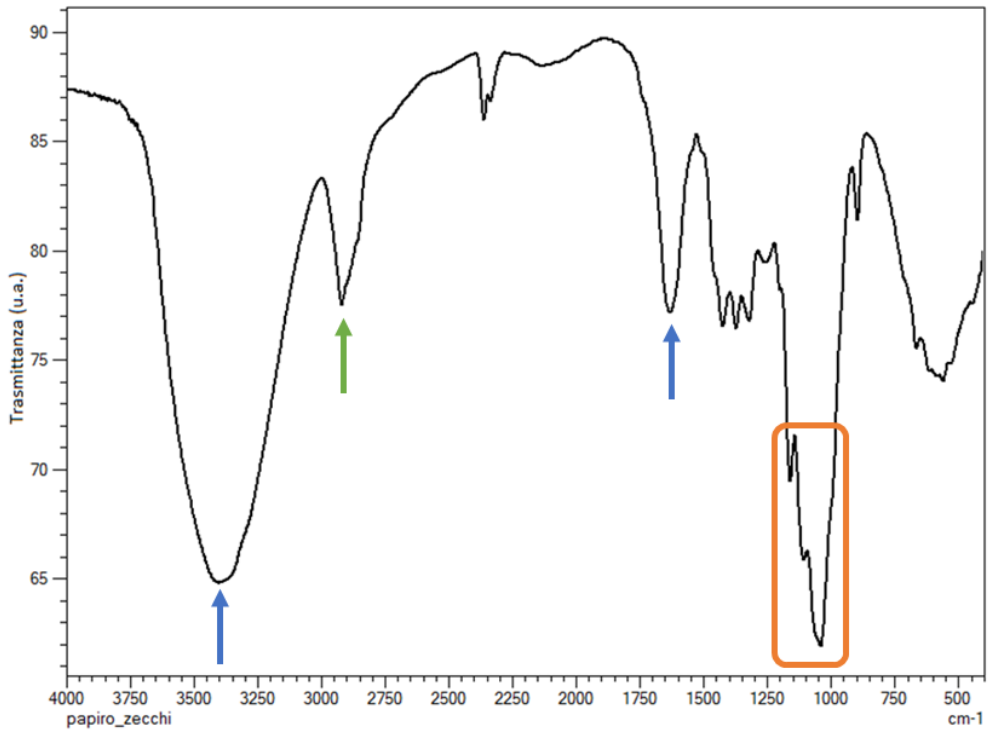

Figure 5. 5 FTIR spectrum of the papyrus sheet used as support for the test samples.

For the extraction procedure, we expect that immersing the written papyrus in water, the Arabic gum will solubilize, releasing the carbon particles of the ink. It is evident, as however expected, that Arabic gum and papyrus are really similar and thus we can guess that the solubility in water of the papyrus extractives is as good as that of Arabic gum. To verify the presence of papyrus extractives in the water solutions and identify and characterize them, blank tiles of the papyrus sheet were immersed in 20 mL of deionized water at about 50°C for 6 hours. After the extraction, the water-soluble extractives were dried using a rotary evaporator and the dried extractives with their respective papyrus blank tiles were analysed by FTIR.

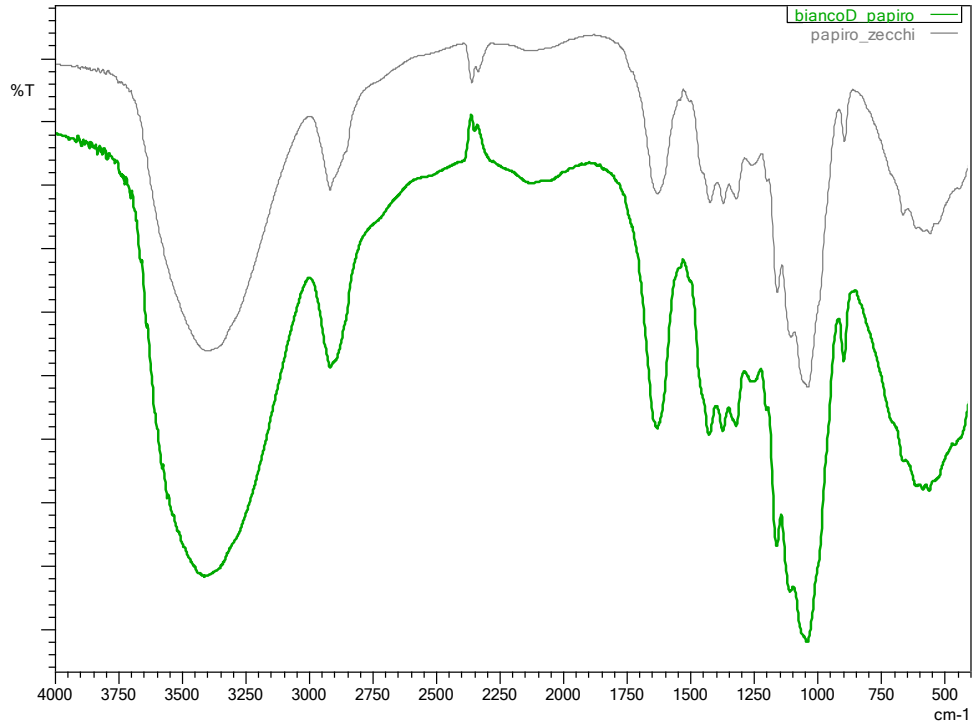

Figure 5. 6 FTIR spectra of the blank papyrus tile before (grey) and after (green) the extraction in water.

In Figure 5.7 the comparison of the spectrum of the blank tile before the extraction in water (grey) and after the extraction (green) is visible. No significant differences between the two spectra can be seen: peaks are, indeed, very similar both in wavelength and in relative intensities. In fact, the natural gums contained in the papyrus have lower concentrations than cellulose, therefore their peaks are not visible in the spectrum since the ones of the cellulose overlap them. Hence it is not possible to observe their removal.

In Figure 5.7 the spectra of the extractives (in blue) and the Arabic gum (in orange) are represented. The two spectra highlight very similar compositions of the compounds, since the peaks fall in the same spectral bands, confirming the polysaccharide nature of the water-soluble materials present in the papyrus.

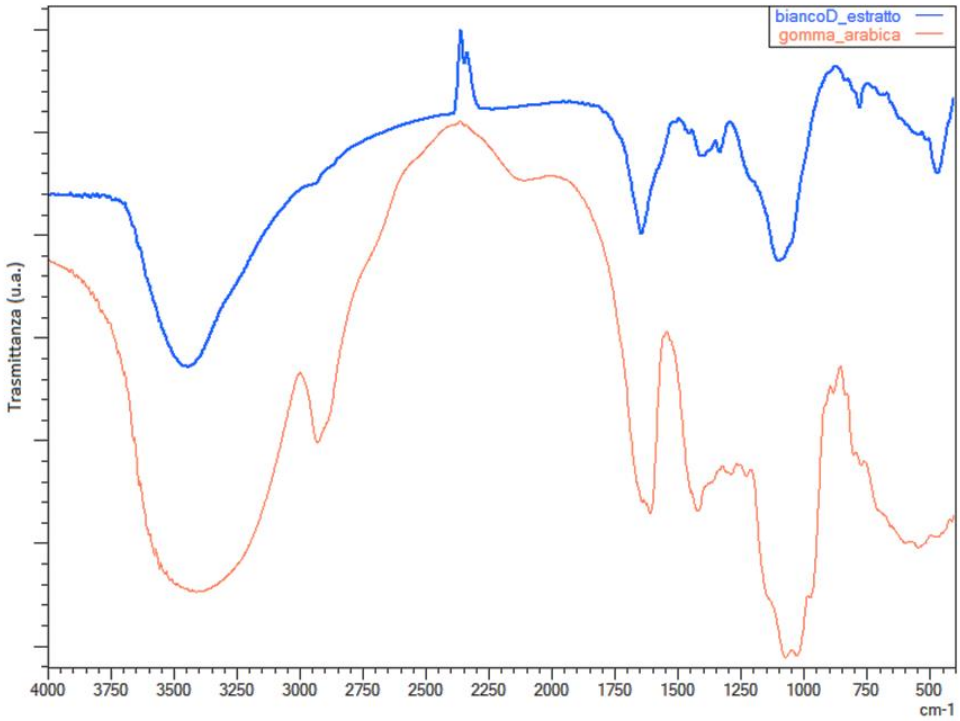

Figure 5. 7 FTIR spectrum of the blank tile extractives (in blue) compared to the spectrum of the Arabic gum (in orange).

Having in mind our goal of dating the ink on papyrus, in principle, we can think to collect the measurable material by immersing the written document in warm water: considering the high solubility in water of the Arabic gum, the ink particles would detach from the support and would be released into the water, while the gum would be completely solubilized, mixed however with papyrus extractives. We could choose if dating the Arabic gum or the ink, however due to the very similar composition of the Arabic gum and the extractives it may result very difficult to separate the two compounds. Therefore, we chose to date the charcoal particles of the ink.

5.4.2 ^{14}C - AMS measurements

As preliminary investigation on the raw materials, we measured the ^{14}C concentration of some fragments collected from the charcoal used to produce the home-made ink, as

well as of the Arabic gum and the papyrus. These experimental data would have represented a sort of reference to evaluate the quality of the charcoal particles extraction procedure and the possible presence of contaminations.

From the charcoal used to make the ink, three different fragments without any discrimination on their provenance were selected. As explained in paragraph 1.3, all the samples to be dated must be pre-treated before the radiocarbon concentration measurement, in order to get rid of all the possible contaminations. In this case, we removed the outer layers of the charcoals and then powdered them into small pieces. Afterwards, the charcoals underwent an acid-base-acid (ABA) treatment, adapted from [71] on purpose; in particular:

- HCl 1M, at about 80°C for 1 hour. This step is needed to remove the possible carbonate contaminants;
- NaOH 0.1M, at room temperature for 30 minutes. With this step, we remove the possible organic contaminants due to the humic acids in the soil;
- HCl 1M at 80°C for 1 hour, to remove the possible CO_2 that may dissolve into the water in the previous step

Between one step and the other, the sample was rinsed with deionized water, until reaching the neutral pH.

At the end of this pre-treatment the three different samples (called *Charcoal_S*, *Charcoal_S1* and *Charcoal_S2*) were dried in oven at 100°C, combusted and graphitized, as explained in paragraph 1.3.1[12].

The radiocarbon concentration was measured also for the Arabic gum and for the blank papyrus extractives. Considering the high solubility in water of the two materials, we did not perform further pre-treatment on them and simply reduced them into graphite pellets.

In Table 5.1 the radiocarbon concentrations measured for the three charcoal samples,

[12] At this step of the feasibility study, we decided to use the experimental set-up optimized for the typical "big" samples. This provided us a better control on precision and accuracy of the measurement.

the Arabic gum and the blank papyrus extract are reported.

Samples	Lab code	14C conc. (pMC)
Charcoal_S	Fi3981	109.79 ± 0.62
Charcoal_S1	Fi4081	105.51 ± 0.59
Charcoal_S2	Fi4082	102.57 ± 0.64
Arabic gum	Fi3980, Fi3989	118.26 ± 0.51
Blank papyrus extract	Fi4354	103.70 ± 0.44

Table 5. 1 Radiocarbon concentrations measured for the charcoal, the Arabic gum and the blank papyrus extract. Regarding the Arabic gum, the weighted average of the concentrations measured for Fi380 and Fi3989 is reported, since the two fractions were consistent one with the other.

The first thing we notice is that the three charcoal samples have radiocarbon concentrations which are not in statistical agreement one with the other. The measured scattering among the three radiocarbon concentrations may appear surprising. Nevertheless, it can be explained if we keep in mind that those charcoals were produced by wood burning, without any control on the collection, and thus on the age, of the used wood and branches. Moreover, if we consider the calibrated ages of the three different samples, these ages cover a period basically starting since the beginning 2000s, that is the expected period in which the wood was cut to make the charcoal. As for the Arabic gum and the papyrus extract, both their concentrations suggest that they can be considered as “contemporary”.

As a further preliminary investigation, we verified the possibility to collect the charcoal particles from the prepared ink without being affected by the Arabic gum used as binder. The carbon insoluble fraction of the ink was collected by centrifugation rinsing it with deionized water for ten times to clean it from any possible residue due to Arabic gum. Afterwards, the collected fragments were treated according to the ABA procedure mentioned above for the raw charcoals. The charcoal extracted in this way was then combusted and graphitized and its radiocarbon concentration was measured. In Figure

5.8 the radiocarbon concentration of the extracted charcoal (C_Ink) is compared to the ones measured for the charcoals used to make the ink.

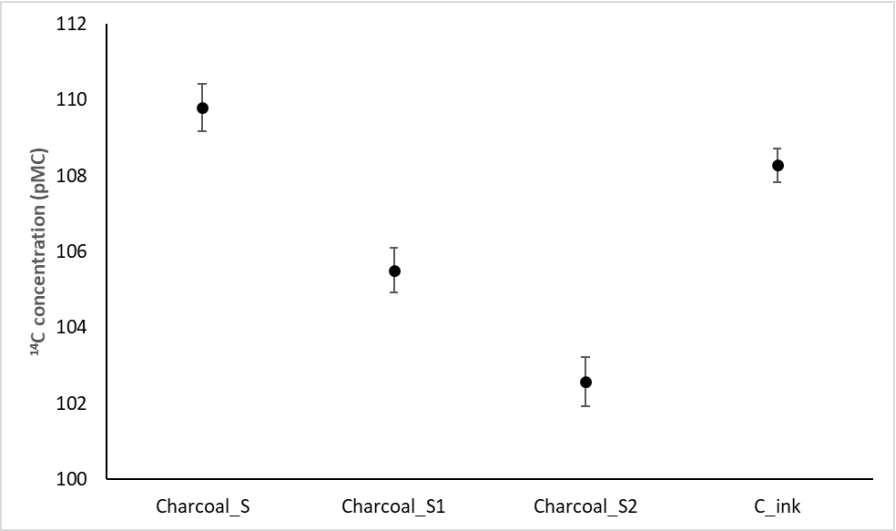

Figure 5. 8 Radiocarbon concentrations measured for the charcoals samples compared to the one measured for the charcoal extracted from the prepared ink.

The measured radiocarbon concentration is in the range of the measured ^{14}C concentrations of the raw charcoals, suggesting that after rinsing several times with water, a possible contamination due to the Arabic gum is very unlikely.

5.5 Tests on the "large tiles"

Before working on more realistic samples, we decided to verify the effectiveness of the extraction procedure on the large tiles samples (Ink_ATR1 and Ink_ATR2).

After the complete drying and the natural ageing, as explained in paragraph 3.3, about 25 mg of ink was estimated to be present on the two samples. To extract the charcoal particles from the samples, the large tiles were immersed in 30 mL of deionized water, at about 50°C for 8 hours: during this period, we observed that at first the binder detached from the support in globular forms, carrying inside the charcoal particles; afterwards, the Arabic gum completely solubilize in the warm water, releasing the

particles. After this extraction, the tubes were left at room temperature for 16 hours, to let the particles deposit as much as possible (Figure 5.9).

Water was finally removed by centrifugation. After the extraction procedure, the collected charcoal particles from the two different samples, underwent slightly different pre-treatment:

- Ink_ATR1 was immersed in deionized water at 50°C for 30 min, then in 1M HCl at 80°C for 1 hour;
- Ink_ATR2 was just put into 1M HCl at 80°C for 1 hour.

To check if the treatment effectively removed the Arabic gum and which of the two methods was more efficient, the two samples were characterized by ATR.

We chose to use ATR instead of FTIR, because with the FTIR spectroscopy we would have not been able to see any signal from the contaminants, due to the too high absorbance of charcoal, which would have covered all the other signals. ATR spectra were acquired using a Shimadzu IRAffinity-1 spectrometer, equipped with a single reflection crystal, and elaborated using Lab Solution IR v. 2.16.

Figure 5. 9 The two samples Ink_ATR1 and Ink_ATR2 after the particle extraction.

As it can be noticed, no "real" signal is present in the spectra (Figure 5.10): no peak associable to any typical Arabic gum or papyrus extractives bonds is visible. Even though

small traces of such components may be hidden in the spectra by the high background due to the great absorption of the black material, this suggests that both pre-treatments were successful in the removal of possible contaminations of the recovered charcoal particles.

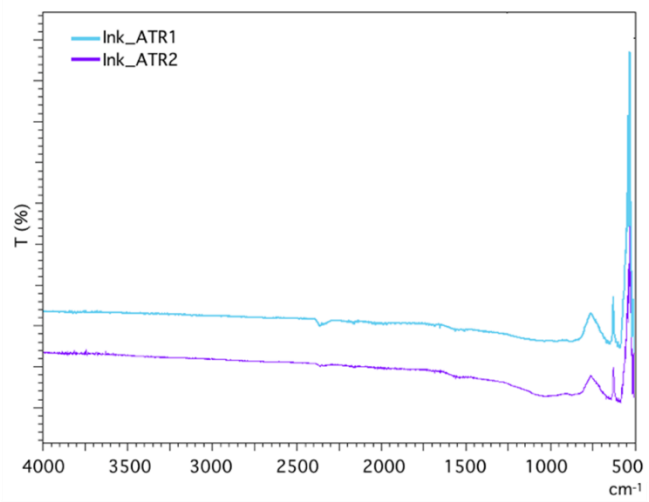

Figure 5. 10 ATR spectra for the samples Ink_ATR1 and Ink_ATR2.

Since both the pre-treatment can be considered efficient, we decided to put Ink_ATR1 and Ink_ATR2 together in a single sample (Ink_ATR), because the masses of the two samples after the ATR measurements were too small to perform the dating on both the samples with our traditional experimental set-up for the large samples.

The sample Ink_ATR was graphitised and measured by AMS, giving a ^{14}C concentration which is compatible with the radiocarbon concentrations obtained for the ink (see Table 5.2 for comparison).

Sample	**Lab code**	**^{14}C conc. (pMC)**
C_ink	Fi4024, Fi4029	108.27 ± 0.44
Ink_ATR	Fi4031	107.62 ± 0.53

Table 5. 2 Radiocarbon concentration reported for the samples C_ink and Ink_ATR. Regarding the C_ink, the weighted average of the concentrations measured for Fi4024 and Fi4029 is reported, since the two fractions were consistent one with the other.

Since the ATR measurements suggested the effectiveness of the two different cleaning procedures applied on Ink_ATR1 and Ink_ATR2 and, in addition, the radiocarbon measurement on the combination of the two samples did not show any presence of contaminations, we decided to set-up the charcoal particles collection procedure by adding the less invasive procedure for the purification material after the extraction in water: 1M HCl at 80°C for 1 hour and then rinsing with ultra-pure water until neutral pH. Indeed, an efficient pre-treatment with few steps guarantees the avoidance of excessive sample mass loss, which is fundamental in applications where samples are already small (like this one).

5.6 The tests on the "6mg" tiles

After the complete drying and the natural ageing, about 1 mg of ink was estimated to be present on the 6mg_0, 6mg_1 and 6mg_2 samples. Charcoal particles were extracted and collected following the same procedure described in the paragraphs above for the "large tile" samples and summarised as followed:

- bath in deionized water at 50°C for 8 hours;
- settling at room temperature for 16 hours to allow for the complete deposition of the charcoals particles (Figure 5.11);
- recovery of the particles by centrifugation;
- bath in 1M HCl at 80 °C for 1 hour;
- neutralization by multiple rinsing with water.

As discussed above in paragraph 5.x, the pre-treatment chosen for the charcoal particles was the simpler one performed on Ink_ATR2, which consisted in less steps, in order to lose as less mass as possible.

To minimize the risk of possible material losses while collecting the charcoal particles from the extraction equipment into the small tin capsules for combustion in the EA (see paragraph 1.3.1), for each sample, the final dispersion was directly pipetted into those capsules, and then let to dry. This operation has been repeated until the whole dispersion was transferred into the capsules. For each sample, about 0.2 – 0.3 mg of

dried charcoal were collected.

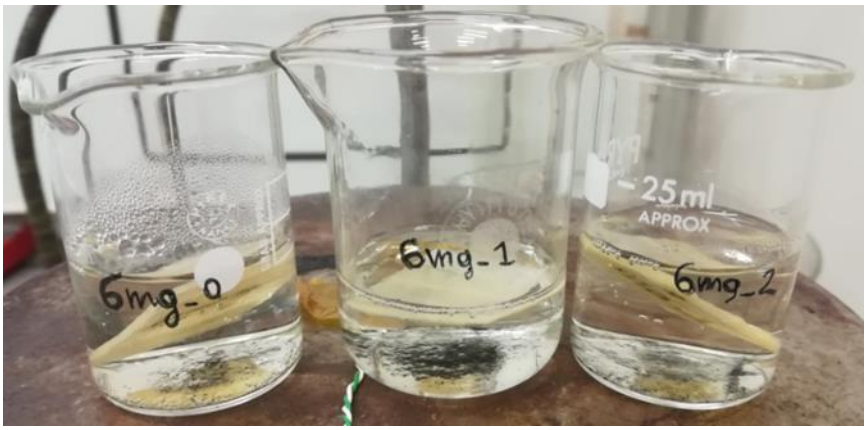

Figure 5. 11 Samples 6mg_0, 6mg_1 and 6mg_2 during the extraction of the charcoal particles.

Considering the amount of mass that we estimated was sufficient to collect 100 mbar of CO_2 for charcoal for the microsamples set-up (about 0.2 mg, see Table 2.1 in paragraph 2.1.1), the masses collected for these test samples were perfect for this application.

The samples were then combusted and graphitized using the new experimental set-up for microsamples described in Chapter 2. In Table 5.3 the masses used for the combustion and the amount of CO_2 collected for each sample are reported. For sample 6mg_2, which was the most abundant in mass, we obtained more CO_2 than the amount that was needed (about 200 mbar). Hence, we decided to reduce the CO2 collected in the reactor down to 100 mbar and transfer the excess of the gas in the other graphitization reactor. In this way, we obtained two different samples to be measured by AMS; doing to this, when possible, it is important, since it allows us to have a better control on the results obtained by the measurements.

Sample	Lab code	Mass (mg)	CO_2 pressure (mbar)
6mg_0	Fi4098	0.2	90
6mg_1	Fi4096	0.2	100
6mg_2	Fi4093 Fi4094	0.3	100 80

Table 5. 3 Burnt masses and respective CO_2 collected for the 6mg - series. For the sample 6mg_2 the CO_2 obtained from the combustion was in excess, thus we reduced it to 100 mbar and trasferred the excess in the other graphitization reactor.

In Table 5.4 the radiocarbon concentration measured for 6mg_0, 6mg_1 and 6mg_2 are reported.

Sample	Lab code	^{14}C conc. (pMC)
6mg_0	Fi4098	109.86 ± 0.81
6mg_1	Fi4096	108.32 ± 0.63
6mg_2	Fi4093, Fi4094	108.68 ± 0.65

Table 5. 4 Radiocarbon concentration measured for the samples 6mg_0, 6mg_1 and 6mg_2. Regarding 6mg_2, the weighted average of the concentrations measured for Fi4093 and Fi4094 is reported, since the two fractions were consistent one with the other.

As we can see, the radiocarbon concentrations of the 6mg-series are compatible one with another. Moreover, if we compare these concentrations with the ones measured for C_ink and Ink_ATR, we can see a satisfying compatibility.

In Figure 5.12 the comparison between the radiocarbon concentrations of the 6mg-series and the data collected from the raw charcoal fragments is presented. Even though the agreement of the charcoal Fi3981 is fully satisfying, the other two charcoal samples do not seem consistent with the 6mg-series samples from the statistical point of view. Nevertheless, as already pointed out above, a significant heterogeneity of the ^{14}C concentrations in the original charcoal fragments "population" can be expected: thus, we can just comment about a general compatibility of the microsamples with the larger ones.

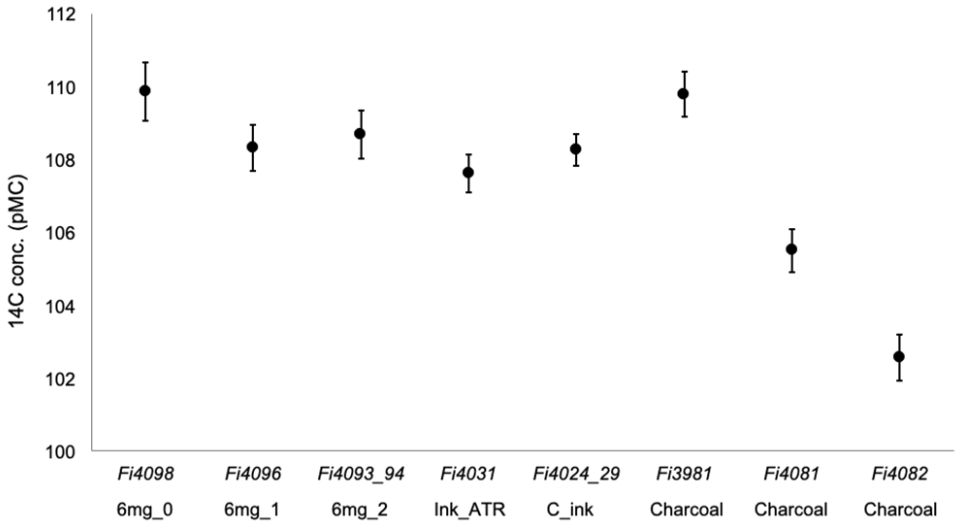

Figure 5. 12 Comparison between all the radiocarbon concentration measured for this application: the charcoals, C_ink, Ink_ATR and the 6mg-series.

5.7 Summary of the feasibility study

In this chapter, the feasibility study to date charcoal-based black inks, in particular when deposited on papyrus, one of the most widespread writing supports in the past, is presented. The issue about this application is that we need to collect a sample that would alter the integrity of the document we want to analyse. Since minimising the mass needed to perform the dating is crucial in order to preserve the document, our new experimental set-up for microsamples is ideal and necessary for this application.

We firstly studied an efficient procedure to extract the charcoal particles from the support, removing all the possible contamination from the binder. To do so, we prepared large test samples, analyzed the materials after the extraction of the charcoal by FTIR and ATR and afterwards we measured the radiocarbon concentrations, to check if they were all compatible one with another (i.e. all the contaminants were removed).

After identifying the right procedure for the extraction, we worked on small test samples (6mg-series). Enough charcoal material was extracted from these test samples

and processed using our new set-up optimized for microsamples. The overall experimental procedure resulted to be reproducible, and measured ^{14}C concentrations were coherent with the data obtained from larger samples and raw materials.

We are now planning to apply the methodology described in this chapter to a real sample. In this case we have to deal with the conservation conditions of the sample, which may even involve the loss of most of the ink particles, leaving us without enough material for the dating. Thus, we must even think of alternative solutions to this problem, which can be the possibility to date the organic binder itself. In any case, the microsample set-up is crucial for pursuing further research in this direction.

Conclusions

In this thesis, I have presented the research conducted during the three years of Ph.D., working at the INFN-LABEC laboratory in Florence.

During these years, we implemented a procedure for ^{14}C-AMS measurements on samples as small as about 50 µg of C (graphite), often referred to as "microsamples". We focused on the upgrade of the pre-existing experimental set-up, as far as both the graphitization instrumentation and the ^{14}C concentration measurements by AMS are concerned. We installed new graphitization reactors optimized for smaller samples: their volume was reduced to have a better efficiency of the graphitization reaction, and to better monitor its trend. In addition, ancillary instruments (small ovens and small Peltier cooling devices) were designed and produced to fit the new reactors.

New copper inserts were designed, in order to prevent possible mass losses between pre-treatment steps: the iron used as catalyst in the graphitization is directly pressed into these inserts, which are then introduced into the reactor, so that the produced graphite deposits directly on the inserts. The Cu inserts are mounted into the aluminium holders of the accelerator source and then are ready to be measured. As for the AMS measurements, the beam transport was further optimized to deal with lower extracted currents, to gain enough statistics at the end of the measurements.

Several tests on the new experimental set-up were performed, verifying a good reproducibility, a satisfying background and fine precision and accuracy.

Since the new microsamples set-up proved to be reliable, we decided to focus on new possible applications in the field of Cultural Heritage:

- Radiocarbon dating of mortars.

  Mortars are very heterogeneous materials and the separation between the carbon fraction of interest (that is the binder) and the possible contaminants (carbonates aggregates) can be very challenging. A crucial point of this application is finding a very selective separation procedure for the removal of the contaminants mentioned above. This procedure should be strongly

selective causing a high mass loss, so that using the typical set-up for large samples is not feasible. Our new microsamples set-up allowed us to deal with this problem: in fact, we were able to keep our procedure selective enough for the application dating carbonate samples as low as few milligrams, thus without increasing the initial mass of our collected mortar core (that is usually not possible in the field of Cultural Heritage).

- Radiocarbon dating of inks.

  The main issue of this kind of application is the invasiveness of the analysis, especially in case of using the typical set-up for large samples. It is clear that to date the ink, we would collect a portion of the text, thus we would risk to spoil the legibility of the document. For this reason, reducing the mass required for the measurements is mandatory. Our microsample set-up allowed us to perform such task with satisfying precision while reducing by an order of magnitude the mass of the sample to be dated, thus efficiently reducing the invasiveness of the dating procedure.

We believe that the optimization of the experimental set-up for the dating of microsamples is necessary and of high importance: the case studies discussed in this thesis prove it, since without the microsamples set-up we could have not performed such analyses.

Obviously, the work here presented does not stop with this thesis. Indeed, multiple different research lines can be explored enjoying the benefits of the new set-up.

We already mentioned the possibility of dating the pigments of an artwork: if we consider the components of a painting, pigments are not the only datable part. Indeed, especially in the past, organic binders were used to apply the pigments on the surface of the painting, giving them adhesion to the surface and cohesion between pigments grains. Following the research shown here, we are going to study a procedure that allows us to extract the organic binder and date it. This kind of application brings issues similar to the one for the dating of organic inks: the invasiveness of the analysis should be kept at minimum in order to preserve the legibility of the artwork. Consequently,

collectable material is expected to be very small. Such a possible application can be clearly studied only thanks to the microsamples set-up.

The relevance of this experimental set-up goes also beyond the aforementioned applications in the field of Cultural Heritages, as already explained in paragraph 1.4; indeed, our research group is currently working on the application of microsamples set-up, as well as the procedures, to the study of atmospheric particulate matter.

Appendix A: Discussion about the assumptions of ^{14}C dating

As said in paragraph 1.1 equation (1.4), radiocarbon dating is based on assumptions, which are true only in first approximation. Here we report the most important correction which have to be taken into account when dealing with the ^{14}C dating method:

- Radiocarbon concentration is constant regardless the place: the production rate of ^{14}C in atmosphere depends on how many cosmic rays reach the atmosphere. Since cosmic rays are made of charged particles, they are deflected by the magnetic field of Earth. Since the intensity of the magnetic field varies accordingly to the latitude, the production of ^{14}C is maximum at the poles and decreases gradually while reaching the equator. This effect is, however, compensated by the atmospheric fluxes, which mix the air masses throughout the globe and even out the concentration of radiocarbon in the atmosphere in a time that is much lower than radiocarbon half-life, hence negligible. Thus, we can consider this assumption true.
- Radiocarbon concentration in the atmosphere has always been constant through time: this assumption is true only in first approximation. Since the early days of radiocarbon measurements, discrepancies between the measured radiocarbon ages and calendar ages measured with independent method (e.g. dendrochronology) have been reported [72]. These discrepancies are caused by variations of the production of ^{14}C in the atmosphere, both for natural reasons (e.g. changes in the Earth magnetic field or variations in the Solar activity) and for anthropogenic reasons. Among the anthropogenic reasons, two important events must be taken into account. The former is called "Suess effect" and is related to the Industrial Revolution: starting from the 19^{th} century, massive amount of CO_2, produced from fossil fuels (with no ^{14}C), has been emitted in the atmosphere; consequently, the radiocarbon concentration in the atmosphere decreased significantly. Another effect is the so-called "bomb peak", related to

the nuclear tests carried out in the atmosphere between 1995 and 1963 [73]: the nuclear tests have caused a significant increase of neutron fluxes in the atmosphere, causing a growth in the ^{14}C production rate. All these reasons make obvious that the conventional radiocarbon age in equation (1.4) is not the real age and corrections and calibration are needed, as explained in the paragraph 1.1.

- ^{14}C concentration in the ocean or lake-like environments is the same as the one in atmosphere: actually, CO_2 solubilize into water starting from the surface and the exchange between the surface and the deep water is very slow, not negligible in respect to the half-life of ^{14}C. These exchanges allow the radiocarbon concentration to uniform in water, but the mean value of the concentration is smaller than the concentration of ^{14}C in the atmosphere. All the living organism living in water exchange with water itself, causing an appearing ageing of marine samples of about 400 years. Regarding lake-like environments, an ageing effect has to be taken into account, linked to the geological $CaCO_3$ enrichment (no ^{14}C) of these environments. In order to date samples from these environments, specific corrections have to be made.
- As long as it lives, every organism has a radiocarbon concentration equal to the one of the atmosphere: even in this case, the assumption is true only in first approximation. As a matter of fact, when chemical reactions happen, different isotopes are assimilated with different mechanism. In particular, the assimilation of lighter isotopes is favourite with respect to the heavier ones. For example, during the photosynthesis, the formation of C-C bonds favourites the assimilation of ^{12}C, decreasing the concentration of ^{13}C and ^{14}C in the sample. This phenomenon is called isotopic fractionation and specific correction must be made in order to avoid the apparent ageing of the sample. Since the fractionation correction cannot be calculated for ^{14}C, since it is an instable isotope, ^{13}C is used. Knowing the correlation between ^{14}C and ^{13}C, it is possible to correct the ^{14}C concentration obtained during the measurements.

- Equation (1.4) is valid only if the sample behaves like a closed system and no other possible reaction with the outer environment happens. Possible contaminations by outer carbon may happen due to natural agents (e.g. the humic acids, carbonates, diagenesis effects) or anthropic agents, causing the apparent ageing of rejuvenation of the sample. To avoid these kind of contaminations, all the samples are pre-treated before the measurements, as explained in paragraph 1.3.

Appendix B: Data analysis

During every measurement with the accelerator, in addition to the unknown samples, internal standards are added to the batch of samples to be put into the ion source:

- NIST Oxalic Acid II, simply called "standard", with a known and certified radiocarbon concentration;
- Cyclohexanone 2.4 DNPH, called "blank", with a nominal null ^{14}C concentration;
- IAEA C7, with a certified ^{14}C concentration.

For each sample ^{14}C counts and ^{13}C and ^{12}C currents are measured. From these measurements, the isotopic ratios of $^{14}C/^{12}C$, needed to determine the conventional radiocarbon age, and $^{13}C/^{12}C$, needed for the isotopic fractionation corrections, are calculated.

The contribution of blanks, which represents the background of the measurements, is subtracted from the isotopic ratios of standards and unknown samples. Besides, the $^{14}C/^{12}C$ ratio of unknown samples is normalized to the isotopic ratios of the standards. The radiocarbon concentration of the unknown samples will be:

$$\left[{}^{14}C\right]_{t,pMC} = \left[{}^{14}C\right]_{std,pMC} \frac{\left[{}^{14}C\right]_t - \left[{}^{14}C\right]_{blk}}{\left[{}^{14}C\right]_{std} - \left[{}^{14}C\right]_{blk}} \left(\frac{\left[{}^{13}C\right]_{std}}{\left[{}^{13}C\right]_t}\right)^2 \qquad \text{(B.1)}$$

In which $\left[{}^{14}C\right]_t$ and $\left[{}^{13}C\right]_t$ are the measured isotopic ratio $^{14}C/^{12}C$ and $^{13}C/^{12}C$ for the unknown samples respectively, $\left[{}^{14}C\right]_{std}$ and $\left[{}^{13}C\right]_{std}$ are the isotopic ratios measured for the standards, $\left[{}^{14}C\right]_{blk}$ is the isotopic ratio measured for the blanks and $\left[{}^{14}C\right]_{std,pMC}$ is the certified radiocarbon concentration of the standard.

The radiocarbon concentration $\left[{}^{14}C\right]_{t,pMC}$ is typically expressed in pMC, percent of Modern Carbon:

$$pMC = \frac{\left[{}^{14}C\right]_{sample}}{\left[{}^{14}C\right]_{0}} \cdot 100 \tag{B.2}$$

In which $\left[{}^{14}C\right]_{sample}$ represents the sample radiocarbon concentration while $\left[{}^{14}C\right]_{0}$ is the radiocarbon concentration measured in 1950 for a reference material (Oxalic Acid I, no more available).

Starting from equation (1.4), the conventional radiocarbon age becomes:

$$t_{RC} = \tau \cdot \ln \frac{\left[{}^{14}C\right]_{0}}{\left[{}^{14}C\right]_{sample}} = \tau \cdot \ln \frac{100}{\left[{}^{14}C\right]_{t,pMC}} \tag{B.3}$$

In which $\left[{}^{14}C\right]_{0}$ is equal to 100 by the definition of pMC.

Following the error propagation laws, we can obtain the experimental error on the conventional radiocarbon age from equation (B.3):

$$\sigma(t_{RC}) = \tau \cdot \frac{\sigma\left(\left[{}^{14}C\right]_{t,pMC}\right)}{\left[{}^{14}C\right]_{t,pMC}} \tag{B.4}$$

In which the errors on τ and $\left[{}^{14}C\right]_{0}$ are neglected.

List of published papers during the Ph.D.

- F. Barile, S. Barone, M. Fedi, L. Liccioli, V. Paticchio, L. Schiavulli, F. Taccetti "The new sample preparation line for radiocarbon measurements at the INFN Bari Laboratory", *Nuclear Instruments and Methods in Physics Research Section A: Accelerators Spectrometers Detectors and Associated Equipment,* 2019

- F. Barile, S. Barone, M. Fedi, L. Liccioli, V. Paticchio, R. Perrino, L. Schiavulli, F. Taccetti "A C-14 beam monitor using silicon solid state sensor for cultural heritage", *Nuclear Instruments and Methods in Physics Research Section A: Accelerators Spectrometers Detectors and Associated Equipment,* 2019

- M. Fedi, S. Barone, F. Barile, L. Liccioli, M. Manetti, "Towards micro-samples radiocarbon dating at INFN-LABEC, Florence", *Nuclear Instruments and Methods in Physics Research Section B: Beam Interactions with Materials and Atoms,* 2020

- M. Mejìa, M. Tascon, D. Gallegos, D. Gonzàlez Pondal, M. Bini, L. Liccioli, S. Barone, L. Giuntini, M. Fedi, F. Taccetti, F. Marte, "The role of restoration and scientific examination for the accurate attribution of a European painting in South America", *Rendiconti Lincei. Scienze Fisiche e Naturali,* 2020

- S. Calandra, S. Barone, E. Cantisani, M. Fedi, C. A. Garzonio, L. Liccioli, B. Salvadori, T. Salvatici, S. Vettori, "The mortars of Giotto's Bell Tower (Florence, Italy): raw materials and technologies", *Construction and Building Materials*, 2020

- M. Fedi, S. Barone, L. Carraresi, S: Dominici, L. Liccioli, "Direct radiocaron dating of charcoal-based ink in papyri: a feasibility study", *Radiocarbon,* accepted - to be published.

Bibliography

[1] M. Ruff, S. Fahrni, H. Gaeggeler, I. Hajdas, M. Suter, H. A. Synal, S. Szidat e L. Wacker, «On-line Radiocarbon Measurements of Small Samples Using Elemental Analyzer and MICADAS Gas Ion Source,» *Radiocarbon,* 2010.

[2] P. Steier, J. Liebl, W. Kutschera, E. Wild e R. Golser, «Preparation Methods of µg Carbon Samples for 14C MeasuremenTS,» *Radiocarbon,* 2017.

[3] A. M. Smith, Q. Hua, A. Williams, V. Levchenko e B. Yang, «Developments in micro-sample 14C AMS at the ANTARES AMS facility,» *Nuclear Instruments and Methods in Physics Research Section B: Beam Interactions with Materials and Atoms,* 2010.

[4] W. Libby, «Radiocarbon Dating,» *Nobel lactures, Chemistry 1942-1962,* 1964.

[5] Q. Hua, «Radiocarbon: A chronological tool for the recent past,» *Quaternary Geochronology,* 2009.

[6] I. Olsson, «Modern aspects of radiocarbon datings,» *Earth-Science reviews,* 1968.

[7] P. J. Reimer e et al., «The IntCal20 Northern Hemisphere radiocarbon age calibration curve (0-55 kcal BP),» *Radicoarbon,* 2020.

[8] T. J. Heaton e et al., «Marine20 - The marine Radiocarbon age calibration curve (0-55000 CAL BP),» *Radiocarbon,* 2020.

[9] C. Bronk Ramsey, «Bayesian analysis of radiocarbon dates,» *Radiocarbon,* 2009.

[10] W. Kutschera, «Applications of Accelerator Mass Spectrometry,» *International Journal of Mass Spectrometry,* 2013.

[11] T. Jull, «AMS Radiocarbon Dating,» *Elsevier B.V.,* 2007.

[12] W. Kutschera , «Progress in isotope analysis at ultra-trace level by AMS,»

International Journal of Mass Spectrometry, 2005.

[13] M. Fedi, A. Cartocci, M. Manetti, F. Taccetti e P. Mandò, «The 14C AMS facility at LABEC, Florence,» *Nuclear Instruments and Methods in Physics Research B,* 2007.

[14] M. Fedi, L. Caforio, L. Liccioli, P. Mandò, A. Salvini e F. Taccetti, «A Simple and Effective Removal Procedure of Synthetic Resins to Obtain Accurate Radiocarbon Dates of Restored Artworks,» *Radiocarbon,* 2014.

[15] M. Fedi, L. Liccioli, L. Castelli, C. Czelusniak, L. Giuntini, P. Mandò, L. Palla e F. Taccetti, «Memory effects using an elemental analyser to combust radiocarbon samples: Failure and recovery,» *Nuclear Instruments and Methods in Physics Research Section B: Beam Interactions with Materials and Atoms,* 2015.

[16] J. Vogel, J. Southon, D. Nelson e T. Brown, «Performance of catalytically condensed carbon for use in accelerator mass spectrometry,» *Nuclear Instruments and Methods in Physics Research Section B: Beam Interactions with Materials and Atoms,* 1984.

[17] L. Hendriks, I. Hajdas, E. Ferreira, N. Scherrer, S. Zumbuhl, M. Kuffner, L. Carlyle, H. Synal e D. Gunther, «Selective dating of paint components: Radiocarbon dating of lead white pigment,» *Radicoarbon,* 2018.

[18] V. Bernardoni, G. Calzolai, M. Chiari, M. Fedi, F. Lucarelli, S. Nava, A. Piazzalunga, F. Riccobono, F. Taccetti, G. Valli e R. Vecchi, «Radiocarbon analysis on organic and elemental carbon in aerosol samples and source apportionment at an urban site in Northern Italy,» *Journal of Aerosol Science,* 2013.

[19] F. Barile, S. Barone, M. Fedi, L. Liccioli, V. Paticchio, L. Schiavulli e F. Taccetti, «A C-14 beam monitor using silicon solid state sensor for cultural heritage,» *Nuclear Inst. and Methods in Physics Research, A,* 2018.

[20] R. Young, «Lime-based plasters, renders and washes,» in *Materials & Skills for Historic Building Conservation*, Blackwell Publishing Ltd, 2008.

[21] E. Pecchioni, F. Fratini e E. Cantisani, Le malte antiche e moderne : tra tradizione ed innovazione, Pàtron, 2018.

[22] D. Von Landsberg, «The history of lime production and use from early times to the industrial revolution,» *Zement-Kalk-Gips,* 1992.

[23] A. Mazar, Archaeology of the Land of the Bible: 10,000-586 B.C.E., Lutterworth Press, 1990.

[24] L. Pheng, «Construction of dwellings and structures in ancient China,» *Structural Survey,* 2001.

[25] W. H. Gourdin e W. D. Kingery, «The Beginnings of Pyrotechnology: Neolithic and Egyptian Lime Plaster,» *Journal of Field Archaeology,* 1975.

[26] D. Carran, J. Hughes, A. Leslie e C. Kennedy, «A Short History of the Use of Lime as a Building Material Beyond Europe and North America,» *International Journal of Architectural Heritage,* 2012.

[27] A. Henry e J. Stewart, Practical Building Conservation: Mortars, plasters and renders, British Standards Insitution, 2012.

[28] R. Veiga, «Air lime mortars: What else do we need to know to apply them in conservation and rehabilitation interventions? A review,» *Construction and Building Materials,* 2017.

[29] J. Spiropoulos, Small scale production of lime for building, Deutsches Zentrum für Entwicklungstechnologien, 1985.

[30] U. Menicali, I materiali dell'edilizia storica: tecnologia e impiego dei materiali tradizionali, Nuova Italia scientifica, 1992.

[31] «The mortar dating project,» [Online]. Available: http://www.mortardating.com/.

[32] K. Elert, C. Rodriguez-Navarro, E. S. Pardo, E. Hansen e O. Cazalla, «Lime mortarts for the conservation of historic buildings,» *Studies in Conservation,* 2002.

[33] A. Rattazzi, Conosci il grassello di calce? Origine, produzione e impiego del grassello nell'architettura, nell'arte e nel restauro, Bologna: Edicom Bologna, 2007.

[34] M. Bohac e R. Necas, «The role of aging on rheological properties of lime putty,» *Procedia Engineering,* 2016.

[35] R. Lawrence, T. J. Mays, S. P. Rigby, P. Walker e D. D'Ayala, «Effects of carbonation on the pore structure of non-hydraulic lime mortars,» *Cement and Concrete Research,* 2007.

[36] J. Heinemeier, H. Jungner, A. Lindroos, A. Ringbom, T. von Konow e N. Rud, «AMS 14C datig of lime mortar,» *Nuclear instruments and methods in Physics reasearch B,* 1997.

[37] J. Labeyrie e G. Delibrias, «Dating of old mortars by the carbon-14,» *Nature,* 1964.

[38] M. S. Baxter e A. Walton, «Radiocarbon dating of mortars,» *Nature,* 1970.

[39] J. Hale, J. Heinemeier, L. Lancaster, A. Lindroos e A. Ringbom, «Dating ancient mortar,» *American Scientist,* 2003.

[40] D. Michalska, «Influence of different pretreatments on mortar dating results,» *Nuclear instruments and methods in Physics research B,* 2019.

[41] R. Folk e S. Valastro, «Successful technique for dating of lime mortar by carbon-14,» *Journal of field archaeology,* 1976.

[42] A. Lindroos, J. Heinemeier e A. Ringbom, «Mortar Dating Using AMS 14C and Sequential Dissolution: Examples from Medieval, Non-Hydraulic Lime Mortars from the Åland Islands, SW Finland,» *Radiocarbon,* 2007.

[43] J. Heinemeier , A. Ringbom, A. Lindroos e A. Sveinbjornsdottir, «Successful AMS 14C dating of non-hydraulic lime mortars from medieval churces of the Aland islands, Finland,» *Radiocarbon,* 2010.

[44] A. Ringbom, «19 years of mortar dating: learning from experience,»

Radiocarbon, 2014.

[45] F. Marzaioli, C. Lubritto, S. Nonni, I. Passariello, M. Capano e F. Terrasi, «Mortar radiocarbon dating: preliminary accuracy evaluation of a novel methodology,» *Analytical chemistry,* 2011.

[46] F. Marzaioli, S. Nonni, I. Passariello, M. Capano, P. Ricci, C. Lubritto, N. De Cesare, G. Eramo, J. A. Quiros Castillo e F. Terrasi, «Aceleratore mass spectrometry 14C dating of lime mortars: methodological aspects and field study applications at CIRCE (Italy),» *Nuclear instruments and methods in Physics research,* 2012.

[47] S. Nonni, F. Marzaioli, M. Secco, I. Passariello, M. Capano, C. Lubritto, S. Mignardi, C. Tonghini e F. Terrasi, «14C mortar dating: the case of the medieval shayza ciradel, Syria,» *Radiocarbon,* 2013.

[48] A. Addis, M. Secco, F. Marzaioli, G. Artioli, A. Chavarria Arnau, I. Passariello, F. Terrasi e G. Brogiolo, «Selecting the most reliable 14C material inside mortars: the origin of the Padua cathedral,» *Radiocarbon,* 2019.

[49] E. Pecchioni, F. Fratini e E. Cantisani, Atlas of the ancient mortars in thin section under microscope, Firenze: Nardini Editore, 2014.

[50] G. Pesce, R. Ball, G. Quarta e L. Calcagnile, Identification, extraction and preparation of reliable lime samples for 14C dating of plasters and mortars with the "pure lime lumps" technique.

[51] A. Lindroos, A. Ringbom, J. Heinemeier, G. Hodgins, P. Sonck-Koota, P. Sjoberg, L. Lancaster, R. Kaisti, F. Brock, H. Ranta, M. Caroselli e S. Lugli, «Radiocarbon dating historical mortars: lime lumps and/or binder carbonate?,» *Radiocarbon,* 2018.

[52] G. Zucconi, Florence: An Architectural Guide, Arsenale Editrice, 1995.

[53] S. Vettori, E. Cantisani, S. Calandra, S. Barone, S. Caciagli, M. Fedi, C. A. Garzonio, L. Liccioli, B. Salvadori e T. Salvatici, «The mortars of Giotto's Bell

Tower (Florence, Italy): raw materials and technologies,» *Constructionand building materials,* 2020.

[54] L. Caforio, M. Fedi, P. Mandò, F. Minarelli, E. Peccenini, V. Pellicori, F. Petrucci, P. Schwartzbaum e F. Taccetti, «Discovering forgeries of modern art by the 14C Bomb Peak,» *The european Physical Journal Plus,* 2014.

[55] G. Bonani, S. Ivy, W. Wolfli, M. Broshi, I. Carmi e J. Strugnell, «Radiocarbon dating offourteen Dead Sea Scrolls,» *Radiocarbon,* 1992.

[56] D. Donahue, J. Olin e G. Harbottle, «Determination of the radiocarbon age of parchment of the Vinland Map,» *Radiocarbon,* 2002.

[57] M. Fedi, L. Carraresi, N. Grassi, A. Migliori, F. Taccetti, F. Terrasi e P. Mandò, «The Artemidorus Papyrus: solving an ancient puzzle with Radiocarbon and Ion Beam Analysis measurements,» *Radiocarbon,* 2010.

[58] L. Hendricks, I. Hajdas, E. Ferreira, N. Scherrer, S. Zumbuhl, G. Smth, C. Welte, L. Wacker, H. A. Synal e D. Gunther, «Uncovering modern paint forgeries by radiocarbon dating,» *Proceedings of the National Academy of Sciences,* 2019.

[59] F. Oliveira, C. Araujo, K. Macario e A. Cid, «Radiocarbon analysis of the Torah scrolls from the National Museum of Brazil collection,» *Nuclear Instruments and Methods in Physics Research Section B: Beam Interactions with Materials and Atoms,* 2015.

[60] O. Wendelbo, «The freeing of papyri from cartonnage,» *Restaurator, International Journal for the Preservation of Library and Archival Material,* 1975.

[61] H. Ragab, Le papyrus, Cairo: Dr. Ragab Institute, 1980.

[62] C. Basile, «A method of making papyrus and fixing and preserving it by means of a chemical treatment,» in *Conservation of Painting and the Graphic Arts*, IIC Lisbon Conference Preprints, 1972.

[63] A. Owen e R. Danzing, «The history and treatment of the papyrus collection at the Brooklyn Museum,» *Journal of the American Institute of Conservation,* 1993.

[64] F. Hepper e T. Reynolds, «apyrus and the adhesive properties in its cell sap in relation to paper making,» *JEA,* 1967.

[65] H. Weidemann e G. Bayer, «Papyrus, the paper of Ancient Egypt,» *Analytical Chemistry,* 1983.

[66] L. Green, «Recent analysis of pigments from Egyptian artefacts,» in *Conservation in Ancient Egyptian Collections: Papers given at the Conferenceof the United Kingdom Institute for Conservation, Archaeology Section, International Academic Projects*, London, 1995.

[67] R. Newman e M. Serpico, «Adhesives and binders,» in *Ancient Egyptian Materials and Technology*, Cambridge University Press , 2000.

[68] L. Green e B. Leach, «Investigation of consolidants and facing adesive for pigments on papyrus,» *British Museum Conservation Section, Internal Report,* 1993.

[69] G. Phillips e P. Williams, «The specification of the gum arabic of commerce,» in *Food Hydrocolloids*, Boston, Springer, 1994.

[70] M. Glicksman, «Gum Arabic (Gum Acacia),» in *Food Hydrocolloids*, New York, CRC Press, 1983.

[71] W. G. Mook, H. J. Streurman e H. T. Waterbolk, «Physical and chemical aspects of radiocarbon dating,» in *Mook, W. G., Streurman, H. J., & Waterbolk, H. T. (1983). Proceedings of the Groningen Symposium 14C and Archaeology*, 1983.

[72] E. M. Scott e P. J. Reimer, «CALIBRATION INTRODUCTION,» *Radicoarbon,* 2009.

[73] C. Turney, J. Palmer, M. Maslin, A. Hogg, C. Fogwill, J. Southon, P. Fenwick, G. Helle, J. Wilmshurst, M. McGlone, C. Bronk Ramsey, Z. Thomas, M. Lipson, B. Beaven, R. Jones, O. Andrews e Q. Huan, «Global Peak in Atmospheric Radiocarbon Provides a Potential Definition for the Onset of the Anthropocene Epoch in 1965,» *Nature,* 2018.

[74] K. Purser, R. Liebert, A. Litherland, R. P. Beukens, H. E. Gove, C. Bennett, M. Clover e W. Sondheim, «An attempt to detect stable N- ions from a sputter ion source and some implications of the results for the design of tandems for ultra-sensitive carbon analysis,» *Revue de Physique Appliquée,* 1977.

[75] C. Bronk Ramsey, «Development of the radiocarbon program OXCAL,» *Radiocarbon,* 2001.

[76] T. Heaton, M. Blaauw, P. Blackwell, C. Ramsey, P. J. Reimer e M. Scott, «The IntCal20 approach to radiocarbon calibration curve construction: a new methodology using bayesian splined and errors-in-variables,» *Radiocarbon,* 2020.

[77] T. Heaton, P. Kohler, M. Butzin, E. Bard, R. Reimer, W. Austin, C. Ramsey, P. Grootes, K. Hughen, B. Kromer, P. Reimer, J. Adkins, A. Burke, M. Cook, J. Olsen e L. Skinner, «Marine20 - The marine radiocabon age calibration curve (0-55000 cal BP),» *Radiocarbon,* 2020.